

University of Alberta

Investigations into Peripheral Nerve Transverse Relaxation Spectra

by

Keith David Wachowicz



A thesis submitted to the Faculty of Graduate Studies and Research in
partial fulfillment of the requirements for the degree of Doctor of Philosophy

in

Medical Sciences-Biomedical Engineering

Edmonton, Alberta
Fall 2004



Library and
Archives Canada

Bibliothèque et
Archives Canada

Published Heritage
Branch

Direction du
Patrimoine de l'édition

395 Wellington Street
Ottawa ON K1A 0N4
Canada

395, rue Wellington
Ottawa ON K1A 0N4
Canada

Your file *Votre référence*
ISBN: 0-612-96036-6
Our file *Notre référence*
ISBN: 0-612-96036-6

The author has granted a non-exclusive license allowing the Library and Archives Canada to reproduce, loan, distribute or sell copies of this thesis in microform, paper or electronic formats.

L'auteur a accordé une licence non exclusive permettant à la Bibliothèque et Archives Canada de reproduire, prêter, distribuer ou vendre des copies de cette thèse sous la forme de microfiche/film, de reproduction sur papier ou sur format électronique.

The author retains ownership of the copyright in this thesis. Neither the thesis nor substantial extracts from it may be printed or otherwise reproduced without the author's permission.

L'auteur conserve la propriété du droit d'auteur qui protège cette thèse. Ni la thèse ni des extraits substantiels de celle-ci ne doivent être imprimés ou autrement reproduits sans son autorisation.

In compliance with the Canadian Privacy Act some supporting forms may have been removed from this thesis.

Conformément à la loi canadienne sur la protection de la vie privée, quelques formulaires secondaires ont été enlevés de cette thèse.

While these forms may be included in the document page count, their removal does not represent any loss of content from the thesis.

Bien que ces formulaires aient inclus dans la pagination, il n'y aura aucun contenu manquant.

Canada

ACKNOWLEDGEMENTS

I would like to take this opportunity to thank some of the people that have helped make this work possible.

First, I'd like to thank my supervisor, Rick Snyder for all his help over the past six years. He has always made the time to discuss project problems, and has been very helpful in offering advice and suggestions. His enthusiasm for this work served as an excellent motivator on many an occasion. I would also like to acknowledge some of the other members of the academic staff, such as Alan Wilman, Christian Beaulieu, and Peter Allen, to whom one could always feel free to ask questions, and be quite sure of getting a good answer.

Thanks to Beau for being around to keep the computers in line.

Thanks to fellow students such as Steven, Atiyah, Kim, Chilo, and Luis, to name a few, for many enlightening conversations (some of them about work), and for being a reminder that indeed, there is life outside the lab.

Thanks to my family for all the support they've given me over the years. It was very much appreciated.

And thanks most importantly to my wife, Mary (a.k.a. the Adobe™ goddess) who has been an enormous source of help and encouragement. In addition to this support of the moral variety, she has proven herself an invaluable diagram and illustrative consultant. ☺ Thanks for everything, Mary.

TABLE OF CONTENTS

CHAPTER 1 -- INTRODUCTION	1
1.1 Motivation.....	1
1.2 Background – Transverse Relaxation.....	2
1.2.1 Formation of the Magnetization Vector.....	2
1.2.2 Perturbing the System.....	4
1.2.3 Observing the Perturbed System.....	6
1.2.4 Reversible Transverse Relaxation.....	8
1.2.5 Irreversible Transverse Relaxation	13
1.2.5.1 Dipolar Interactions.....	13
1.2.5.2 Chemical Exchange.....	17
1.2.5.3 Cross Relaxation.....	17
1.2.5.4 Diffusion.....	18
1.2.6 Relaxation Agents.....	18
1.3 Peripheral Nerve Structures	19
1.4 Transverse Relaxation in a Multi-compartmental Tissue Medium.....	21
1.5 Spectral Analysis of Decay Data	24
1.6 References.....	27
CHAPTER 2 -- REVIEW OF REPORTS AND INTERPRETATION OF MULTI-COMPONENT T₂ DECAY CURVES IN NERVE TISSUE	30
2.1 Introduction.....	30
2.2 Interpretation of short-lived component	31
2.3 Interpretation of Longer-Lived Spectral Components.....	32
2.4 References.....	36

**CHAPTER 3 -- A CONTINUOUS FLOW PERFUSION SYSTEM FOR
THE MAINTENANCE AND NMR STUDY OF SMALL TISSUE**

SAMPLES *IN VITRO*..... 39

3.1 Introduction..... 39

3.2 Method..... 40

3.3 Results..... 46

 3.3.1 Perfusion Chamber Material..... 46

 3.3.2 Comparison of Spectral-Parameter Precision between Chamber
 and NMR Tube..... 47

 3.3.3 Variation with Flow Rate..... 50

 3.3.4 Two-Coil System..... 52

 3.3.5 Temperature Control System..... 53

 3.3.6 Illustrative Studies..... 53

3.4 Discussion..... 55

3.5 Conclusions..... 58

3.6 References..... 59

**CHAPTER 4 -- ASSIGNMENT OF THE T₂ COMPONENTS OF
AMPHIBIAN PERIPHERAL NERVE TO THEIR MICROANATOMICAL
COMPARTMENTS 63**

4.1 Introduction..... 63

4.2 Method..... 64

4.3 Results..... 66

4.4 Discussion..... 69

4.5 Conclusions..... 78

4.6 References..... 79

CHAPTER 5 -- AN EXAMINATION OF MAMMALIAN NERVE T₂	
SPECTRAL CHARACTERISTICS	83
5.1 Introduction.....	83
5.2 Method.....	84
5.3 Results and Discussion	86
5.3.1 The effect of water and removal of the epineurium on rat nerve tissue.....	86
5.3.2 The use of Mn ²⁺ to assign components to physical compartments.....	90
5.4 Conclusions.....	100
5.5 References.....	101
CHAPTER 6 -- T₂ SPECTRAL CHARACTERISTICS OF HUMAN	
PERIPHERAL NERVE <i>IN VITRO</i>	104
6.1 Introduction.....	104
6.2 Method.....	104
6.2.1 Experimental Procedure.....	104
6.2.2 Analysis	106
6.3 Results.....	106
6.4 Conclusions.....	111
6.5 References.....	113
CHAPTER 7 -- CONCLUSIONS	115
7.1 Component to Compartment Assignment of Frog and Rat Nerve.....	115
7.2 Human Peripheral Nerve Studies.....	116
7.3 NMR In-Vitro Perfusion System.....	117
7.4 Future Directions	117
7.4.1 Human Nerve.....	117
7.4.2 Analysis Technique.....	118

APPENDIX 1 -- ALTERNATIVE ANALYSIS TECHNIQUE	119
A1.1 Introduction.....	119
A1.2 Theory	119
A1.3 Method	124
A1.4 Results and Discussion.....	124
A1.5 Conclusions.....	128

LIST OF TABLES

Table 2-1. T ₂ Spectral parameters of frog sciatic nerve from 4 different <i>in-vitro</i> studies.	30
Table 3-1. Means and standard deviations for transverse relaxation component parameters in frog sciatic nerve, as evaluated by an NNLS (non-negative least squares) algorithm. Note: In the first of the four columns, one nerve preparation was viewed 20 times using the two-coil perfusion chamber. In the second column, a different nerve preparation was viewed 20 times in a conventional NMR tube. The third column utilized the same nerve preparation as in Column 2, but this time the nerve was repositioned in the NMR tube between each spectra acquired. In the last column, 7 spectra were acquired using 7 different nerve preparations placed in NMR tubes.	49
Table 5-1. Average T ₂ spectral parameters from rat sciatic nerve in four different circumstances.....	88
Table 6-1. Spectral parameters for human peripheral nerves acquired in vitro while bathed in a water based tissue medium.....	107

LIST OF FIGURES

Figure 1-1. The equilibrium condition.....	3
Figure 1-2. Laboratory and rotating frames.....	4
Figure 1-3. Perturbation of the system from equilibrium.....	5
Figure 1-4. Trajectory of the magnetization vector with an off-resonance B_1 condition.....	6
Figure 1-5. Plane rotation pulse.....	7
Figure 1-6. Reversible losses and their recovery via a plane rotation pulse.....	8
Figure 1-7. The Carr-Purcell sequence. Both the transmitted B_1 field (grey blocks), and the received transverse magnetization signal (solid line) are displayed on the same axis. However, the received magnetization signal is greatly exaggerated with respect to the transmit field for visualization purposes.....	10
Figure 1-8 Error accumulation from inaccurate B_1 pulses in the C-P sequence.....	11
Figure 1-9. Self-correcting mechanism in the C-P-M-G sequence.....	12
Figure 1-10. The Carr-Purcell-Meiboom-Gill sequence. As in Figure 1-8, the received signal (solid line) is greatly exaggerated.....	12
Figure 1-11. The spectral density function for a correlation time of 1 ns. The three important regions of this function are circled and marked A , B , and C . A marks the quasi-static region of the spectral density function, and B and C mark the spectrum at ω_0 and $2\omega_0$, the frequencies (shown here for 3 Tesla) that lead to transitions and relaxation.....	14
Figure 1-12. Transition energies between the states of a two spin system. α represents a spin in its lower energy state (parallel to the applied magnetic field), and β represents one in its higher energy state (antiparallel).....	16
Figure 1-13. T_2 as it varies with correlation time τ_c	17
Figure 1-14. Variance of water T_2 with concentration of Mn^{2+}	19
Figure 1-15. Schematic of myelinated axon. The white cylindrical structure is the axon, surrounded by darker grey sections of myelin wrappings. Surrounding these and the axon in the Nodes of Ranvier are the Schwann cells (lighter grey).....	20

Figure 1-16. Schematic of fasciculated peripheral nerve.....	21
Figure 2-1. An NMR microscopy image (left) taken from Menon et al. [11] of a crayfish abdominal nerve, with a light histology micrograph on the right.....	33
Figure 3-1. Schematic of a single-coil (a) and two-coil (b) system for excitation and reception of RF signals. In both systems a valve (not shown and outside of the RF Transmit Coil) is included in the inflow tubing that allows for the switching between different buffer solutions.....	41
Figure 3-2. Actively-decoupled birdcage coil, designed for use in conjunction with a receive-only solenoid coil.....	42
Figure 3-3. Schematic for the birdcage coil circuitry. The elements are displayed flat here for the purpose of clarity, rather than being arranged on a cylindrical surface. Below the elements are the baluns (consisting of C_2 and L_2) which serve to match the impedance of the coil to that of the input (50 Ohm). Inductors (L_3) in series with the PIN diodes are placed in parallel with the capacitors, C above the upper end ring serve as principle elements in the decoupling circuitry (The PIN diodes can be turned on or off by the voltage supply circuits above them.)	43
Figure 3-4. Circuit diagram for the receive-only solenoid coil. Capacitors C_T and C_M are used for manual tuning and matching, respectively. The loop containing L_1 , C_1 , and the crossed diode elements (D) is responsible for shutting the coil off during transmission. L_1 and C_1 are chosen to resonate at ω_0 , causing the loop to behave like an open circuit at that frequency. However, the crossed diodes will not allow current through the inductor L_1 after the birdcage coil has stopped transmitting, since the voltages across the diodes during reception will not be sufficient to drive them into forward bias (<0.7 V).	44
Figure 3-5. Echo sampling method. 16 samples were obtained during the span marked above each echo (100 kHz sampling rate, 10 μ s / sample).....	45

Figure 3-6. Comparison of typical experimental frog sciatic nerve T_2 spectra from NMR tube (solid) and perfusion chamber (dashed). The first three components shown in both spectra (labeled A, B, and C) result from the nerve tissue, and the last originates from the buffer solution. 47

Figure 3-7. Variance of nerve and buffer component sizes with changes in flow rate. (a) Experimental results from a nerve sample in the single-coil system. (b) Results generated when theoretical flow loss curves for 1 to 14 mL/h are subtracted from the zero flow data in (a). (c) Experimental results from a nerve sample (different from (a)) in the two-coil system. Note the lack of variation of the components with flow rate..... 49

Figure 3-8. (a) Experimentally determined flow loss curves for the one-coil system (solid) as well as theoretical loss curves (dashed) based on the flow model. (b) Experimentally determined flow loss curves for the two-coil system..... 51

Figure 3-9. Illustrative study with frog sciatic nerve. The component sizes of calculated T_2 spectra are plotted as a function of time, during which the buffer composition was changed from isotonic to hypotonic (by reduction of NaCl content to $\frac{1}{4}$ that of normal), and then back to isotonic..... 54

Figure 3-10. A plot of the sizes obtained from a nerve sample before and after switching the perfusate from a normal solution to one containing 30-mM Gd-DTPA at time = 0. Open circles, grey squares, and solid circles represent the sizes of the short-lived, intermediate-lived, and long-lived nerve components, respectively. The rise and fall of the short-lived component (open circles) has been demonstrated to be an artifact of the changes in the intermediate-lived component (grey squares) [5]..... 54

Figure 3-11. Comparison of the theoretical fractional loss curve for a drop in T_2 from 1.6 to 1.5 seconds (dashed), with the experimentally determined loss curve at 15 mL/hr measured with the two-coil setup (solid). 57

Figure 4-1. Plots of the sizes of the a) perfusate and b) sum of the three nerve T_2 components following switching of the perfusate from an H_2O - to a D_2O -based solution..... 67

- Figure 4-2.** A plot of the T_2 component sizes (top) and their corresponding T_2 times (bottom) obtained from a sheathed nerve sample before and after switching the perfusate at time = 0 from a normal solution to one containing 10-mM Mn^{2+} 68
- Figure 4-3.** A plot of the T_2 component sizes (top) and their corresponding T_2 times (bottom) obtained from a desheathed nerve sample before and after switching the perfusate at time = 0 from a normal solution to one containing 10-mM- Mn^{2+} 69
- Figure 4-4.** Geometric construction of a sheathed cylinder for the purposes of simulation. D_1 and D_2 refer to the diffusion coefficients assigned to the inner section and the outer sheath, respectively..... 72
- Figure 4-5.** A computer simulation of the T_2 component sizes (top) and corresponding T_2 times (bottom) from a nerve with perineurial sheath intact in which 10-mM Mn^{2+} is introduced to the surrounding bathing solution at time = 0. In this simulation, the radius of the nerve was taken to be 0.735 mm, and surrounding this was a 15- μ m thick sheath. The diffusion coefficients of the nerve tissue and perineurial sheath were taken to be 3×10^{-7} cm²/s and 5×10^{-9} cm²/s, respectively. Here, it was assumed that the intermediate-lived component corresponded to the endoneurium. 75
- Figure 4-6.** A computer simulation of the T_2 component sizes (top) and corresponding T_2 times (bottom) from a nerve with perineurial sheath intact in which 10-mM Mn^{2+} is introduced to the surrounding bathing solution at time = 0. All dimensions and coefficients were kept the same as those for the simulation shown in Figure 4-5, the only difference being that in this simulation it was assumed that the longest-lived component corresponded to the endoneurium. 76
- Figure 5-1.** Spectra from rat sciatic nerve in four different circumstances. Spectra were reconstructed from average parameters in each case, using gaussian peaks of equal width for easy visual comparison from one to another. Normalization of the spectra was achieved by setting the short-lived component to a constant magnitude of 10. ... 87
- Figure 5-2.** a. Rat nerve with epineurium intact. b. Rat nerve with epineurium removed (single fascicle). Note the increased spacing between axons. 89
- Figure 5-3.** Frog nerve with 10-mM Mn^{2+} ions infused at time zero..... 91

Figure 5-4. Solved spectral parameters for rat sciatic nerve. 10-mM Mn^{2+} ions were infused at time zero (dashed line).	93
Figure 5-5. Experiment on rat sciatic nerve, with 10-mM Mn^{2+} ions infused at time zero. The short-lived and intermediate-lived components cannot be resolved after the introduction of manganese. The resultant merged component is represented with filled squares.	94
Figure 5-6. Repeat of experiment displayed in Figure 4, but using a single fascicle taken from rat sciatic nerve, instead of the entire nerve. Infusion of 10 mM Mn^{2+} begins at time zero (dashed line).	95
Figure 5-7. Spectral parameters of a rat sciatic nerve briefly exposed to Mn^{2+} , and then bathed in fluorinert.	96
Figure 5-8. a and b: Modified spectral parameters of the data set shown in Figure 7. c: An estimate of the paramagnetic ion concentration based on the values in b	97
Figure 5-9. a. Rat sciatic nerve. b. Frog sciatic nerve. Both these micrographs were acquired with the same magnification.	99
Figure 5-10. Comparison between normal spectral parameters of a single fascicle and one which was first rinsed in 3-mM Mn^{2+} for 6 seconds.	100
Figure 6-1. A typical T_2 spectrum of human peripheral nerve (saphenous) bathed in a water-based medium (RPMI).	107
Figure 6-2. Plot of average component parameters for human nerve. The error bars represent the standard deviations of these parameters for T_2 time and spectral size. The error bars for the T_2 times are derived from the standard deviation in logarithmic space.	108
Figure 6-3. Human peripheral nerve sample (saphenous) in Fluorinert FC-77. The long-lived component is present, albeit small.	109
Figure 6-4. The relative magnitude and T_2 time of nerve components calculated from the data set involving Gd-DTPA. The nerve was dipped for 10 seconds in 500 mM Gd-DTPA 2 minutes before time 0.	110

Figure A1-1. a) A plot of a monoexponential decay curve (solid) with a decay constant of 100 ms against a plot of the average (dashed) of two different curves, with decay constants increased and decreased by a factor of 1.2 from 100 ms. b) The difference function (single decay minus average) of the two lines described in a).
..... 120

Figure A1-2. The difference function as varies over a range of factor values (f). An increasing f value has the primary effect of vertically magnifying the difference function. 121

Figure A1-3. A schematic of how one might obtain compressed and magnified data sets $Y^-(x)$ and $Y^+(x)$ if data were sampled logarithmically. 122

Figure A1-4. A comparison of the techniques when applied to a data set with a delta function source spectrum (dashed). 125

Figure A1-5. A comparison of the techniques when applied to a data set with a continuous Gaussian line source spectrum (dashed), SNR=1000. 125

Figure A1-6. A comparison of the techniques when applied to a data set with a continuous Gaussian line source spectrum (dashed), SNR=6000. 126

Figure A1-7. A comparison of the techniques when applied to a data set with a continuous Gaussian line source spectrum (dashed), SNR=100. 126

Figure A1-8. A comparison of the techniques when applied to a data set with Rician noise. The dashed line represents the ideal source spectrum. 127

CHAPTER 1

INTRODUCTION

1.1 Motivation

Transverse relaxation (T_2) spectroscopy is one method of obtaining sub-voxel information using NMR. Because of the inherent difficulty in producing well-resolved spectra using this technique, its clinical use to date has been limited. However, despite its shortcomings, it has been demonstrated capable of probing information about sample microstructures, wherever there is a significant barrier to diffusion between neighbouring microstructural compartments. This has been applied in muscle tissues [1], plants [2], and even rocks [3]. But of particular interest are applications of this spectroscopic technique to nerve tissue. The compartmentalisation of nerve tissue on a microscopic scale is highly visible using this technique, due to effective diffusion barriers separating its compartments (particularly in myelinated nerve).

This technique has been successfully used to visualise myelin content in white matter [4], which has large implications for the diagnosis and monitoring of demyelinating disorders such as multiple sclerosis. However, myelin water only accounts for signal found in one region of the transverse relaxation spectrum, both in white matter and in peripheral nerve. The components found in other spectral regions have not been well attributed to nerve microstructures. The following work is therefore dedicated towards a better understanding of these other spectral components generated by peripheral nerve, so that nerve pathologies may be better discerned by NMR technology.

While *in-vivo* tissues are clearly in an optimal state for analysis of characteristics, there are many challenges to obtaining T_2 spectra in this manner. For one, the signal to noise (SNR) levels achieved through *in-vivo* studies of peripheral are generally low, as is the density of time-domain data points one can acquire. Both these issues become a

concern during analysis of the data, which will be discussed. For these reasons, and for the freedom to expose nerves to various agent during experiments, it was decided that all studies for this work be done using excised tissues *in vitro*. The knowledge gained from this work can then be applied back into an imaging protocol.

Since the T_2 spectra of frog nerve had already been well documented [5,6], it was decided that this tissue would be a good place to begin investigating the meaning of spectral components, with the intention of moving onto mammalian (rat) nerve preparations, and finally onto human peripheral nerve, as the hurdles in each successive study were overcome. Studies from all three tissues are therefore included in this work. Additionally, a flow system was designed to continuously perfuse the tissue with fresh buffer, and became invaluable to nerve studies in its ability to switch the buffer content from one type to another while acquiring NMR data on-the-fly. Developing a system with these capabilities (while not degrading the quality of acquired data) presented challenges of its own, and these issues and solutions to them are therefore included herein.

1.2 Background – Transverse Relaxation

1.2.1 Formation of the Magnetization Vector

Transverse relaxation is a process that will begin immediately after a polarized collection of spins (NMR visible nuclei) is perturbed from its equilibrium state. First, let us describe the equilibrium state. In order for protons (the nucleus that will be considered in this work) to align their magnetic moments to become capable of producing measurable signal, the object containing them (hereon referred to as “the sample”) must be placed in a magnetic field. Under these conditions the spins will align either parallel or antiparallel to the field direction. If the probabilities for each of these states were equal, then no resultant vector would be produced. However, the energy levels of the two states are not equal, and have the following energy eigenstates:

$$E = \pm \frac{1}{2} \gamma \hbar B_0, \quad [1.1]$$

where γ is the gyromagnetic ratio (a constant associated with the nucleus in question), and B_0 is the strength of the polarizing magnetic field. Given that the spin states follow Maxwell-Boltzmann statistics, the relative populations will be governed by the temperature and the energy eigenvalues, and the lower energy eigenstate will be favoured. The probability that a spin is in the energy state E_n is governed by the equation:

$$P_n = \frac{\exp(-\beta E_n)}{\exp(-\beta E_1) + \exp(-\beta E_2)}, \quad [1.2]$$

where $\beta = 1/kT$, with k being the Boltzmann constant, and T being the temperature in degrees Kelvin. The difference between these probabilities defines the portion of spins that will contribute to the overall sample magnetization vector. That portion is actually quite small. For example, for a proton study at room temperature and at a B_0 field of 3 Tesla, only $\sim 0.001\%$ of the spins will be visible, but will sum up to form a magnetization vector \vec{M} , which in equilibrium will be aligned with B_0 .

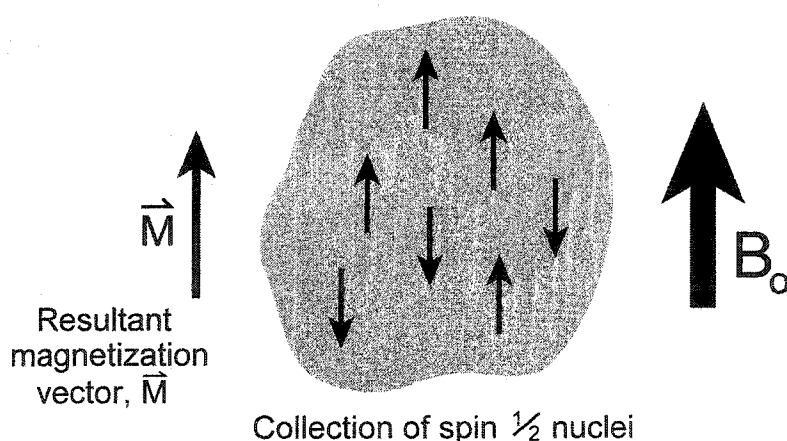


Figure 1-1. The equilibrium condition.

1.2.2 Perturbing the System

In a classical description, when a nuclear magnetic moment is exposed to a magnetic field, \mathbf{B}_0 , it will precess about an axis defined by the direction of the \mathbf{B}_0 vector. The rate of this precession, termed the Larmor frequency, will be determined solely by the strength of the magnetic field and the gyromagnetic constant, γ , associated with the nucleus in question. i.e.:

$$\omega_0 = \gamma B_0 \quad [1.3]$$

It is convenient to consider the system in the rotating frame of reference, where the observer rotates around the \mathbf{B}_0 axis at the Larmor frequency (Figure 1-2). In this rotating frame of reference, one can consider that the magnetization vector \mathbf{M} is stationary and for the purposes of explanation, no longer affected by a magnetic field. If one then adds a circularly polarized time varying magnetic field \mathbf{B}_1 , which rotates around the laboratory frame at the Larmor frequency, one can then cause the magnetic moment to rotate away from its equilibrium alignment (Figure 1-3).

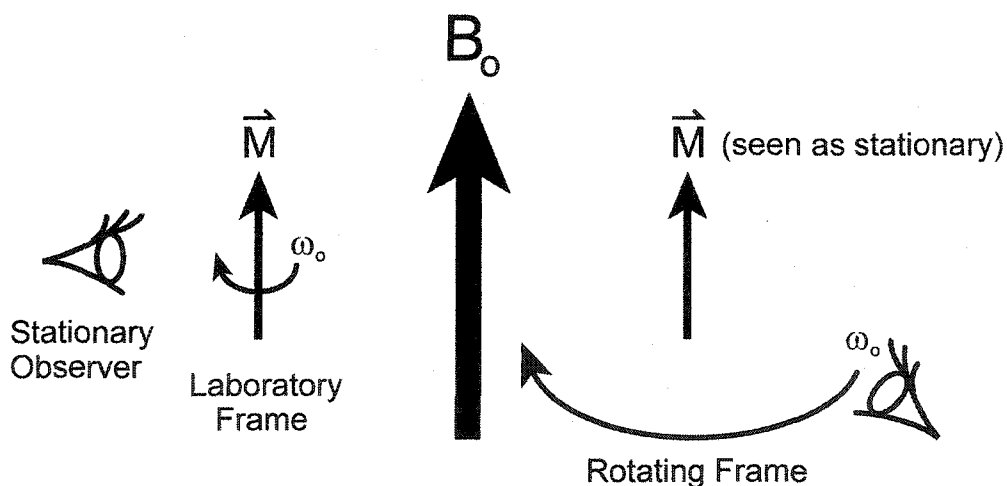


Figure 1-2. Laboratory and rotating frames.

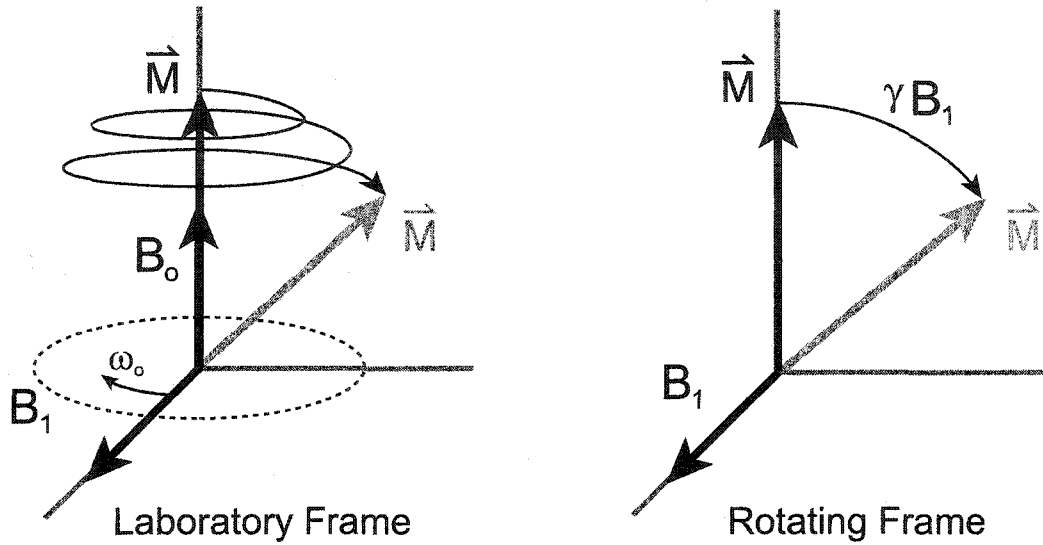


Figure 1-3. Perturbation of the system from equilibrium.

The added time varying field \mathbf{B}_1 is in practice implemented by placing the sample in a region surrounded by current carrying elements, which resonate electronically at or very close to the Larmor frequency. If the \mathbf{B}_1 field is off resonance, say at $\omega = \omega_0 + \Delta\omega$, then the \mathbf{B}_0 vector can no longer be completely neglected in the rotating frame. In this case, a resultant \mathbf{B} field will perturb the system, being the resultant vector of the \mathbf{B}_1 field and a fraction of \mathbf{B}_0 . Equation 1.4 describes the resultant magnetic field that would perturb the magnetization vector in a rotating frame coincident with \mathbf{B}_1 (Figure 1-4).

$$\vec{B} = \frac{\Delta\omega}{\omega_0} B_0 \hat{z} + B_1 \hat{x} \quad [1.4]$$

As is seen in Figure 1-4, the off resonance condition will change the trajectory of the magnetization vector as it is perturbed from equilibrium. The greater the off-resonance nature of the \mathbf{B}_1 field, the greater will be the distortion of this trajectory. The magnitude of \mathbf{B}_1 is typically many orders of magnitude smaller than B_0 (B_1 typically lies in the μT range, and B_0 is typically on the order of 1 T or more), so it will only take a

small shift in ω to render the \mathbf{B}_1 field ineffective. For example, for a situation where the \mathbf{B}_1 is $10 \mu\text{T}$, and \mathbf{B}_0 is 3 T , the \mathbf{B}_1 rotation frequency would only have to be off by 76 ppm for the maximum perturbation of the magnetization to be just 5 degrees off equilibrium.

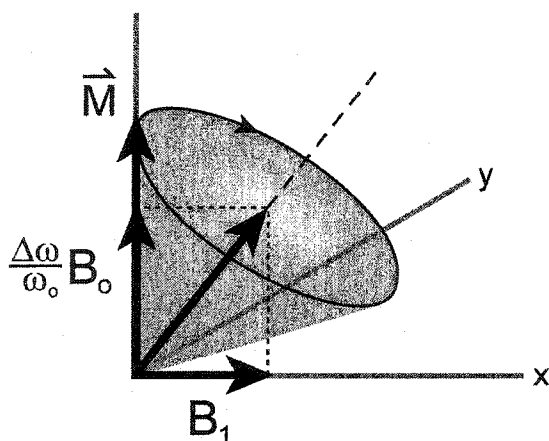


Figure 1-4. Trajectory of the magnetization vector with an off-resonance \mathbf{B}_1 condition.

1.2.3 Observing the Perturbed System

The presence of the magnetization vector can be detected by induced voltages in conductive current elements surrounding the sample (often the same device used to transmit the \mathbf{B}_1 field). However, this receiver device, or coil, can only detect time-varying changes in the magnetization vector, and hence can only detect vector components that are in a plane perpendicular to the \mathbf{B}_0 field as they rotate around this plane at ω_0 . Thus, the system will reach a maximum visibility when it is perturbed into the plane perpendicular to \mathbf{B}_0 , or transverse plane. A \mathbf{B}_1 pulse that achieves this will therefore be termed an excitation, 90 degree, or $\pi/2$ pulse.

Another type of pulse that will be used heavily in this work is called a plane rotation, or refocusing pulse. As will be shown later, this pulse is often required in order to correct for inhomogeneities present in \mathbf{B}_0 . As implied in its name, this pulse rotates the

magnetization components about an axis in the rotating frame from one side of the transverse plane to the other (Figure 1-5).

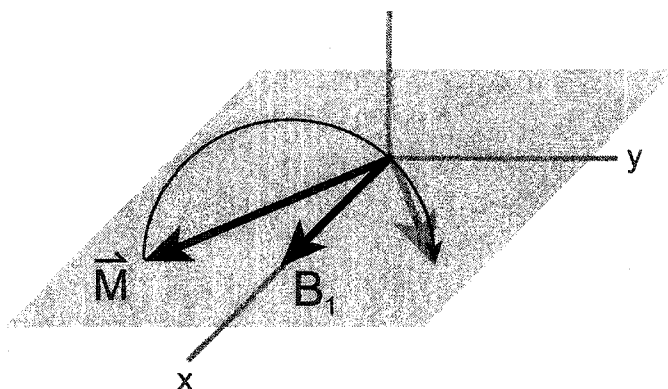


Figure 1-5. Plane rotation pulse.

Once visible, the observed signal from the perturbed magnetization vector will deteriorate, or relax through time in two coincident and independent ways. In one way, the magnetization perturbed from equilibrium will gradually return to equilibrium by gradually re-aligning with B_0 . The rate at which this will occur will be characterized by the time T_1 . Equation 1.5 describes the change of the unobservable M_z component as it undergoes longitudinal, or T_1 relaxation.

$$M_z(t) = M_0 - (M_0 - M_z(0))\exp(-t/T_1) \quad [1.5]$$

Longitudinal relaxation will not play a major role in this work, so it will not be discussed further. The other mode of relaxation in NMR is referred to as transverse relaxation, and it involves the reduction of observable signal originating from a loss in spin coherence. This relaxation can be separated into two general subsections: reversible and irreversible.

1.2.4 Reversible Transverse Relaxation

If left on its own, magnetization in the transverse plane will decay exponentially with a rate T_2^* . I.e.:

$$M_{xy} = \exp(-t/T_2^*) \quad [1.6]$$

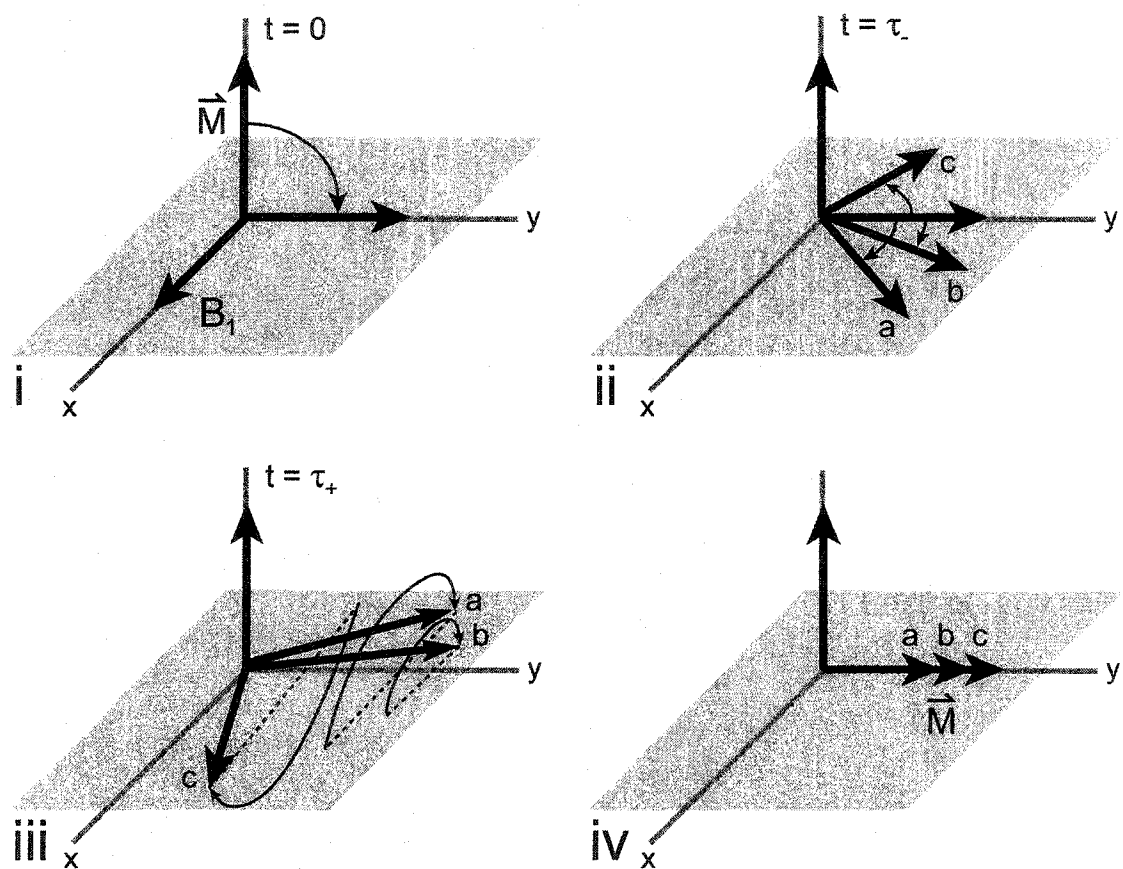


Figure 1-6. Reversible losses and their recovery via a plane rotation pulse.

Part of these exponential losses can be recovered, and are hence known as reversible. These losses originate from B_0 inhomogeneities that are static on the timescale of an NMR experiment. A visualization of how these losses occur and how they are recovered is shown in Figure 1-6 (assuming only reversible losses are present). In the first frame of

this figure, a $\pi/2$ pulse tips the magnetization vector onto the y axis. Static B_0 inhomogeneities will cause components of the magnetization vector \mathbf{M} to precess at slightly different Larmor frequencies. This will be seen in the rotating frame as a dispersion of the \mathbf{M} vector in the transverse plane away from the y axis. This dispersion is represented in the second frame by three arbitrary vectors \mathbf{a} , \mathbf{b} , and \mathbf{c} , which rotate away from the y axis at different rates and directions. A plane rotation pulse is shown in the third frame, which inverts the position of these three vectors about the y axis, but does nothing to the rate and direction of angular rotation, since the B_0 inhomogeneities that are affecting them are static. It is for this reason that following the pulse, after the same interval of time t that they were initially allowed to disperse, the vectors completely refocus to re-form \mathbf{M} .

This process of recovering losses is a type of spin echo, or Hahn echo [7]. In order to observe transverse magnetization as it plays out over time while regularly compensating for B_0 inhomogeneities, a technique was proposed by Carr and Purcell [8] in which a train of successive refocusing pulses would play out after an initial excitation pulse. In this case, the magnetization vector would be allowed to dephase, then would be refocused, allowed to dephase again, then refocused, and so on. However, in the original Carr-Purcell sequence, the B_1 field would be applied along the same axis for the refocusing pulses as in the initial excitation pulses (unlike the case illustrated in Figure 1-6). In this manner, provided one has a perfectly calibrated and homogeneous B_1 field, the effects of irreversible losses alone can be seen in the form of a signal envelope (represented by the dashed line in Figure 1-7), having the equation:

$$M_{xy} = \exp(-t/T_2) \quad [1.7]$$

Because the refocusing pulses are along the same axis as the excitation pulse, the even echoes as seen by an RF receiver will be opposite in polarity to the odd.

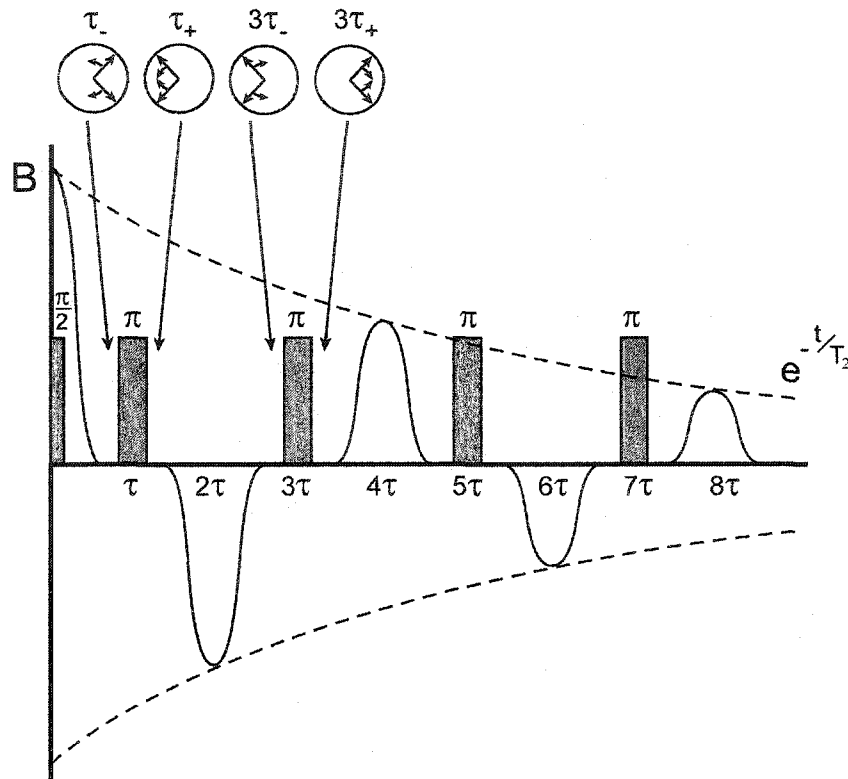


Figure 1-7. The Carr-Purcell sequence. Both the transmitted B_1 field (grey blocks), and the received transverse magnetization signal (solid line) are displayed on the same axis. However, the received magnetization signal is greatly exaggerated with respect to the transmit field for visualization purposes.

Unfortunately, this sequence is highly sensitive to pulse imperfections, for unless the B_1 pulses are exactly calibrated and homogeneous, errors in the angles of rotation during the pulses will accumulate, causing the signal envelope to decay at a higher rate than the ideal T_2 . This error accumulation is demonstrated in Figure 1-8. In this figure, the x axis, to which (in this sequence) the B_1 field is always aligned, is pointing out of the page. Note how the observable M_y magnetization component deteriorates as the result of a relatively small initial B_1 inaccuracy. Alas, because of this oversight (or perhaps lack of technological means), Carr and Purcell will forever have to share the glory for this concept with two other gentlemen.

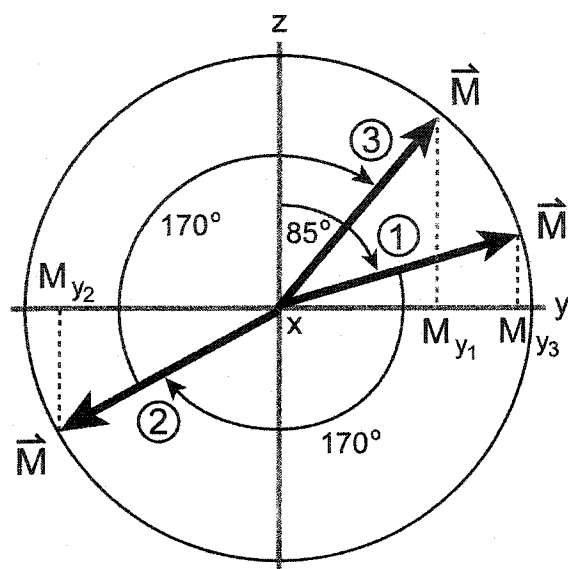


Figure 1-8 Error accumulation from inaccurate B_1 pulses in the C-P sequence.

In 1958 Meiboom and Gill proposed a modification to the Carr-Purcell sequence, in which there was a $\pi/2$ shift in phase of the B_1 pulse between the initial excitation pulse, and the refocusing pulses to follow [9]. This simple modification allowed this valuable technique to become very robust, and insensitive to moderate miscalibrations and inhomogeneities in the B_1 field. To illustrate this robustness, Figure 1-9 follows the path of a perfectly coherent magnetization vector experiencing a uniform but miscalibrated B_1 pulse train. This diagram displays the spatial axes in the rotating frame with the y axis (to which the refocusing B_1 pulses are aligned) pointing out of the page. In this example, the refocusing pulses are mis-set to 170 degree rotations, but the excitation pulse was assumed to be accurate. Although the sequence will remain robust even if the $\pi/2$ pulse contains a rotation error, the self-correcting mechanism in the sequence is more clearly illustrated in this manner. Note how every second echo (4τ versus 2τ) will result in a more-or-less corrected M vector position (marked as dots on the sphere surface).

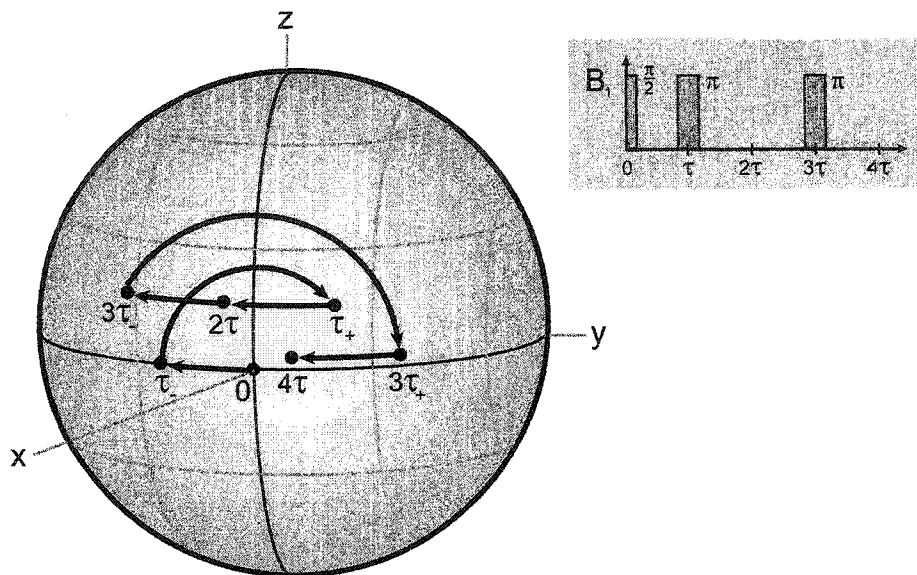


Figure 1-9. Self-correcting mechanism in the C-P-M-G sequence.

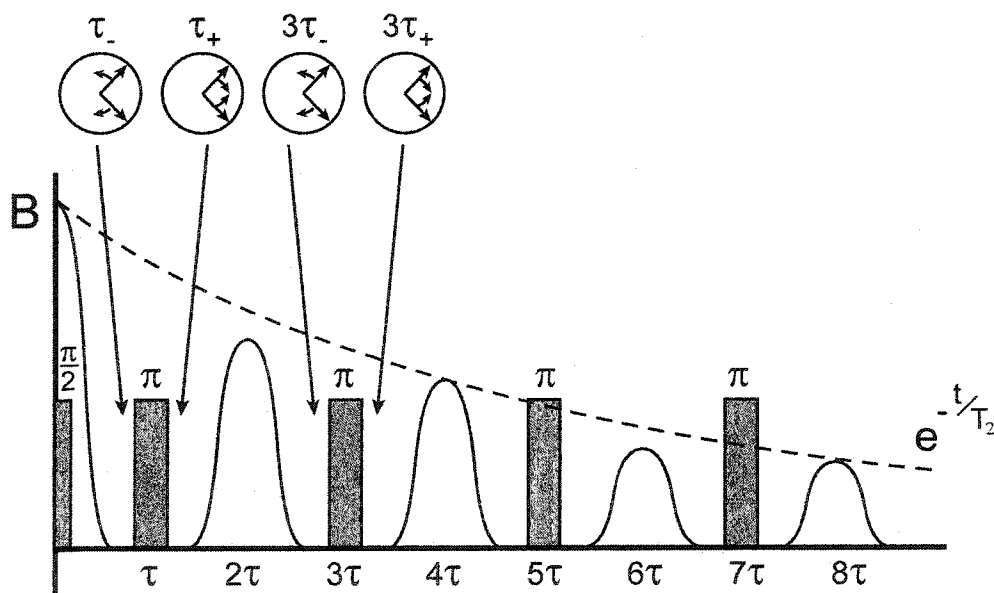


Figure 1-10. The Carr-Purcell-Meiboom-Gill sequence. As in Figure 1-8, the received signal (solid line) is greatly exaggerated.

It should be noted that T_1 relaxation does not have a significant effect on the measured T_2 decay with this method, because the continuous administration of refocusing

pulses inverts any longitudinal relaxation that can occur during an echo interval. Figure 1-10 illustrates the nature of the signal one would detect using the C-P-M-G sequence when B_1 is inhomogeneous or inaccurate. Theoretically, only the even echoes will be precise, but for practical purposes, unless there is a gross pulse inaccuracy, all echoes will be close to an ideal T_2 decay.

1.2.5 Irreversible Transverse Relaxation

This section will be a broad and general overview of the mechanisms that lead to transverse relaxation.

1.2.5.1 Dipolar Interactions

The rotational and translational movement of magnetic nuclei with respect to each other will inevitably and continuously result in interactions and energy exchange via their magnetic fields through space. Since the dipolar field will fall off as the cube of the distance, only dipoles in close proximity to each other need be considered. From a relaxation point of view only magnetic field fluctuations of several different frequencies are significant. In order to illustrate, the Debye spectral density function should first be discussed.

If one were to observe the magnetic field experienced by a single dipole from surrounding neighbours, say, in the x direction, the fluctuations would appear much as white noise. However, an analysis of these fluctuations would reveal a certain degree of time correlation. This correlation can be described as the time-averaged product of the magnetic field at time t and $(t+\tau)$. i.e.:

$$G(\tau) = \overline{B_x(t) \cdot B_x(t + \tau)} \quad [1.8]$$

The function G , or the autocorrelation function, can on first order be taken to decay exponentially [10] with τ , having a time constant τ_c :

$$G(\tau) = G(0) \cdot e^{-|\tau|/\tau_c}, \quad [1.9]$$

where $G(0) = \overline{B_x^2(t)}$.

A spectral density function can be described as twice the Fourier transform of the auto correlation function, which in this case, being a decaying exponential, yields a Lorentzian lineshape. This is what is referred to as the Debye spectral density function, which, has the following form:

$$J(\omega) = 2 \cdot G(0) \cdot \frac{\tau_c}{1 + \omega^2 \tau_c^2} \quad [1.10]$$

The normalized form of $J(\omega)$, in which the constant $2G(0)$ is dropped, will be used for the rest of this discussion.

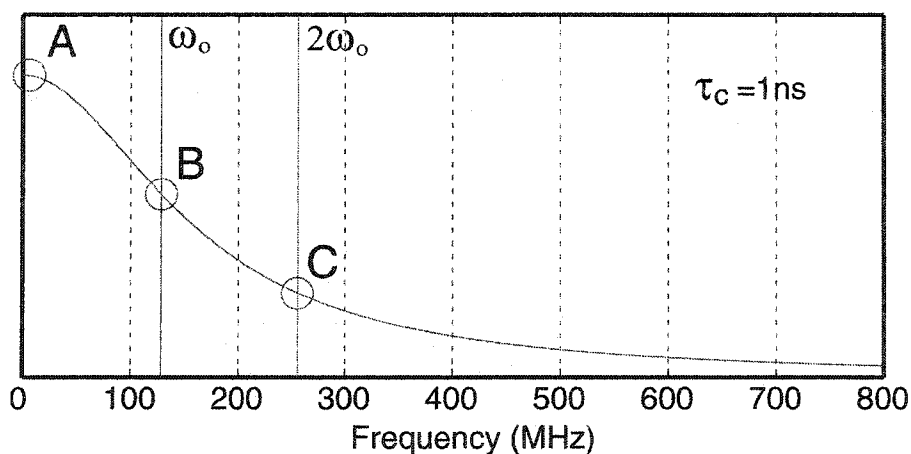


Figure 1-11. The spectral density function for a correlation time of 1 ns. The three important regions of this function are circled and marked **A**, **B**, and **C**. **A** marks the quasi-static region of the spectral density function, and **B** and **C** mark the spectrum at ω_0 and $2\omega_0$, the frequencies (shown here for 3 Tesla) that lead to transitions and relaxation.

Figure 1-11 displays a sample Debye spectral density function with a correlation time at 1 ns. The three regions circled and labelled as A, B, and C are the significant regions for relaxation through dipolar field interactions.

Quasi-Static Region

The region labelled A contributes to irreversible transverse relaxation through the dephasing of coherent spins in the transverse plane. Unlike the dephasing depicted in Figure 1-6, which could be refocused with a plane-rotation pulse, this dephasing is permanent. One can think of the permanent nature of the signal loss as resulting from the particular time-course of the fluctuations in the quasi-static region. These fluctuations occur too quickly to be negated by refocusing pulses (refocusing requires a constant precession rate), and too slowly to average to zero. This region plays a very important role with respect to how transverse relaxation varies with correlation time (related to the rotational speed of molecules), particularly at short correlation times.

Transition Frequencies

The regions labelled B and C are the spectral components that correspond to the resonant frequency of the system, ω_0 , and twice the resonant frequency, $2\omega_0$. These frequencies are those that can cause energy transitions between spins, leading to relaxation. The significance of these frequencies is seen from the transition energies possible when moving from one two spin state to another (Figure 1-12).

As is seen in Equation 1.1, the energy separation between the different energy states of a $\frac{1}{2}$ spin particle is $\gamma\hbar B_0$, or $\hbar\omega_0$. Since only one spin is involved in the E_1 transitions, $E_1 \sim \hbar\omega_0$, and using a similar argument, $E_2 \sim \hbar(2\omega_0)$. The greater the probability for these transitions, the greater will be the relaxation rate of the spin ensemble. (The two zero energy interactions labelled E_0 are the technical reason underlying the dephasing mentioned in the section above, corresponding to the zero frequency spectral density.)

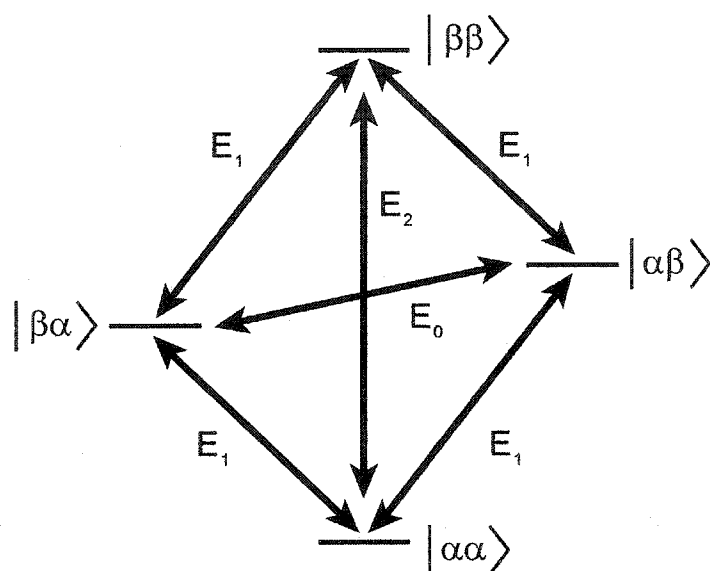


Figure 1-12. Transition energies between the states of a two spin system. α represents a spin in its lower energy state (parallel to the applied magnetic field), and β represents one in its higher energy state (antiparallel).

The transition probabilities for these interactions can be calculated and used to define the relaxation rates [11,12]. The transverse relaxation time on the basis of dipolar interactions can be given in terms of the Debye spectral characteristics as follows:

$$T_2^{-1} = \frac{3}{20} b^2 \{3J(0) + 5J(\omega_o) + 2J(2\omega_o)\}, \quad [1.11]$$

where $J(\omega)$ is the normalized Debye spectral density, and

$$b = -\frac{\mu_o}{4\pi} \cdot \frac{\hbar\gamma^2}{r^3}, \quad [1.12]$$

where r is the spin separation distance. Figure 1-13 shows a plot of transverse relaxation times calculated according to Equation 1.11, as they vary over the correlation time τ_c , using an ω_0 corresponding to the Larmor frequency at 3 Tesla, and an assumed inter-proton distance of 0.2 nm.

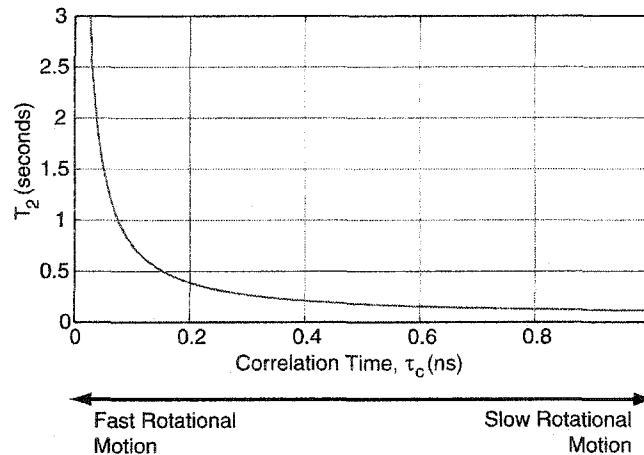


Figure 1-13. T_2 as it varies with correlation time τ_c .

1.2.5.2 Chemical Exchange

Another process by which irreversible losses in transverse signal can occur is through chemical exchange. Chemical exchange involves the reconfiguration or breaking and forming of bonds. Since the electronic structure will be different in the altered molecule, the magnetic field experienced by the protons will likely undergo subtle change as well, causing altered precession rates, and therefore altered T_2 . In a tissue environment, this process often occurs as water molecules bind and unbind to and from macromolecules.

1.2.5.3 Cross Relaxation

Cross relaxation, while primarily a phenomenon associated with longitudinal relaxation, can play in transverse relaxation as well. In order for transverse cross relaxation to occur, the precession rates of the two spins in question must be the same

[10]. This is thought to account for some relaxation of the water of hydration around a macromolecule.

1.2.5.4 Diffusion

Diffusion of excited molecules can also contribute to their relaxation provided the diffusion path takes the molecules through inhomogeneous B_0 environments. In this situation, refocusing pulses will not be able to compensate for the dephasing of these spins, as their precession rate will have varied over the course of travel. Factors affecting the efficiency of this relaxation mechanism are the diffusion coefficient of the molecule, as well as the inhomogeneity gradient. Decreasing the space between refocusing pulses in the C-P-M-G sequence will reduce the effect of this phenomenon on measured T_2 times.

1.2.6 Relaxation Agents

Certain molecules, when added to free water, can have a reducing effect on the overall measured T_2 time. Types of molecules that can have this effect on T_2 are large macromolecules, any molecules that offer binding sites for water, and molecules with a paramagnetic field. Basically, any type of molecule that can interfere with the motion of water molecules and slow its movement will reduce its T_2 by increasing its correlation time (Figure 1-13). The ability of water to bind to these molecules will also permit relaxation mechanisms like chemical exchange and cross relaxation. The diffusion of paramagnetic molecules with respect to water will cause time-dependent B_0 inhomogeneities that lead to increased relaxation through the means described in section 1.2.5.4. Paramagnetic relaxation agents can be ionic such as Mn^{2+} or Ni^{2+} , or present in large macromolecules such as iron dextran. The effect of any relaxation agent can be described to first order by the following equation [13]:

$$\frac{1}{T_2} = \frac{1}{T_{2o}} + R_T \cdot C, \quad [1.13]$$

where T_{2o} is the original T_2 time before addition of the agent, R_T is the transverse relaxivity coefficient in $\text{mol}^{-1}\cdot\text{s}^{-1}$, and C is the concentration of the relaxation agent. Depending on the relaxivity coefficient, it can take just a small concentration of agent to have a very significant effect on the T_2 . For example, only a concentration of 10-mM Mn^{2+} (with an R_T of 50 mM/s) will reduce water from a T_2 time of 2 seconds to 2 ms (Figure 1-14).

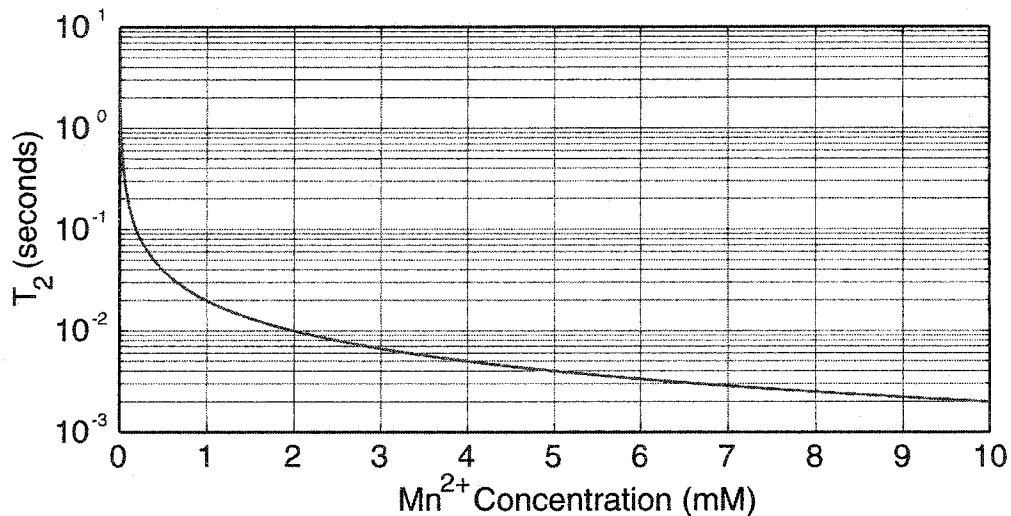


Figure 1-14. Variance of water T_2 with concentration of Mn^{2+} .

1.3 Peripheral Nerve Structures

Nerve Fibre

The nerve fibre is the conducting unit of the nerve, consisting of a number of components. At its core is the axon, a cylindrical body, bordered by its cell membrane, or axolemma. The diameter of an axon can typically vary from $0.5 \mu\text{m}$ to $10 \mu\text{m}$ [14]. Neurofilaments and microtubules, which are instrumental in axonal growth and transport, constitute the primary structural components of the axoplasm. The axoplasm, being a major constituent of peripheral nerve (estimated in rat sciatic nerve to have fractional

area of 24 percent [15]), will make a significant contribution to the signal acquired in a transverse relaxation experiment.

Surrounding each axon is a Schwann cell. In myelinated nerve, these Schwann cells are dedicated to a segment of one axon, and form a single spiral process around it, composed of many foldings of lipid bilayers. Each Schwann cell will myelinate approximately 1-mm segments of the axon, and only a small gap, termed a Node of Ranvier, will be left between adjacent processes. At the node, neighbouring Schwann cells form finger-like interlocking process (Figure 1-15). The node lengths will vary somewhat according to the diameter of the nerves, but will have a typical dimension of $0.5 \mu\text{m}$ [16].

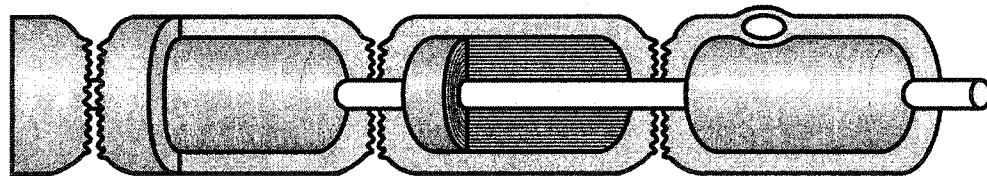


Figure 1-15. Schematic of myelinated axon. The white cylindrical structure is the axon, surrounded by darker grey sections of myelin wrappings. Surrounding these and the axon in the Nodes of Ranvier are the Schwann cells (lighter grey).

Myelin also will contribute a major component to NMR signal. Even though it has a very compact microstructure, it contains a significant amount of water (40 percent by volume determined by X-ray diffraction [17]).

Endoneurium

Nerve fibres as discussed above are arranged in bundles (fascicles) and surrounded by a perineurial sheath, composed of lamella cells arranged in concentric layers. The connective tissue surrounding the nerve fibres within the perineurium is called the endoneurium (Figure 1-16). This contains a significant amount of collagen, which forms

a very important connective tissue skeleton [18]. Water volume within the endoneurium is significant, and is therefore a third important contributor to NMR signal.

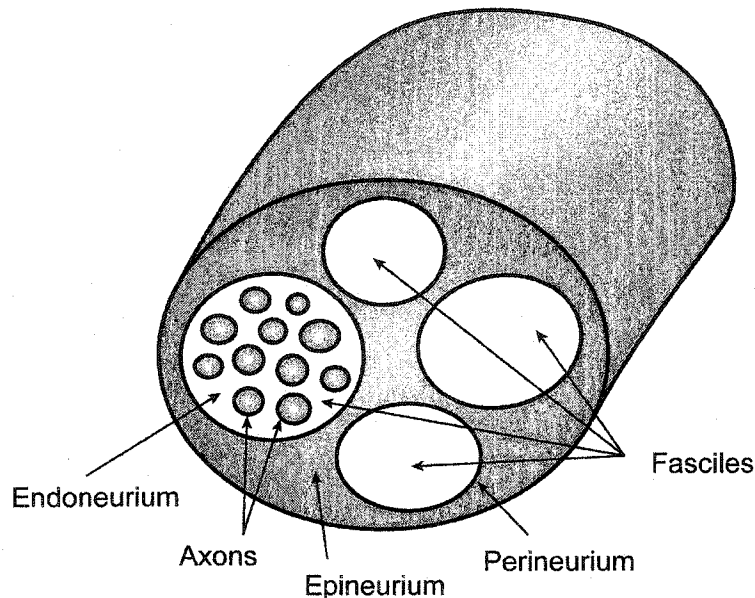


Figure 1-16. Schematic of fasciculated peripheral nerve.

Epineurium

As is seen in the schematic in Figure 1-16, the epineurium, which surrounds nerve bundles, can form another major compartment in peripheral nerve. The amount of epineurium present around a fascicle or fascicles can vary greatly between nerve trunks. In general, nerves with few fascicles will have a smaller proportion of epineurium [14]. This was seen to be the case in the frog and rat sciatic nerves studied in this work, where the number of fascicles was usually two or less.

1.4 Transverse Relaxation in a Multi-compartmental Tissue Medium

Many things can happen to a water molecule through the course of an NMR experiment. It can bind and unbind to macromolecules, diffuse through microscopic inhomogeneities, and diffuse from one molecular environment to another to name a few.

What effect do all these changes have on the measured T_2 ? The answer has to do with the rapidity of these changes compared with the timescale of the NMR parameter being measured.

The manner in which water T_2 will change when in association with two different states, or phases, has been investigated [19]. Consider the fractional spin populations in the two phases, p_a and p_b , with transverse relaxation times T_{2a} and T_{2b} . The lifetime of water molecules in each phase is τ_a and τ_b . The general equation for transverse magnetization that was derived is given in Equation 1.14.

$$\Phi_2(t) = \lambda^+ e^{-t/T_2^+} + \lambda^- e^{-t/T_2^-}, \quad [1.14]$$

where the signal is normalized so λ^+ and λ^- sum to 1,

$$\lambda^\pm = \pm \left[\left(\frac{1}{T_2^o} - \frac{1}{T_2^\pm} \right) / \left(\frac{1}{T_2^+} - \frac{1}{T_2^-} \right) \right], \quad [1.15]$$

$$\frac{1}{T_2^\pm} = \frac{1}{2} \cdot \left\{ \left(\frac{1}{T_{2a}} + \frac{1}{T_{2b}} + \frac{1}{\tau_a} + \frac{1}{\tau_b} \right) \pm \left[\left(\frac{1}{T_{2a}} - \frac{1}{T_{2b}} + \frac{1}{\tau_a} - \frac{1}{\tau_b} \right)^2 + \frac{4}{\tau_a \tau_b} \right]^{1/2} \right\}, [1.16]$$

$$\text{and } \frac{1}{T_2^o} = \frac{p_a}{T_{2a}} + \frac{p_b}{T_{2b}}. \quad [1.17]$$

λ^\pm and T_2^\pm are therefore the new fractional populations and T_2 times. The theory reduces to simpler expressions in two important limits. When τ_a and τ_b are much smaller than T_{2a} and T_{2b} , the system is said to be in fast exchange, and reduces to a single exponential decay:

$$\Phi(t) = e^{-t/T_{2o}}, \quad [1.18]$$

where the rate of decay is a weighted average of the intrinsic ones. The transition between bound and unbound phases is usually considered to be in fast exchange. For example, water within the axonal space of a nerve can be taken as a single exponential decay (assuming it is completely isolated from other compartments), due to the rapid exchange it would have between bound and unbound phases.

On the other extreme, when τ_a and τ_b are much greater than T_{2a} and T_{2b} , the system is said to be in slow exchange, and the relaxation can be described as a multi-exponential decay true to the intrinsic T_2 s and fractional populations of the compartments:

$$\Phi_2(t) = p_a \cdot e^{-t/T_{2a}} + p_b \cdot e^{-t/T_{2b}}, \quad [1.14]$$

According to this theory, the intermediate regime will continue to exhibit multi-exponential relaxation, but the relaxation times and the measured population sizes will be distorted from their intrinsic values.

To what degree the three primary compartments in nerve, endoneurium, axoplasm, and myelin water can be taken to be in slow exchange has been estimated on the basis of the belief that myelin, which forms a barrier between the other two compartments, is a significant diffusion barrier. Indeed, estimates have been made that roughly 64 ms would be needed for axonal water to mix with the 10th layer of myelin [20]. Considering that many more layers of myelin are often present in myelinated nerve, it does seem reasonable to consider the system to be nearing the slow exchange condition. However, there is doubtless some contribution of exchange to the system, and as such one must be careful not to be too cavalier in making the assumption of the slow exchange limit, as a

small deviation from this condition can alter population sizes and relaxation times from their intrinsic values.

1.5 Spectral Analysis of Decay Data

In the previous section it was shown that compartmentalized tissue can give rise to relaxation curves with multiple decay constants. In order to extract out the information pertaining to component sizes and relaxation rates, the multi-exponential data has to be treated mathematically. As straightforward as it sounds, the solution is anything but trivial, owing largely to the non-orthogonal nature of the exponential curve [21]. As a result, a number of techniques have been used, some more successful than others. The technique used in this work is the NNLS method of Lawson and Hanson [22], which was later adapted and used with NMR data [23].

A multi-exponential curve can be represented by the summation of all its constituent exponentially decaying components, represented by the following equation:

$$D(t) = \int S(\tau) \cdot \exp\left(\frac{-t}{\tau}\right) \cdot d\tau \quad [1.15]$$

Discretised into N decay constants, this equation can be written as:

$$D(t) = \sum_{n=1}^N S_n \exp\left(\frac{-t}{\tau_n}\right) \quad [1.16]$$

Finally, with time discretised as well into M sample times, the equation can be written:

$$\begin{bmatrix} D_1 \\ D_2 \\ \vdots \\ D_M \end{bmatrix} = \begin{bmatrix} \exp(-t_1/\tau_1) & \exp(-t_1/\tau_2) & \dots & \exp(-t_1/\tau_N) \\ \exp(-t_2/\tau_1) & \exp(-t_2/\tau_2) & \dots & \exp(-t_2/\tau_N) \\ \vdots & \vdots & \ddots & \vdots \\ \exp(-t_M/\tau_1) & \exp(-t_M/\tau_2) & \dots & \exp(-t_M/\tau_N) \end{bmatrix} * \begin{bmatrix} S_1 \\ S_2 \\ \vdots \\ S_N \end{bmatrix} \quad [1.17]$$

In this form only the column vector of S values is unknown. The NNLS routine can now be applied in this form. A set of S values is determined that minimizes the χ^2 parameter while prohibiting negative solutions. The χ^2 parameter is defined as:

$$\chi^2 = \sum_{m=1}^M \frac{\left\{ \left[\sum_{n=1}^N S_n \exp\left(\frac{-t_m}{\tau_n}\right) \right] - D_m \right\}^2}{\sigma_m} \quad , \quad [1.18]$$

where σ_m is the standard deviation of the m^{th} data point. As is, the routine will find a delta function solution. These, although producing minimal χ^2 parameters, are difficult to interpret. This technique can easily be adjusted to produce smooth solutions, however. Here, constraints can be added to force the solution to be continuous, at the expense of a larger χ^2 [24]. These constraints add cost to the solution for certain spectral features, such as a large gradient, or change in gradient over neighbouring solution points. The type of constraint used in this work was called a “minimum” energy constraint, because it minimized the square of the solution points, having the effect of reduced solution amplitudes and smoothly varying spectra. The minimum energy constraint was implemented as follows:

$$\begin{bmatrix} D_1 \\ D_2 \\ \vdots \\ D_M \\ 0 \\ 0 \\ \vdots \\ 0 \end{bmatrix} = \begin{bmatrix} \exp(-t_1/\tau_1) & \exp(-t_1/\tau_2) & \cdots & \exp(-t_1/\tau_N) \\ \exp(-t_2/\tau_1) & \exp(-t_2/\tau_2) & \cdots & \exp(-t_2/\tau_N) \\ \vdots & \vdots & \ddots & \vdots \\ \exp(-t_M/\tau_1) & \exp(-t_M/\tau_2) & \cdots & \exp(-t_M/\tau_N) \\ \mu & 0 & \cdots & 0 \\ 0 & \mu & \cdots & 0 \\ \vdots & \vdots & \ddots & \vdots \\ 0 & 0 & 0 & \mu \end{bmatrix} * \begin{bmatrix} S_1 \\ S_2 \\ \vdots \\ S_N \end{bmatrix} \quad [1.19]$$

As the factor μ is increased, the χ^2 parameter will monotonically increase. Thus, a criterion for an acceptable χ^2 parameter can be selected to determine an appropriate μ . In this work, the target χ^2 parameter was taken to be a selected multiple of the delta function χ^2 ($\mu=0$). This method was seen to give more consistency than another alternative, which set the χ^2 parameter to the number of data points, M , used to find the solution (assuming each data point had been normalized to its standard deviation) [24].

The generation of relaxation spectra from multi-exponential decay data with NNLS has its limitations. The non-orthogonal nature of the exponential function reduces the ability of the routine to resolve spectra to reliable spectral precision. Indeed, this problem is bound to plague any algorithm when applied to this problem. Fenrich et al. [25] investigated the ability of NNLS to separate closely spaced peaks, and found it was dependent on SNR, time separation between data points (echo spacing), and the time acquisition window. In our work, spectral peaks could not usually be discriminated if the T_2 times of the peaks were roughly a factor of 2 or less apart. Even when one does achieve a well-resolved spectrum, it is important to remember that this spectrum is only a rough estimate of the intrinsic decay spectrum, and no one data set can be viewed with too much confidence. It would be of significant benefit to this technique if the spectral resolution of generated spectra could be improved.

1.6 References

- [1] Ploutz-Snyder LL, Nyren S, Cooper TG, Potchen EJ, Meyer RA. Different effects of exercise and edema on T_2 relaxation in skeletal muscle. *Magn Reson Med.* 1997; 37: 676-682.
- [2] Van der Weerd L, Vergeldt FJ, Adrie de Jager P, Van As H. Evaluation of algorithms for analysis of NMR relaxation decay curves. *Magn Reson Imaging.* 2000; 18: 1151-1157.
- [3] Kleinberg RL. Pore size distributions, pore coupling, and transverse relaxation spectra of porous rocks. *Magn Reson Imaging.* 1994; 12: 271-274.
- [4] Mackay AL, Whittall KP, Adler J, Li D, Paty D, Graeb D. In-vivo visualization of myelin water in brain by magnetic resonance. *Magn Reson Med.* 1994; 31: 673-677.
- [5] Vasilescu V, Katona E, Simplaceanu V, Demco D. Water compartments in the myelinated nerve, III: pulsed NMR results. *Experientia.* 1978; 34: 1443-1444.
- [6] Does MD, Snyder RE. T_2 relaxation of peripheral nerve measured in vivo. *Magn Reson Imag.* 1995; 13: 575-580.
- [7] Hahn EL. Spin Echoes. *Physical Review.* 1950; 80: 580-594.
- [8] Carr HY, Purcell EM. Effects of diffusion on free precession in nuclear magnetic resonance experiments. *Physical Review.* 1954; 94: 630-638.
- [9] Meiboom S, Gill D. Modified spin-echo method for measuring nuclear relaxation times. *The Review of Scientific Instruments.* 1958; 29: 688-691.
- [10] Levitt MH. *Spin dynamics: basics of nuclear magnetic resonance.* Wiley, Chichester. 2002.

- [11] Abragam A. The principles of nuclear magnetism. Clarendon Press, Oxford. 1961.
- [12] Slichter CP. Principles of magnetic resonance (3rd Edition). Springer, Berlin. 1989.
- [13] Haacke EM, Brown RW, Thompson MR, Venkatesan R. Magnetic resonance imaging: physical principles and sequence design. Wiley, New York. 1999.
- [14] Sunderland Sir S. Nerve injuries and their repair: a critical appraisal. Edinburgh, New York : Churchill Livingstone, 1991.
- [15] Webb S, Munro CA, Midha R, Stanisiz GJ. Is multicomponent T_2 a good measure of myelin content in peripheral nerve? 2003; 49: 638-645
- [16] Davison AN, Peters A. Myelination. Chareles Thomas, Springfield, Illinois. 1970.
- [17] Morell P. Myelin. Plenum Press, New York, 1984.
- [18] Olsson Y. Microenvironment of the peripheral nervous system under normal and pathological conditions. Critical Reviews in Neurobiology. 1990; 5: 265-311.
- [19] Zeimmerman JR, Brittin WE. Nuclear magnetic resonance studies in multiple phase systems: lifetime of a water molecule in an adsorbing phase on silica gel. J Phys Chem. 1957; 61:1328.
- [20] Finkelstein A. Water movement through lipid bilayers, pores and plasma membranes: theory and reality. Wiley, New York. 1987.
- [21] Gardner DG, Gardner JC, Laush G, Meinke WW. Method for the analysis of multicomponent exponential decay curves. The Journal of Chemical Physics. 1959; 31: 978-986.

- [22] Lawson CL, Hanson RJ. Solving least squares problems. Enlewood Cliffs, NJ, Prentice Hall, Inc. 1974.
- [23] Whittall KP, MacKay AL. Quantitative interpretation of NMR relaxation data. J Magn Reson. 1989; 84:134-152.
- [24] Graham SJ, Stanchev PL, Bronskill MJ. Criteria for analysis of multicomponent tissue T2 relaxation data. Magn Reson Med. 1996; 35: 370-378.
- [25] Fenrich FRE, Beaulieu C, Allen PS. Relaxation times and microstructures. NMR in Biomedicine. 2001; 14: 133-139.

CHAPTER 2

REVIEW OF REPORTS AND INTERPRETATION OF MULTI-COMPONENT T_2 DECAY CURVES IN NERVE TISSUE

2.1 Introduction

Multi-exponential transverse relaxation studies on *in-vitro* peripheral nerve were first reported in the 1970s with the work of Vasilescu et al. [1]. This work was performed on frog sciatic nerve, and yielded three distinctly separate nerve relaxation rates (Table 2-1). For analysis, a graphical exponential stripping approach was taken, which, although less robust than more modern techniques now available, the method performed reasonably given the spectral distance between components (separate by more than a factor of 4), and the significant population sizes of all three (the smallest was found to be 21 percent). Other groups later repeated this experiment on frog sciatic nerve and obtained comparable three-component spectra [2-4] (Table 2-1). Multi-exponential T_2 studies were also performed on *in-vitro* peripheral nerve in other species, consistently revealing multiple components [5-7]. The form of T_2 spectra from a number of different species had been fairly reliably determined, but the obvious question regarding the physical meaning of the constituent components had inconsistent answers.

	Vasilescu et al.		Does et al.		Peled et al.		Wachowicz et al.	
	Mean	Std. Dev.	Mean	Std. Dev.	Mean	Std. Dev.	Mean	Std. Dev.
Size A (%)	29	-	16	2	17	4	19	2
Size B (%)	50	-	48	3	54	3	39	4
Size C (%)	21	-	36	3	29	4	42	4
T_2 A (ms)	17	6	16	2	18	1	17	1
T_2 B (ms)	70	14	78	6	68	16	83	4
T_2 C (ms)	310	21	317	18	281	34	232	15

Table 2-1. T_2 Spectral parameters of frog sciatic nerve from 4 different *in-vitro* studies.

2.2 Interpretation of short-lived component

The component which is least disputed in physical interpretation is the shortest-lived component, with an average reported value of approximately 17 ms in frog sciatic nerve. It has been well associated with water occupying space between the lipid bi-layers in myelin sheaths. This correlation was accomplished through studies involving nerve tissue from a variety of different species. Jolesz et. al. [8] found that the T_2 of rat sciatic nerve would increase during Wallerian degeneration induced by nerve section, a process which is characterized, in part, by a fragmentation and phagocytosis of the myelin sheath [9]. A later experiment by the same group compared the relaxation rates between myelinated and nonmyelinated garfish nerve [10]. From these studies it was suggested that water associated with myelin membranes may be responsible, and that the myelin sheaths provides an impediment to exchange between extracellular and axonal regions.

A more thorough comparison of myelinated and nonmyelinated garfish nerves was done by Fenrich [6] and Beaulieu [7]. In these transverse-relaxation studies, multi-component spectra were obtained from excised optic, trigeminal, and olfactory garfish nerves. Of these, the trigeminal and optic nerves are myelinated, but the olfactory nerve is not. When spectra from the three nerves were compared, a T_2 component between 30 and 50 ms was observed for both myelinated nerves, but was conspicuously absent in the olfactory. This study also used histological area estimates of the different compartments to verify the myelin water assignment to short-lived T_2 signal, as did Menon et al. with abdominal crayfish nerves [11].

Further evidence for this assignment was found in guinea pig, cat, and human CNS tissues [12-14], using a similar argument as above. In all these studies, a T_2 spectral component at roughly 10 ms was found when white matter was examined. In nonmyelinated grey matter, however, this component was not discovered. Stewart et al. [12] also triggered demyelination in some white matter samples through induced encephalomyelitis, and found that the short-lived 10 ms peak was absent in these

samples. Further, experiments in which white matter samples were homogenized were performed. This process mixes the contents of the nerve tissue together, while leaving the myelin layers intact [15]. When T_2 spectra of this homogenized tissue were obtained, the longer-lived portion of the spectrum was narrower than normal, indicating a breakdown of compartmentation of its component sources. However, the short-lived component remained in its 10-ms location, and did not narrow, suggesting that it corresponds to the myelin layers which were left intact.

Does and Snyder performed experiments in which T_2 spectra were obtained both *in vivo* and *in vitro* from frog sciatic nerve in a number of different timeframes after the onset of Wallerian degeneration [16]. The Wallerian degeneration was induced by a crush injury, administered with a nylon thread against a glass rod for thirty seconds. As degeneration progressed, histology revealed myelin breakdown after 1 and 2 weeks post-injury. Following this at 4 weeks, significant myelin loss is evident. Both the *in-vitro* and *in-vivo* data revealed a severe loss of short-lived signal after 28 days, lending support to the idea that this short-lived signal corresponds to myelin water.

2.3 Interpretation of Longer-Lived Spectral Components

Beginning with Vasilescu et al. [1] in their work with frog sciatic nerve, attempts were made to assign the relaxation components to physical microstructures. The populations they derived from T_2 spectroscopy were compared to compartment sizes that the same authors had determined through a D_2O mediated exchange experiment in a previous work [17]. The close correspondence between population sizes in the two methods led them to propose that the intermediate and long-lived components are associated with the axonal space and the extracellular space, respectively.

Fenrich [6] and Beaulieu [7] also used a population comparison to make an assignment of the spectral components to nerve microstructures. In this case, the spectral populations were compared with histological area estimates. After the areas were

measured, they were compensated for the different water densities that would be present in the different micro-anatomical regions. Using this method, a similar assignment to that of Vasilescu was determined. However, there are some inherent dangers in using spectral component sizes to determine assignments, particularly when the population sizes are similar. As was noted in the previous chapter, whether the measured component sizes can accurately represent associated spin populations will depend on the extent to which the slow exchange regime can be assumed. Even if this assumption is generally valid, a small deviation from this regime can result in a situation where spectral component sizes do not quantitatively represent the water population from their source microstructures, even though distinct multi-component relaxation is observed.

Menon et al. [11] used a different technique on crayfish abdominal nerve. Using NMR microscopy, a long TE image was acquired. Special attention was paid to the 4 giant axons present in this type of nerve, as they were big enough for multiple pixels to fit inside. In this way, the axonal space alone could be compared with the rest of the nerve. Their results showed darker regions inside the axons than in the rest of the nerve (which contained much smaller axons), leading them to believe that the axonal space has a shorter T_2 than the extracellular space (Figure 2-1).

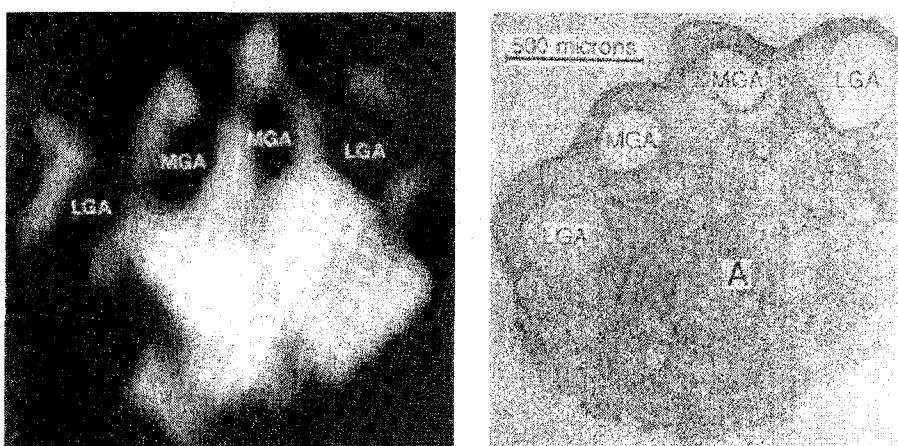


Figure 2-1. An NMR microscopy image (left) taken from Menon et al. [11] of a crayfish abdominal nerve, with a light histology micrograph on the right.

While this work is interesting, and does provide evidence for their assignment, care must be taken when applying interpretations from one species to nerve in general, as slight changes in proteins present could have significant effects of T_2 . This could be of particular concern when comparing nerve from distant species (i.e. invertebrate to vertebrate).

Peled et al. [3] found evidence for a reversal of the assignments listed above by measuring the diffusion characteristics of the individual T_2 components in frog sciatic. The ADC value of the long-lived component was found to vary considerably over diffusion times from 6 ms to 100 ms, whereas the ADC values for the intermediate component was found to be fairly constant over the same range. Based on the unrestricted nature of the diffusion seen in the intermediate-lived component led to the conclusion of its being associated with the extracellular space. The long-lived component, being seen as being a more restricted water component, was assigned to the axonal space.

Wachowicz et al. [18] found further evidence for this interpretation of the two longer-lived components seen in frog sciatic nerve by viewing the effects of Mn^{2+} diffusing into the tissue. In such experiments, the intermediate-lived component was seen to quite dramatically disappear long before that of the long or short-lived. Reasoning that the extracellular space would be the compartment first affected by the paramagnetic ions (since the myelin sheaths should provide a significant diffusion barrier for the Mn^{2+}) it was concluded that the intermediate and long-lived components corresponded to the extracellular and axonal space, respectively. This work will be presented in Chapter 4.

Work has also been done on rat peripheral nerve, both *in vitro* and *in vivo*. *In-vitro* work has been presented by Stanisiz et al. in a number of studies [5,19,20], and in all

cases, three T_2 components were observed. They postulate that both axonal water and endoneurium are represented by the intermediate component in rapid exchange, and that the long-lived component is originating from connective tissue in the perineurium and epineurium. However, studies with the epineurium removed [18] in frog nerve still show a well-defined long-lived component; one, moreover, that remains after the introduction of manganese. Thus, if the same exchange model can be applied to both rat and frog peripheral nerve, this assignment seems doubtful.

Does et al. reported a three-component T_2 spectrum of rat trigeminal nerve examined *in vivo* [21]. However, the relaxation constants quoted for the three components (12 ms, 33 ms, and 105 ms) were much smaller than in *in-vitro* measurements of rat sciatic nerve [5,22]. It is unclear why these values appear so low. Perhaps it simply reflected difficulties encountered performing this task in an imaging protocol. Alternatively, these differences could be a result of their performing the study *in vivo* at 37 degrees C as opposed to room temperature. On the other hand, in one report the T_2 spectrum of rat sciatic nerve was observed over changes in temperature and no statistically significant variation in parameters was seen [22].

To the best of this author's knowledge, there are no reports of *in-vitro* human peripheral nerve T_2 studies. However, imaging sequences have been performed on human peripheral nerve in which the nerve can be made to appear bright compared to the surrounding muscle [23-25]. This was done by using a fast spin echo sequence giving heavy T_2 weighting, suggestive that a longer-lived component may exist in human peripheral nerve. It is interesting that in the cross-sectional image of the sciatic nerve [24,25], it is the fascicles that appear bright, suggesting that epineurium is not a long-lived compartment.

2.4 References

- [1] Vasilescu V, Katona E, Simplaceanu V, Demco D. Water compartments in the myelinated nerve, III: pulsed NMR results. *Experientia*. 1978; 34: 1443-1444.
- [2] Does MD, Snyder RE. T₂ relaxation of peripheral nerve measured in vivo. *Magn Reson Imag*. 1995; 13: 575-580.
- [3] Peled S, Cory DG, Raymond SA, Kirschner DA, Jolesz FA. Water diffusion, T₂, and compartmentation in frog sciatic nerve. *Magn Reson Med*. 1999; 42: 911-918.
- [4] Wachowicz K, Snyder RE. A continuous flow perfusion system for the maintenance and NMR study of small tissue samples in vitro. *Magma*. Accepted for publication.
- [5] Stanisz GJ, Midha R, Munro CA, Henkelman RM. MR properties of rat sciatic nerve following trauma. *Magnetic Resonance in Medicine*. 2001; 45: 415-20.
- [6] Fenrich FR. MSc thesis: A simulation and experimental study of water proton relaxation in white matter model. University of Alberta; 1992.
- [7] Beaulieu C, Fenrich FR, Allen PS. Multicomponent water proton transverse relaxation and T₂-discriminated water diffusion in myelinated and nonmyelinated nerve. *Magn Reson Imag*. 1998; 16: 1201-1210.
- [8] Jolesz FA, Polak JF, Ruenzel PW, Adams DF. Wallerian degeneration demonstrated by magnetic resonance: spectroscopic measurements on peripheral nerve. *Radiology*. 1984; 152: 85-87.
- [9] Stoll G, Muller HW. Nerve injury, axonal degeneration and neural regeneration: basic insights. *Brain Pathol*. 1999; 9: 313-325.

- [10] Jolesz FA, Polak JF, Adams DF, Ruenzel PW. Myelinated and nonmyelinated nerves: comparison of proton MR properties. *Radiology*. 1987; 164: 89-91.
- [11] Menon RS, Rusinko MS, Allen PS. Proton relaxation studies of water compartmentalization in a model neurological system. *Magn Reson Med*. 1992; 28: 264-274.
- [12] Stewart WA, MacKay AL, Whittall KP, Moore GR, Paty DW. Spin-spin relaxation in experimental allergic encephalomyelitis. Analysis of CPMG data using a non-linear least squares method and linear inverse theory. *Magn Reson Med*. 1993; 29: 767-775.
- [13] Menon, RS, Rusinko, MS, Allen, PS. Multiexponential proton relaxation in model cellular systems. *Magn Reson Med*. 1991; 20:196-213.
- [14] Fischer HW, Rinck PA, Van Haverbeke Y, Muller RN. Nuclear relaxation of human brain gray and white matter: analysis of field dependence and implications for MRI. *Magn Reson Med*. 1990;16: 317-334.
- [15] Norton WT, Cammer W. in "Myelin," (P. Morell, Ed.), 2nd ed. p155, Plenum Press, New York, 1984.
- [16] Does MD, Snyder RE. Multi-exponential T2 relaxation in degenerating peripheral nerve. *Magn Reson Med*. 1996; 35: 207-213.
- [17] Vasilescu V, Margineanu DG, Katona E. Heavy water intake in tissues, II: H₂O-D₂O exchange in the myelinated nerve of the frog. *Experientia*. 1977; 33: 192-194.

- [18] Wachowicz K, Snyder RE. Assignment of the T₂ components of amphibian peripheral nerve to their microanatomical compartments. *Magn Reson Med.* 2002; 47: 239-245.
- [19] Webb S, Munro CA, Midha R, Stanisiz GJ. Is multicomponent T₂ a good measure of myelin content in peripheral nerve? 2003; 49: 638-645.
- [20] Stanisiz GJ, Webb S, Munro CA, Pun T, Midha R. MR properties of excised neural tissue following experimentally induced inflammation. [Journal Article] *Magnetic Resonance in Medicine.* 2004; 51: 473-479.
- [21] Does MD, Gore JC. Compartmental study of T(1) and T(2) in rat brain and trigeminal nerve in vivo. *Magnetic Resonance in Medicine.* 2002; 47: 274-83.
- [22] Wachowicz K, Snyder RE. Temperature dependence of the T₂ spectrum of peripheral nerve. In: *Proceedings of the 9th Annual Meeting of ISMRM, Glasgow, 2001*; p 1368.
- [23] Dailey AT, Tsuruda JS, Filler AG, Maravilla KR, Goodkin R, Kliot M. Magnetic resonance neurography of peripheral nerve degeneration and regeneration. *Lancet.* 1997; 350: 1221-2.
- [24] Filler AG, Howe FA, Hayes CE, Kliot M, Winn HR, Bell BA, Griffiths JR, Tsuruda JS. Magnetic resonance neurography. *Lancet.* 1993; 341: 659-61.
- [25] Maravilla KR, Bowen BC. Imaging of the peripheral nervous system: evaluation of peripheral neuropathy and plexopathy. *American Journal of Neuroradiology.* 1998; 19: 1011-1023.

CHAPTER 3

A CONTINUOUS FLOW PERFUSION SYSTEM FOR THE MAINTENANCE AND NMR STUDY OF SMALL TISSUE SAMPLES *IN VITRO*†

3.1 Introduction

Samples of excised tissue are frequently studied *in vitro* to better understand the nuclear magnetic resonance (NMR) characteristics and properties of the tissue. While it would be desirable that all investigations of tissue be performed *in vivo*, there are advantages to *in-vitro* work. Partial volume complications can be eliminated through the removal of extraneous tissues present during *in-vivo* studies. For many applications, once these tissues have been removed no further localization using gradient pulses is required, resulting in the elimination of eddy currents and shortened echo times. The ability to use smaller RF coils that tightly wrap around the sample chamber generally results in an improved signal-to-noise ratio (SNR). Moreover, it is possible to expose tissues maintained *in vitro* to drugs and agents not possible *in vivo* [1-5]. Thus, although excised tissues can never completely mimic tissues studied *in vivo*, the quality of data acquired can make *in-vitro* studies advantageous in many circumstances.

It would be poor practice to examine samples *in vitro* without taking care to provide them with an environment as close as possible to that *in vivo*. *In-vitro* imaging and non-proton studies have been performed in which excised tissue is maintained in a chamber while continuously perfused with a physiologically appropriate buffer solution [1-3,6-10]. In contrast, *in vitro*, non-imaging proton studies of relaxation and diffusion are generally performed in one of two conditions: with the tissue placed in an NMR tube and submersed in a static buffer solution, or with the tissue covered by a sealant to prevent dehydration [11-19]. In proton studies, movement of a buffer solution can distort the otherwise simpler data recorded from a static solution. However, if a static solution is

† A version of this chapter has been accepted for publication in MAGMA.

used, the environment surrounding the sample may be unable to meet the oxygen requirements of the tissue and suffer loss of viability over the course of an experiment. The use of a chamber to house the tissue sample through which a buffer solution is allowed to flow offers the advantage of a continuous supply of oxygen and nutrients to the tissue, and in particular, the ability to make rapid, on-the-fly changes in the composition of the solution.

This chapter describes a system that continuously supplies a fresh, oxygenated buffer solution to an excised tissue sample throughout the course of an NMR study. It will demonstrate how this system can be used as an investigative tool using the multi-component proton T_2 -relaxation spectrum of frog sciatic nerve as an example. Brief reports of preliminary studies have been published [20,21].

3.2 Methods

Chambers to house the tissue samples to be studied were constructed from two types of material: one was machined from polycarbonate and a second assembled from interlocking sections of polyethylene tubing. Both types of chamber were cylindrical, having inside dimensions of approximately 4-5 mm in diameter and 4 mm in height. Polyethylene tubing, having an internal diameter of approximately 0.8 mm, was pressure-fitted to the chambers through holes in either end to allow a physiologically appropriate buffer solution to flow through the chamber and about the tissue (Figure 3-1 a). These pressure fits were sufficient to maintain a leak-proof system without any sealing agents. The solution was forced through the chamber against gravity by a dual infusion pump (KD Scientific Inc., Model 210) located approximately 4 m from the magnet. The pump maintained a constant flow rate that was varied from between zero and 21 mL/h, and could continue uninterrupted for as long as the syringe reservoir (60 mL) lasted. A manual valve was placed in the inflow tubing approximately 15 cm before the chamber that could select one of two solutions to flow through the chamber. By adjusting the

valve it was possible to change the solution flowing through chamber within approximately 30 s. For comparison, during a different set of studies designed to assess the precision of measured parameters, samples of tissue were placed in a 5-mm NMR tube containing a buffer solution.

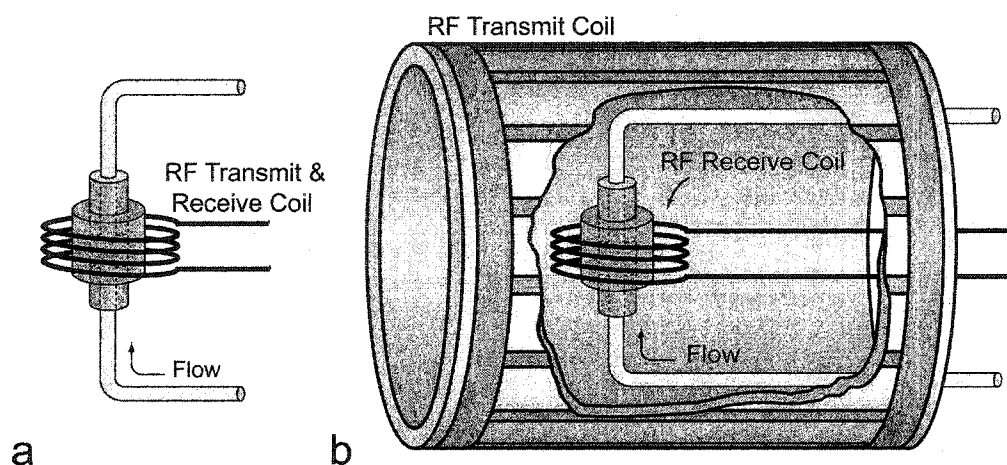


Figure 3-1. Schematic of a single-coil (a) and two-coil (b) system for excitation and reception of RF signals. In both systems a valve (not shown and outside of the RF Transmit Coil) is included in the inflow tubing that allows for the switching between different buffer solutions.

Frog sciatic nerve has been reported to have an oxygen consumption rate of $6\text{-}12 \times 10^{-6}$ mol/h/g (dry weight) at 20 °C [22-24], corresponding to an estimated consumption rate of $40\text{-}80 \times 10^{-9}$ mol/h for a typical nerve sample (estimated at just under 7 mg dry weight) used in our studies. Allowing a buffer solution whose oxygen content was initially at equilibrium with room air at atmospheric pressure ($pO_2 = 159$ mmHg) to deplete through consumption to 40 mmHg would deliver approximately 1.5×10^{-7} moles of oxygen per mL of solution. Thus, an adequate delivery of oxygen would require a flow rate of 0.27-0.54 mL/h. If one were to use such a flow rate, 30-60 minutes would be required for 99% replacement of the previous buffer when switching from one solution to another (assuming a well-stirred solution). We thus used flow rates of typically 5-8 mL/h that afforded sufficient oxygenation of the tissue, a reasonable switching time (2-3 min), and the avoidance of turbulence that might disturb the tissue with a higher flow rate. Rat

sciatic nerve at 35 °C has been reported [25] to have an oxygen consumption rate of 4-8 times that of frog nerve, thus requiring a flow rate of up to 4 mL/h. While extraction of all available oxygen from the flowing solution is doubtful, additional oxygen could be supplied in the case of mammalian tissue, if warranted, by saturating the buffer solution with pure oxygen at atmospheric pressure.

For all experiments performed, the perfusion chamber was centred in the bore of a 3-T, 80-cm-bore, whole-body NMR system controlled by a SMIS console. In an attempt to allow accurate data acquisition during continuous buffer flow, an RF system was developed in which a larger volume coil surrounded the entire chamber apparatus, and a smaller, four-loop, tight-fitting solenoid coil surrounded the chamber (Figure 3-1 b). During some studies, the smaller coil both transmitted and received RF signals (single-coil system), while during others, the larger volume coil transmitted and the smaller coil received the signals (two-coil system). The larger was a shielded birdcage coil having 16 elements and active decoupling circuitry [26] to turn it off during RF acquisition by the smaller coil (Figure 3-2). The birdcage coil was constructed with element lengths

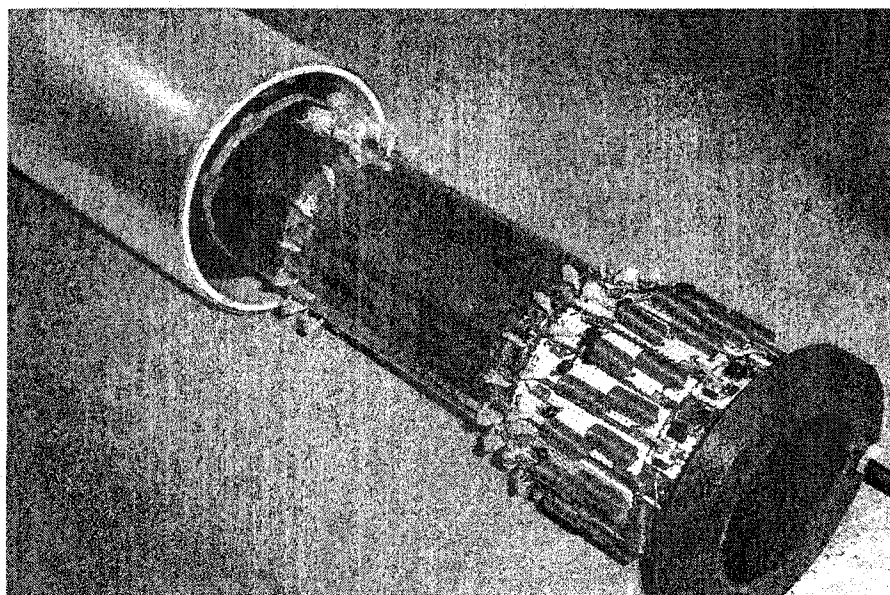


Figure 3-2. Actively-decoupled birdcage coil, designed for use in conjunction with a receive-only solenoid coil.

approximately 12.3 cm in length (between mid-points on the end rings), and 7.3 cm in diameter. The end rings of the coil were constructed with $\frac{1}{2}$ inch copper tape, and the “ladder” elements with $\frac{1}{4}$ inch copper tape. With these dimensions, the capacitors straddling the gaps in the end rings were set to 68 pF for a resonant frequency of 127.72 MHz. A schematic of this coil is displayed in Figure 3-3. The smaller coil was equipped with a crossed diode circuit to prevent interaction of the coils during transmission by the larger coil (Figure 3-4).

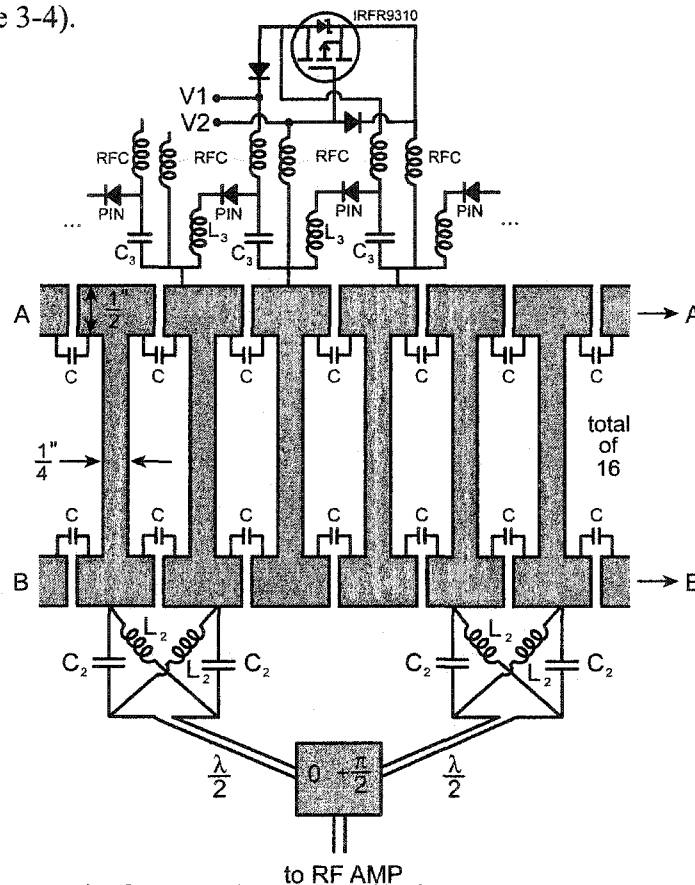


Figure 3-3. Schematic for the birdcage coil circuitry. The elements are displayed flat here for the purpose of clarity, rather than being arranged on a cylindrical surface. Below the elements are the baluns (consisting of C_2 and L_2) which serve to match the impedance of the coil to that of the input (50 Ohm). Inductors L_3 (in series with the PIN diodes and placed in parallel with the capacitors C and C_3) above the upper end ring serve as principal elements in the decoupling circuitry (The PIN diodes can be turned on or off by the voltage supply circuits above them.) The HEXFET circuits were designed in an attempt to provide supply voltages V_1 and V_2 without drawing too much current from the voltage source. Each of these FET circuits supply a pair of adjacent elements.

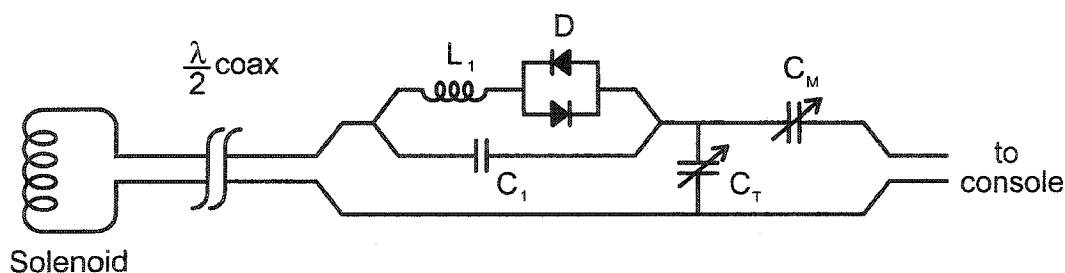


Figure 3-4. Circuit diagram for the receive-only solenoid coil. Capacitors C_T and C_M are used for manual tuning and matching, respectively. The loop containing L_1 , C_1 , and the crossed diode elements (D) is responsible for shutting the coil off during transmission. L_1 and C_1 are chosen to resonate at ω_0 , causing the loop to behave like an open circuit at that frequency. However, the crossed diodes will not allow current through the inductor L_1 after the birdcage coil has stopped transmitting, since the voltages across the diodes during reception will not be sufficient to drive them into forward bias (<0.7 V).

When it was desired to increase the temperature of the buffer solution flowing through the chamber above ambient, a section of the polyethylene tubing that supplied solution to the chamber was passed through a circulating water bath located just outside the chamber. Water to the bath was supplied through insulated 1-cm diameter polyethylene tubing that passed through a variable-temperature heating system located outside of the magnet. To monitor the chamber temperature, a fibre-optic temperature sensor (Model FOT-M, FISO Technologies) was placed in the tubing immediately beyond the outflow opening of the chamber.

The tissue used to evaluate the system was sciatic nerve taken from *Xenopus laevis*, the African clawed frog. Frog sciatic nerve was chosen, as it has a well-characterized multi-component T_2 spectrum [19,27] that can serve to assess performance of the system. Two to three centimetre lengths of nerve having a diameter of approximately 1 mm were removed from adult female specimens following euthanasia in an aqueous solution of 0.1% MS-222 (3-aminobenzoic acid ethyl ester) for 30 min. The nerve segments were carefully cleaned of any extraneous material while keeping the perineurial sheath intact.

One or two segments were placed in the perfusion chamber for testing. The standard buffer solution contained 112-mM NaCl, 3.0-mM KCl, 1.6-mM MgSO₄, 3.0-mM CaCl₂, 5.0-mM Glucose, and 3.0-mM HEPES, with a pH of 7.4 and oxygenated with room air. For some studies, the solution was made hypotonic through the reduction of the NaCl content. For other studies, a paramagnetic agent in the form of MnCl₂ or Gd-DTPA was added to the buffer solution, and in these cases the osmotic pressure of the solution was maintained at that of the standard through adjustment of the NaCl concentration. Except where noted, all studies were performed at room temperature. All animal procedures were approved by the Health Sciences Animal Policy and Welfare Committee of our institute.

Transverse-relaxation decay curves were acquired using a phase-cycled CPMG sequence that included 4, 8, or 16 averages. Four thousand echoes were acquired with an inter-echo time of 1.6 ms and π -pulses either 20 or 200 μ s in duration. 16 samples were acquired at the centre of each echo with a sampling rate of 100 kHz (Figure 3-5). The maximum of each echo was normally taken to be the mean value of these samples, since there was usually very little curvature over the short sampling region, assuming a good shim had been obtained. In rare cases where the shim was not sufficient to prevent a visible curvature in the echo over the sampling region, the 16 samples were fit with a 2nd order polynomial function, and the maximum point of the fitting curve was taken to represent the echo. A TR of 14 seconds was used to ensure complete relaxation between

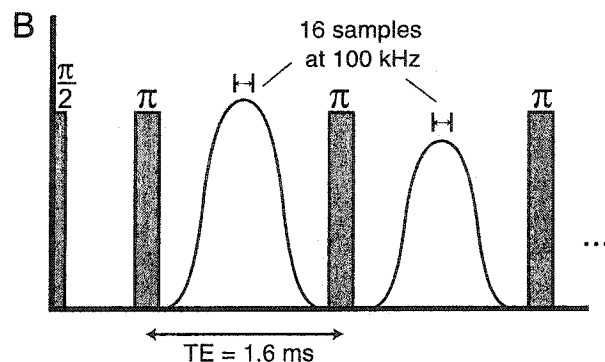


Figure 3-5. Echo sampling method. 16 samples were obtained during the span marked above each echo (100 kHz sampling rate, 10 μ s / sample).

excitations. One hundred and forty data points were sampled from each decay curve in a randomized, quasi-logarithmic pattern. The sampled points were fitted in a non-negative least squares (NNLS) sense [28] to a set of 105 decaying exponentials, logarithmically spaced between 0.5 ms and 3 s, and smoothed with a minimum energy constraint to produce an estimate of the T_2 -relaxation spectrum. In order to improve precision, this procedure was repeated 20 times using newly randomized points. The T_2 spectrum used for subsequent evaluation was taken as the average of those obtained from the 20 sets of data points.

Occasionally, when the number of components in the T_2 spectrum was constant throughout an entire experiment (as determined by the NNLS algorithm), another analysis routine was implemented. In this routine, each of the components was modeled by a Gaussian line in logarithmic decay space. Three parameters defined the position and shape of each spectral line: width at half maximum, magnitude, and spectral location [29]. The routine begins by taking seed values for all these parameters (supplied by the NNLS results) and then optimizing them to minimize the χ^2 parameter of the fit. For some data sets this routine was found to improve the precision of fitted spectral components.

3.3 Results

3.3.1 Perfusion Chamber Material

Transverse-relaxation spectra were obtained for the two types of chamber (polycarbonate and polyethylene) while perfused with water at flow rates of 5-8 mL/h. The single-coil system was used for this experiment, and no tissue was present. Both chambers yielded the expected T_2 spectral line at approximately 1,600 ms resulting from the water protons. However, the polycarbonate chamber produced artifactual T_2 lines (over 10 percent of the total signal), particularly in the region between 10 and 500 ms

where T_2 components of soft tissue are most often reported. The relatively large amount of unwanted signal in this region made it necessary to rule out the use of machined polycarbonate chambers. The polyethylene chamber had significantly fewer artifactual lines in this region, and was therefore used in all subsequent studies. There was, however, one large spectral line originating from the use of the polyethylene at approximately 1 ms, but as its T_2 relaxation time was considerably lower than that of the tissue components, it did not prove to be a significant problem.

3.3.2 Comparison of Spectral-Parameter Precision between Chamber and NMR Tube

Transverse-relaxation spectra were obtained from nerve contained in either an NMR tube or the perfusion chamber using the single-coil system. (Buffer flow was always maintained in the perfusion chamber unless otherwise stated.) Both yielded three-component nerve spectra (Figure 3-6) similar to spectra reported in the literature [19,27], thus demonstrating a comparative performance of the perfusion chamber to an NMR tube, the latter considered the gold standard for *in-vitro* analysis.

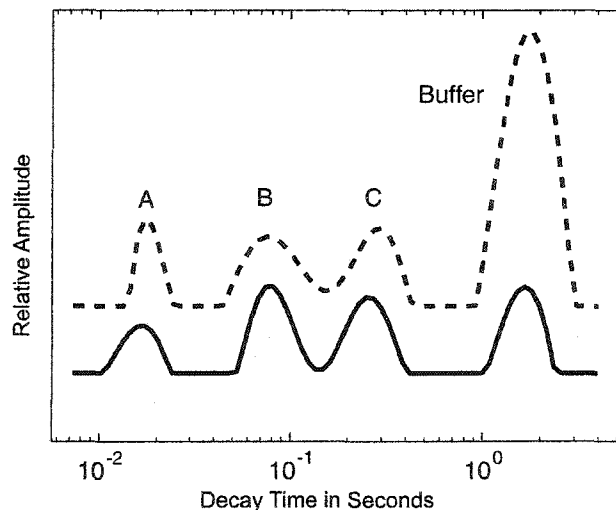


Figure 3-6. Comparison of typical experimental frog sciatic nerve T_2 spectra from NMR tube (solid) and perfusion chamber (dashed). The first three components shown in both spectra (labeled A, B, and C) result from the nerve tissue, and the last originates from the buffer solution.

In studies in which the buffer solution is altered from one composition to another, the tissue is generally removed from an NMR tube, placed in the altered solution for a period of time, and then re-introduced into the tube together with the altered solution. This presents the possibility of variation in results due to the repositioning of the tissue, and thus could limit sensitivity to changes in buffer composition. The perfusion chamber could remove this variation through seamless transitions from one buffer composition to another. A study consisting of four experiments was thus performed to determine the level of precision in T_2 spectral component parameters due to repositioning as well as inter-preparation variation. In the first experiment, a freshly excised piece of nerve was placed in the two-coil perfusion chamber, and 20 T_2 spectra were acquired. In the second experiment, the same procedure was repeated using a conventional NMR tube and a single transmit/receive RF coil. (A different nerve preparation was used in the second experiment.) In the third experiment, 8 T_2 spectra were acquired from the same nerve preparation as in Experiment 2, except that in this case, the nerve was repositioned in the NMR tube before each acquisition. Finally, in a fourth experiment, 7 T_2 spectra were acquired from 7 different nerve preparations and placed in NMR tubes in an attempt to assess inter-preparation variation. The statistical variances of the resulting T_2 spectral parameters were calculated and are presented in Table 3-1. To summarize, multiple spectral measures using either the chamber or NMR tube (columns 1 and 2) yielded similar standard deviations for corresponding parameters; however, repositioning (column 3) increased the standard deviations by a factor of approximately 5. Inter-preparation standard deviations (column 4) were fairly close to those of the repositioning experiment. These results serve to emphasize the detrimental effects that repositioning a tissue sample can have on the ability to observe subtle tissue changes over time, and underscore the advantages of introducing environmental changes via the perfusion system.

	Chamber (N=20)		NMR tube (N=20)		Repositioning (N=8)		Inter-prep (N=7)	
	Mean	Std. Dev.	Mean	Std. Dev.	Mean	Std. Dev.	Mean	Std. Dev.
Size A (%)	22.16	0.33	22.69	0.42	20.58	0.76	19.54	1.95
Size B (%)	41.63	0.94	39.69	0.63	38.82	3.26	38.71	4.06
Size C (%)	36.21	0.55	37.62	0.86	40.60	4.66	41.75	3.98
T ₂ A (ms)	18.09	0.27	17.07	0.54	17.54	1.56	16.97	1.13
T ₂ B (ms)	82.33	0.58	96.17	0.77	97.60	8.55	82.87	3.96
T ₂ C (ms)	268.68	3.01	301.25	4.10	287.75	24.71	231.61	15.46

Table 3-1. Means and standard deviations for transverse relaxation component parameters in frog sciatic nerve, as evaluated by an NNLS (non-negative least squares) algorithm. **Note:** In the first of the four columns, one nerve preparation was viewed 20 times using the two-coil perfusion chamber. In the second column, a different nerve preparation was viewed 20 times in a conventional NMR tube. The third column utilized the same nerve preparation as in Column 2, but this time the nerve was repositioned in the NMR tube between each spectra acquired. In the last column, 7 spectra were acquired using 7 different nerve preparations placed in NMR tubes.

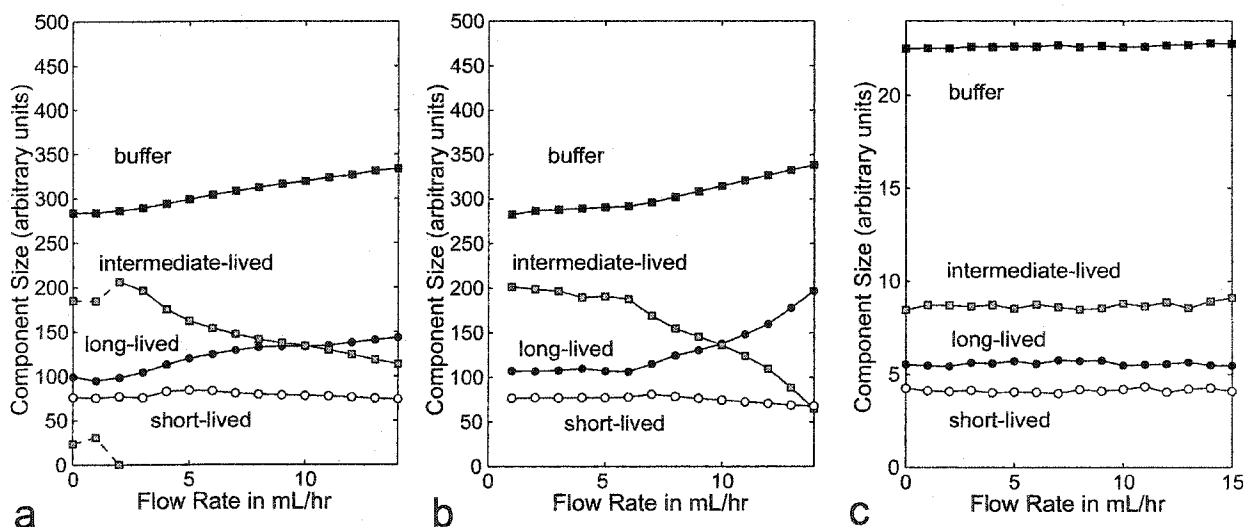


Figure 3-7. Variance of nerve and buffer component sizes with changes in flow rate. (a) Experimental results from a nerve sample in the single-coil system. (b) Results generated when theoretical flow loss curves for 1 to 14 mL/h are subtracted from the zero flow data in (a). (c) Experimental results from a nerve sample (different from (a)) in the two-coil system. Note the lack of variation of the components with flow rate.

3.3.3 Variation with Flow Rate

Measurements were made to assess the stability of results with change in flow rate. Freshly excised nerve was placed in the perfusion chamber using the single-coil system, and T_2 spectra were recorded for 15 different flow rates varying from 0 to 14 mL/h. All spectra contained three components attributable to the nerve plus one resulting from the buffer solution. As a function of flow rate, only minor variation was observed in component T_2 -relaxation times (data not shown); however, relative component sizes did exhibit variation (Figure 3-7 a). To account for this variation, it was theorized that the decay curve of flowing buffer solution encountered differing levels of distortion, dependent on the flow rate. Two different factors could account for this distortion: signal loss from solution flowing outside the sensitive range of the RF coil, and errant signal from the solution within the inflow and outflow tubes that received imperfect excitation and refocussing pulses. These differences in the buffer decay curve could then affect the nerve and buffer component sizes as seen through the analysis routine.

A computer simulation was performed to test the above theory in order to determine whether a newly designed coil system was justified. In the simulation it was assumed that the primary source of variation with flow rate resulted from signal losses derived from excited buffer flowing beyond the range of sensitivity of the RF coil during the acquisition period (causing a loss since the buffer flowing in had not received the initial excitation pulse). The loss of excited buffer was taken to increase linearly with time, generating a signal loss having the form of a linearly increasing plot modulated by an exponentially decaying envelope associated with the transverse signal decay of the buffer solution. The simulation assumed immediate transitions in coil sensitivity, and thus neglected any period of transition, both on the inflow and outflow sides of the chamber. The predicted signal losses were calculated with the following equation:

$$\text{SignalLoss}(n) = S_V \cdot R_F \cdot nTE \cdot e^{-nTE/T_{2\text{buffer}}}, \quad [3.1]$$

where n is the echo number, S_V is the estimated signal strength per unit volume, and R_F is the flow rate. S_V had to be estimated because the exact volume of buffer in the chamber was unknown. A rough calculation based on the signal proportions of nerve to buffer and the inner dimensions of the chamber yielded an estimated volume of 0.03 mL. S_V was then taken as the signal strength of the buffer divided by this volume. The predicted signal loss versus acquisition (echo) time for a range of flow rates is shown in Figure 3-8 a (dashed), where it is compared to a measured loss at the same rates (solid). The latter were obtained by measuring the signal difference between nerve experiments with flowing and static buffer solutions, and normalizing to the total amount of buffer signal present. Qualitative comparison of these two sets of curves suggests that the outflow of solution excited while in the chamber may account for a substantial portion of signal loss.

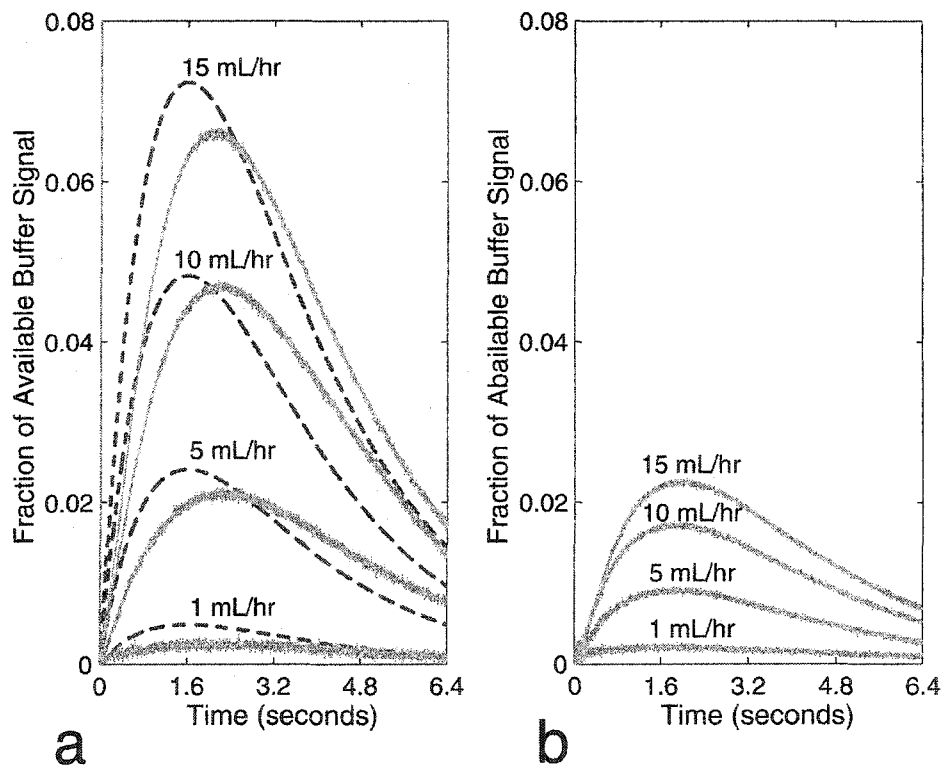


Figure 3-8. (a) Experimentally determined flow loss curves for the one-coil system (solid) as well as theoretical loss curves (dashed) based on the flow model. (b) Experimentally determined flow loss curves for the two-coil system.

To determine whether the predicted signal loss could account for the variation of component size with flow rate (as seen in Figure 3-7 a), loss prediction curves were generated for flow rates between 1 and 14 mL/h, such as those displayed with dashed lines in Figure 3-8 a. These loss prediction curves were then each subtracted from an experimental decay curve, specifically the decay curve that was the source data for the zero flow results in Figure 3-7 a. The resulting simulated decay curves for each flow rate were then converted to T_2 spectra with the NNLS algorithm. The magnitudes of the components from the resulting spectra are shown in Figure 3-7 b and show qualitative agreement with the trends experimentally determined in Figure 3-7 a.

3.3.4 Two-Coil System

In order to allow for more precise quantitative studies, a new experimental setup had to be devised to reduce the dependency of measured parameters on flow rate. Thus, as a means to avoid flow-related signal losses, it was decided that the RF transmission and reception responsibilities should be assumed by two separate coils. In this two-coil system, a larger birdcage coil would transmit RF energy over a region of the apparatus that included the chamber as well as the inflow and outflow perfusate tubing. The smaller single coil that circumscribes the perfusion chamber would then act as a dedicated receive-only coil (Figure 3-1 b). As a result of the larger coil, all buffer solution from which signal is acquired (whether in the chamber or the tubing) would receive correct excitation and inversion pulses.

To test for signal loss as a function of acquisition time, decay curves were acquired from buffer solution and frog sciatic nerve over a number of different flow rates, varying between 0 and 15 mL/h (using the two-coil system). All the flow data sets were then subtracted from the static buffer data set to measure experimental loss curves due to flow. A sampling of loss curves measured over a range of flow rates is shown in Figure 3-8 b. As can be seen, the results show a marked reduction in signal losses when the two-coil system is used. (The experiments for both Figure 3-8 a and b were performed on the

same sample consecutively and produced raw data of roughly equal magnitude. In this way, the size of the loss curves can be compared directly.) To determine the effect of the two-coil system on variation in component size with flow rate, T_2 spectra were calculated from the decay curves obtained above. The resulting component sizes are displayed in Figure 3-7 c. Comparing these to results using only the single-coil system (Figure 3-7 a) shows a marked improvement in stability.

3.3.5 Temperature Control System

Since *in-vitro* examination of tissue could involve mammalian tissues, it is desirable to be able to investigate their NMR characteristics at mammalian temperatures. Using the temperature system described in the Methods section, temperatures of up to 40 °C in the chamber can be achieved and maintained with a variation of $< \pm 1$ °C. The temperature within the chamber stabilized within approximately 10 minutes following selection of a new bath temperature.

3.3.6 Illustrative Studies

Two studies were performed to illustrate the use of the perfusion system. In the first, using the two-coil system, an experiment was performed in three stages. First, data was acquired from a nerve sample perfused with an isotonic buffer solution for ~80 minutes. In the next stage, the perfusate was switched to a hypotonic solution and again observed for 80 minutes. In the third and final stage, the perfusate was switched back to the isotonic solution and data was again taken for an 80-minute interval (Figure 3-9). Switching to the hypotonic solution showed a distinct increase in size of the long-lived T_2 component of the nerve, followed by a slow return towards its initial size upon re-introduction of the isotonic solution.

In a second study, a paramagnetic agent was introduced into the perfusate following acquisition of data from a nerve sample in normal buffer solution (Figure 3-10). As is

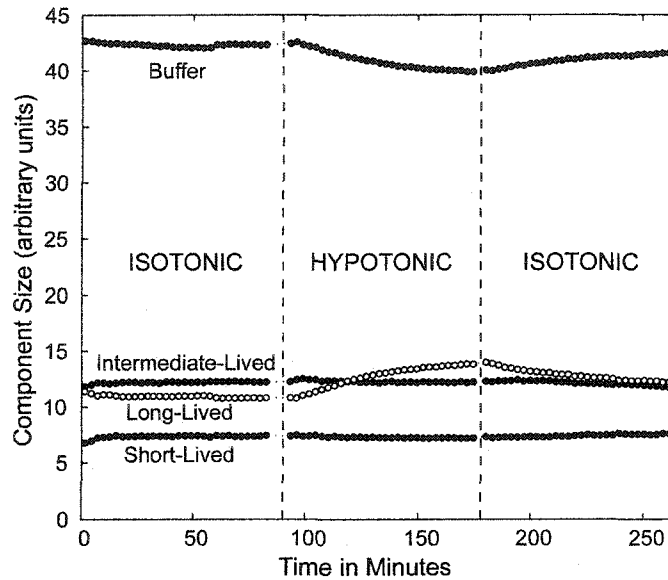


Figure 3-9. Illustrative study with frog sciatic nerve. The component sizes of calculated T_2 spectra are plotted as a function of time, during which the buffer composition was changed from isotonic to hypotonic (by reduction of NaCl content to $\frac{1}{4}$ that of normal), and then back to isotonic.

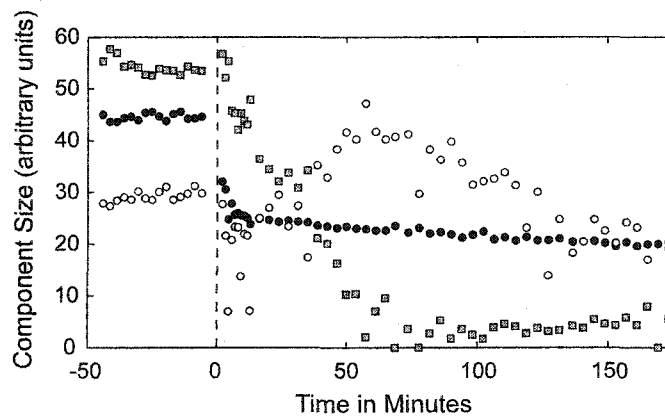


Figure 3-10. A plot of the sizes obtained from a nerve sample before and after switching the perfusate from a normal solution to one containing 30-mM Gd-DTPA at time = 0. Open circles, grey squares, and solid circles represent the sizes of the short-lived, intermediate-lived, and long-lived nerve components, respectively. The rise and fall of the short-lived component (open circles) has been demonstrated to be an artifact of the changes in the intermediate-lived component (grey squares) [5].

clear, within a period of approximately 40 minutes the majority of the signal from the intermediate-lived component had disappeared.

Both these studies were used to reveal information about the physical structure of nerve tissue. This information would have been more difficult to obtain with a traditional NMR tube approach. Using an NMR tube would have required the removal of the sample each time the bathing solution was altered. This procedure would have introduced extra variation in measured parameters due to sample repositioning, as well as incorporating time delays after every change before data acquisition could be resumed.

3.4 Discussion

The perfusion chamber was shown to generate results with comparable values and standard deviations to those of a simple NMR tube (Table 3-1, columns 1 and 2). Moreover, an advantage to the perfusion chamber was demonstrated in that significant uncertainties resulting from repositioning of the tissue (Table 3-1, column 3) could be avoided by maintaining the tissue in the flow chamber, and administering altered solutions via the input tubing. For example, standard deviations of results from repositioned nerve were approximately 5 times as great as those of undisturbed samples. One would therefore have to repeat the experiment on the order of 25 times in order to duplicate the same level of precision.

The two-coil system data demonstrates a much greater stability than that seen in using the single coil (Figures 3-7 a and c). This is of obvious advantage when acquiring data for quantitative purposes, but could also be of value in studies where one is interested in small relative changes in tissue characteristics. Suppose, for example, the buffer solution was switched from one type to another to investigate the response of the tissue, and the T_2 of the second buffer solution was different from the first. Since the single-coil set-up is likely vulnerable to flow artefacts which are T_2 dependent (Equation 3.1), even a slight variation in buffer T_2 may well cause a small relative change to appear

in the solved parameters of the tissue. This apparent relative change could easily be interpreted as real if the expected tissue response could occur over a rapid timeframe.

The greater stability with respect to flow as described above is due to the separation of the transmit/receive tasks between two decoupled coils, as well as their relative geometries. Provided that the transmit coil is indeed able, as it was designed, to transmit uniform pulses over the entire sensitive range of the receive coil and a significant portion of the inflow tubing next to the chamber, the two-coil system should theoretically be immune to most flow effects, regardless of flow rate, flow distribution throughout the perfusion system (including turbulence), and the sensitivity profile of the receiver. The only flow effect uncorrected by this apparatus would be irreversible losses encountered by the buffer as it travels through inhomogeneities in the local B_0 field. The ability of this coil configuration to overcome the aforementioned flow effects is demonstrated in Equations 3.2-3.4. Here, any signal within range of the receive coil is integrated over all volume, where S_v is a spatially dependent function representing signal strength per unit volume.

$$\text{Receive Signal (t)} = \int_V S_v(\vec{r}) \cdot e^{-t/T_2 \text{buffer}} \cdot dv \quad [3.2]$$

$$= e^{-t/T_2 \text{buffer}} \int_V S_v(\vec{r}) \cdot dv \quad [3.3]$$

$$= C_S \cdot e^{-t/T_2 \text{buffer}} \quad [3.4]$$

Even though the buffer may be flowing from one region of the sensitivity gradient to another, the decay rate in each fixed differential volume will be spatially constant at $e^{-\left(\frac{t}{T_2 \text{buffer}}\right)}$. (Each portion of the buffer occupying space within range of the receive coil during the experiment will (assuming homogeneous B_0) be receiving a near perfect pulse train.) Therefore, the time dependent term can be pulled outside the integral, reducing

the integral to a constant (C_S), and leaving a monexponential term that will apply for any and all flow profiles.

The fact that the measured loss curves for the two-coil system (Figure 3-7 c) are not negligible serve to demonstrate that although a significant portion of the flow effects have been removed by this coil configuration, some still remain. As was stated above, the only flow effect that the two-coil setup should theoretically be unable to remedy is a reduction in the buffer T_2 due to flow through inhomogeneous B_0 , and the resulting irreversible relaxation. A decrease in buffer T_2 with flow could indeed result in this type of loss curve. Figure 3-11 illustrates a simulated loss curve caused by a reduction of the T_2 from 1.6 s to 1.5 s (the measured drop in buffer T_2 between 0 and 15 mL/hr in Fig 3-3 c), compared against the experimental two-coil loss curve at 15 mL/hr.

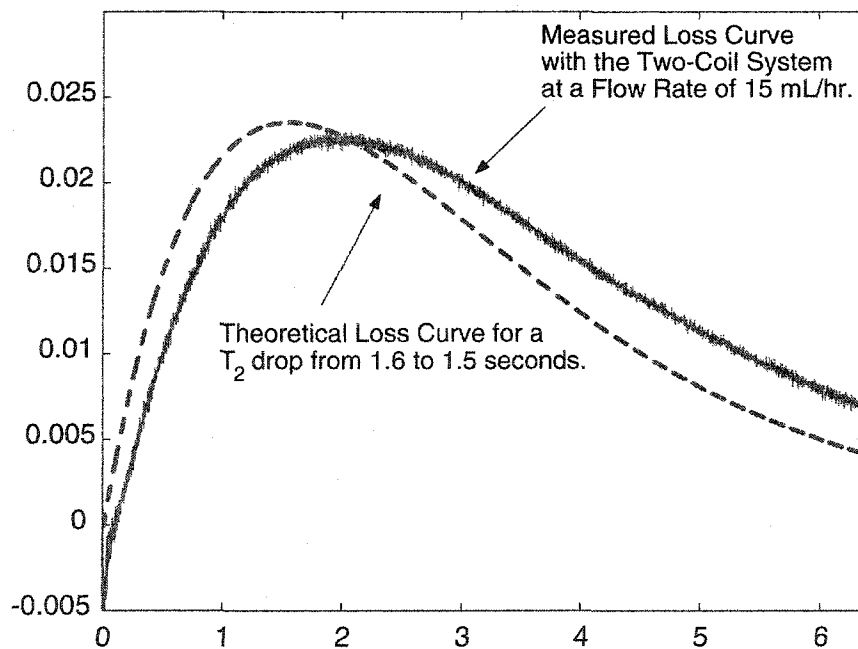


Figure 3-11. Comparison of the theoretical fractional loss curve for a drop in T_2 from 1.6 to 1.5 seconds (dashed), with the experimentally determined loss curve at 15 mL/hr measured with the two-coil setup (solid).

This figure reveals how little the T_2 has to decline to account for loss curves on the same order as those seen in Figure 3-7 c. However, unlike the loss curves generated by the theory in Equation 3.1, these losses can be fully defined by monoexponential decay terms in the immediate vicinity of the initial buffer T_2 , and would likely not interfere with the tissue spectral components, as was seen in Figure 3-7 a.

3.5 Conclusions

Experimental data from use of the perfusion chamber were found to equal the quality of those obtained using standard NMR tubes. This novel perfusion chamber is able to offer several advantages, however. Fresh buffer solution can be supplied to a tissue sample at flow rates high enough to provide for its oxygen requirements. Agents can also be introduced into the chamber in a longitudinal study without the need to reposition the sample. This is of significant benefit, as repositioning the sample was found to cause a 5-fold reduction in the precision of measured parameters. The two-coil system was successful in minimizing effects of the flowing buffer on the results, and allowed quantitative measurement of NMR parameters while the buffer composition was changed on the fly. The system is also capable of controlling the temperature of the sample between 25-40 °C.

3.6 References

- [1] O'Shea JM, Williams SR, Van Bruggen N, Gardner-Medwin AR. Apparent diffusion coefficient and MR relaxation during osmotic manipulation in isolated turtle cerebellum. *Magn. Reson. Med.* 2000; 44: 427-432.
- [2] Beauvieux MC, Tissier P, Couzigou P, Gin H, Canioni P, Gallis JL. Ethanol perfusion increases the yield of oxidative phosphorylation in isolated liver of fed rats. *Biochim. et Biophys. Acta.* 2002; 1570: 135-140.
- [3] Blackband SJ, Bui JD, Buckley DL, Zelles T, Plant HD, Inglis BA, Phillips MI. MR microscopy of perfused brain slices. *Magn. Reson. Med.* 1997; 38: 1012-1015.
- [4] Buckley DL, Bui JD, Phillips MI, Zelles T, Inglis BA, Plant HD, Blankband SJ. The effect of ouabain on water diffusion in the rat hippocampal slice measured by high resolution NMR imaging. *Magn. Reson. Med.* 1997; 41: 137-142.
- [5] Wachowicz K, Snyder RE. Assignment of the T₂ components of amphibian peripheral nerve to their microanatomical compartments. *Magn. Reson. Med.* 2002; 47: 239-245.
- [6] Freyer JP, Fink NH, Schor PL, Coulter JR, Neeman M, Sillerud IO. A system for viably maintaining a stirred suspension of multicellular spheroids during NMR spectroscopy. *NMR in Biomed.* 1990; 3: 195-205.
- [7] Tian G, Xiang B, Dai G, Sun J, Lindsay WG, Deslauriers R. Simultaneous antegrade/retrograde cardioplegia protects myocardium distal to a coronary occlusions: a study in isolated pig hearts. *Magn. Reson. Med.* 2001; 46: 773-780.

- [8] Burgess SC, Babcock EE, Jeffrey FM, Sherry AD, Malloy CR. NMR indirect detection of glutamate to measure citric acid cycle flux in the isolated perfused mouse heart. *FEBS Letters*. 2001; 505: 163-167.
- [9] Espanol MT, Litt L, Chang LH, James TL, Weinstein PR, Chan PH. Adult rat brain-slice preparation for nuclear magnetic resonance spectroscopy. *Anesthesiology*. 1996; 84: 201-210.
- [10] Van Emous JG, van Echteld CJA. Changes of intracellular sodium T₂ relaxation times during ischemia and reperfusion in isolated rat hearts. *Magn. Reson. Med*. 1998; 40: 679-683.
- [11] Bertram HC, Rasmussen M, Busk H, Oksbjerg N, Karlsson AH, Andersen HJ. Changes in porcine muscle water characterized during growth - an in vitro low-field NMR relaxation study. *J. Magn. Reson*. 2002; 157: 267-276.
- [12] Does MD, Beaulieu C, Allen PS, Snyder RE. Multicomponent T₁ relaxation and magnetization transfer in peripheral nerve. *Magn. Reson. Imaging*. 1998; 16: 1033-1041.
- [13] English AE, Joy MLG, Henkelman RM. Pulsed NMR relaxometry of striated muscle fibers. *Magn Reson Med*. 1991; 21: 264-281.
- [14] Cutillo AG, Chan PH, Ailion DC, Watanabe S, Albertine KH, Durney CH, Hansen CB, Laicher G, Scheel RF, Morris AH. Effects of endotoxin lung injury on NMR T₂ relaxation. *Magn Reson Med*. 1998. 39: 190-197.
- [15] Henkelman RM, Stanisz GJ, Kim JK, Bronskill MJ. Anisotropy of NMR properties of tissue. *Magn Reson Med*. 1994; 32: 592-601.

- [16] Graham SJ, Ness S, Hamilton BS, Bronskill MJ. Magnetic resonance properties of ex vivo breast tissue at 1.5 T. *Magn Reson Med.* 1997; 38: 669-677.
- [17] Nightingale T, MacKay A, Pearce RH, Whittall KP, Flak B. A model of unloaded human intervertebral disc based on NMR relaxation. *Magn Reson Med.* 2000; 43: 34-44.
- [18] Beaulieu C, Fenrich FRE, Allen PS. Multicomponent water proton transverse relaxation and T₂ discriminated water diffusion in myelinated and non-myelinated nerve. *Magn. Reson. Imag.* 1998; 16: 1201-1210.
- [19] Peled S, Cory DG, Raymond SA, Kirchner DA, Jolez FA. Water diffusion, T₂, and compartmentation in frog sciatic nerve. *Magn Reson Med.* 1999; 42: 911-918.
- [20] Wachowicz K, Bonilla I, Snyder RE. The use of a decoupled coil system and relaxation agents to improve perfusion chamber data. In: *Proceedings of the 11th Annual Meeting of ISMRM, Toronto, 2003*; p 2427.
- [21] Wachowicz K, Snyder RE. A perfusion chamber suitable for the measurement of transverse relaxation spectra of tissue maintained in vitro. In: *Proceedings of the 8th Annual Meeting of ISMRM, Denver, 2000*; p 1987.
- [22] Connelly CM. Recovery processes and metabolism of nerve. *Rev. Mod. Phys.* 1959; 31: 475-484.
- [23] Hurlbut WP. Effects of azide and chloretone on the sodium and potassium contents and the respiration of frog sciatic nerves. *J. Gen. Physiol.* 1958; 41: 959-988.
- [24] Brink F Jr. Components of O₂-uptake by excised frog nerve dependent upon external supplied sodium ions. *Proc. Nat. Acad. Sci. USA.* 1975; 72: 3988-3992.

- [25] Low PA, Schmelzer JD, Ward KK. The effect of age on energy metabolism and resistance to ischaemic conduction failure in rat peripheral nerve. *J. Physiol.* (London) 1986; 374: 263-271.
- [26] Barberi EA, Gati JS, Rutt BK, Menon RS. A transmit-only/receive-only (TORO) RF system for high-field MRI/MRS applications. *Magn Reson Med.* 2000; 43: 284-289.
- [27] Does MD, Snyder RE. T₂ relaxation of peripheral nerve measured in vivo. *Magn. Reson. Imag.* 1995; 13: 575-580.
- [28] Whittall KP, MacKay AL. Quantitative interpretation of NMR relaxation data. *J. Magn. Reson.* 1989; 84: 134-152.
- [29] Stanisz GJ, Henkelman RM. Diffusional anisotropy of T₂ components in bovine optic nerve. *Magn. Reson. Imag.* 1998; 40: 405-410.

CHAPTER 4

ASSIGNMENT OF THE T_2 COMPONENTS OF AMPHIBIAN PERIPHERAL NERVE TO THEIR MICROANATOMICAL COMPARTMENTS†

4.1 Introduction

Certain quantities measurable by proton NMR, such as relaxation and diffusion, have been observed to exhibit non-exponential decay curves in a number of tissues [1-12]. Often, these curves may be approximated as a sum of exponentially decaying components. Multiple components may result from the compartmentalization of tissue water at the microanatomical level, for example, into intra- and extracellular compartments, provided the exchange rate of the water between the compartments is slow on the time scale of the quantity measured. The components may contain diagnostic information since tissue pathology often results in changes in the relative size of two or more specific tissue compartments. Examples of such pathologies are vasogenic versus cytotoxic edema, and axonal loss in neural tissue. For an observed change in the size of a component to be of increased diagnostic value, it is important that the relationship is known between the component and the tissue compartment from which it arises.

Neural tissue that contains myelinated fibres has been reported to exhibit multi-exponential proton T_2 decay curves. Transverse-relaxation spectra of peripheral nerves generally contain three well-resolved peaks, while two-component tissues such as white matter often do not exhibit the longest-lived peak. Evidence suggests that in all such tissues the shortest-lived peak results from myelin water [7,9,13-16]. In the case of two-component tissues, it has been proposed that the axonal and endoneurium waters exhibit similar, unresolvable T_2 peaks [8].

† A version of this chapter has been published in *Magnetic Resonance in Medicine*. (2002 Feb; 47(2): 239-45)

While there is evidence to support the assignment of the shortest-lived T_2 component to myelin water, the relationship between the two longest-lived components and their associated compartments in three-component peripheral systems is not as clear. Comparisons between component and compartment sizes have been used to suggest that the intermediate-lived component results from axonal water, and the longest-lived from endoneurium water [10,17,18]. However, Peled et al. [11] have recently proposed this assignment be reversed, with the axonal water giving rise to the longest-lived component. Their proposal was based upon diffusion characteristics of water in amphibian nerve.

In this study, we investigated the relationship between the two longest-lived T_2 components of amphibian nerve and the microanatomical water compartments present in the nerve tissue. The study utilized *in-vitro* experiments where the molecular composition of the nerve water compartments was altered. Proton T_2 decay curves were recorded from samples of nerve maintained first in a physiological saline solution, followed by the addition of a paramagnetic agent to the solution or with the replacement of H_2O by D_2O . Upon altering the solution it was expected that the endoneurium and its associated spectral T_2 component would be affected prior to the other compartments and components due to its closer proximity to the outside environment.

4.2 Methods

All samples used in this study were sciatic nerves taken from female adult *Xenopus laevis*, the African clawed frog, which had been housed in an aquatic environment at room temperature. In total, nine nerve samples were studied. Following euthanasia in MS-222 (3-aminobenzoic acid ethyl ester), 2-3 cm segments of nerve were removed from the frog and immediately placed in an oxygenated physiological saline solution (see below for composition). In some studies, the epineurium surrounding the nerve was removed. Within 1-2 hours following removal, the samples were transferred to a perfusion chamber where they remained undisturbed for the remainder of the experiment. The chamber had inside dimensions of approximately 5 mm in diameter by 4 mm in

height and was perfused at a constant rate of 6-8 ml/hr. The use of a perfusion chamber [19], in contrast with placing the sample in a NMR tube, allowed the composition of the bathing solution (perfusate) to be changed more rapidly and without disturbance to the sample. The chamber was then placed inside a small solenoid RF coil[†] and positioned at the isocentre of a 3-T, 80-cm bore system controlled by a SMIS console. The temperature of the chamber and its contents were maintained at approximately 21 °C.

The primary focus of this study involved introducing a relaxation agent into the perfusate and observing how the transverse relaxation of the nerve was affected over time. This was achieved by switching the perfusate from a physiological saline solution, hereafter referred to as normal solution (of composition 112-mM NaCl, 3.0-mM KCl, 1.6-mM MgSO₄, 3.0-mM CaCl₂, 5.0-mM Glucose, and 3.0-mM HEPES), to one where 10-mM MnCl₂ or 30-mM Gd-DTPA had been added. (When either of these paramagnetic agents was present, the NaCl content of the solution was reduced to maintain an osmotic pressure equal to that of the normal solution.) In a few studies the H₂O in normal solution was replaced with D₂O.

Transverse-relaxation decay curves were acquired using a phase-cycled CPMG sequence that included 4, 8, or 16 averages. Four thousand echoes were acquired with an inter-echo time of 1.6 ms and π pulses of 20 μ s in duration. A TR of 14 s was used to ensure complete relaxation between averages. Decay curves were initially acquired for 40-150 min with normal solution as the perfusate, followed by acquisition for 60-240 min with a modified perfusate.

[†] These experiments were performed before the two-coil system outlined in the previous chapter was built. Although the use of a single coil with flow may have caused some distortion in measured spectral parameters, the conclusions drawn from this study will still be valid, since the goal here was to observe relative changes in spectral parameters over time, not to obtain quantitative values.

Analysis

One hundred and forty data points were sampled from each decay curve in a randomized, quasi-logarithmic pattern. These sampled points were fitted in a non-negative least squares (NNLS) sense [20] to a set of 105 decaying exponentials, logarithmically spaced between 3.2 ms and 3 s, then smoothed with a minimum energy constraint to produce an estimate of the T_2 spectrum. In order to improve precision, this procedure was repeated 20 times using newly-randomized points. The T_2 spectrum used for subsequent analysis was taken as the average of those obtained from the 20 sets of data points. From the average T_2 spectra determined for a given study, the size and T_2 times of the resulting components were plotted against time to view any trends that occurred.

4.3 Results

All T_2 spectra obtained from nerve preparations (both those perfused with a normal solution and those obtained immediately upon switching to a modified solution) were characterized by four spectral peaks having T_2 decay times and relative sizes similar to those reported in the literature [10-12]. Of these, the longest-lived was attributed to the perfusate and the three shortest to the nerve. This assignment was based on the fact that only the longest-lived peak, having a T_2 time of approximately 1500 ms, was observed when nerve was not present in the chamber. In addition to this single peak, a small amount of signal (< 5%) was scattered throughout the lower T_2 region. This scattered signal appeared inconsistently, however, and did not give rise to specific peaks.

Experiments were performed in which the perfusate was switched from an H_2O - to a D_2O -based solution. The spectral peak resulting from the perfusate disappeared completely within ~3 minutes after the switch (Figure 4-1a), revealing the time required to alter the composition of the solution bathing the nerve. Although the size of all three components of the nerve T_2 spectra decreased with time following introduction of the D_2O -based perfusate, it was not possible to determine the order in which the components

were affected by the replacement. However, these studies revealed that > 98% of the signal from the nerve arose from water protons exchangeable with those in the perfusate (Figure 4-1b).

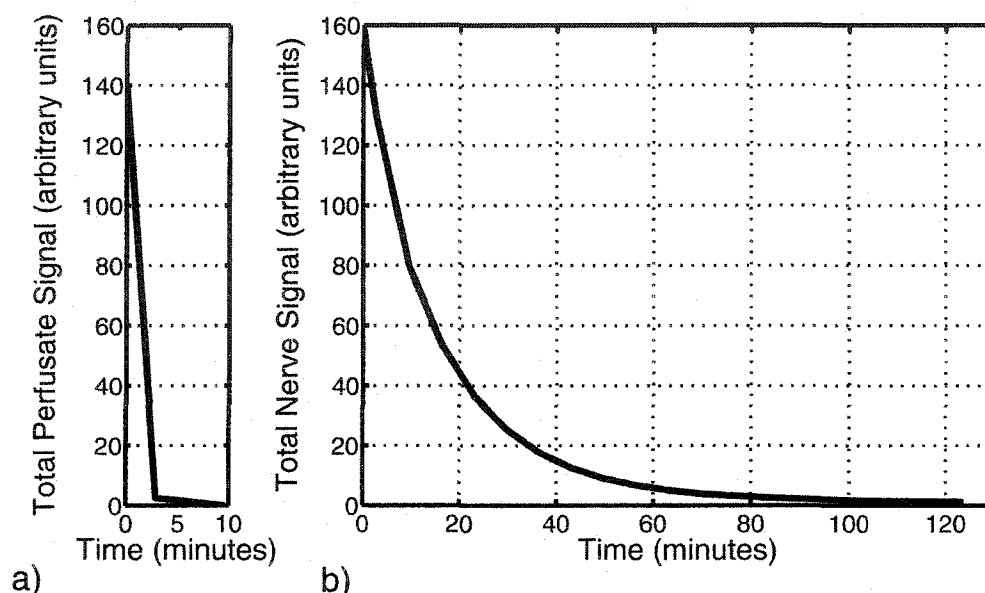


Figure 4-1. Plots of the sizes of the a) perfusate and b) sum of the three nerve T_2 components following switching of the perfusate from an H_2O - to a D_2O -based solution.

In order to determine which of the nerve T_2 components results from the endoneurium, experiments were performed in which a paramagnetic agent (to which the myelin and axonal space may have restricted access in comparison to the endoneurium [21]), was introduced into the perfusate. A plot of the component sizes and T_2 times for a nerve with intact epineurium and perfused with a Mn^{2+} solution is displayed in Figure 4-2. The results of this and two similar experiments showed a clear and rapid reduction in the size of the intermediate-lived component beginning minutes following the introduction of the Mn^{2+} perfusate. After 40 minutes, the signal originating from this component had almost completely disappeared, although a small residual amount (~5 %) remained for the duration of the experiments. In marked contrast, the size of the longest-lived component showed little change in response to the introduction of the Mn^{2+} ions

(Figure 4-2), although a gradual decrease in the relaxation time of this component was observed throughout the course of an experiment. A consistent feature of these studies, however, was a significant increase in the size of the shortest-lived component concurrent with the decline in that of the intermediate-lived component. This increase continued until the size of the intermediate-lived component had fallen to its residual level, after which that of the shortest-lived returned to a near-original size.

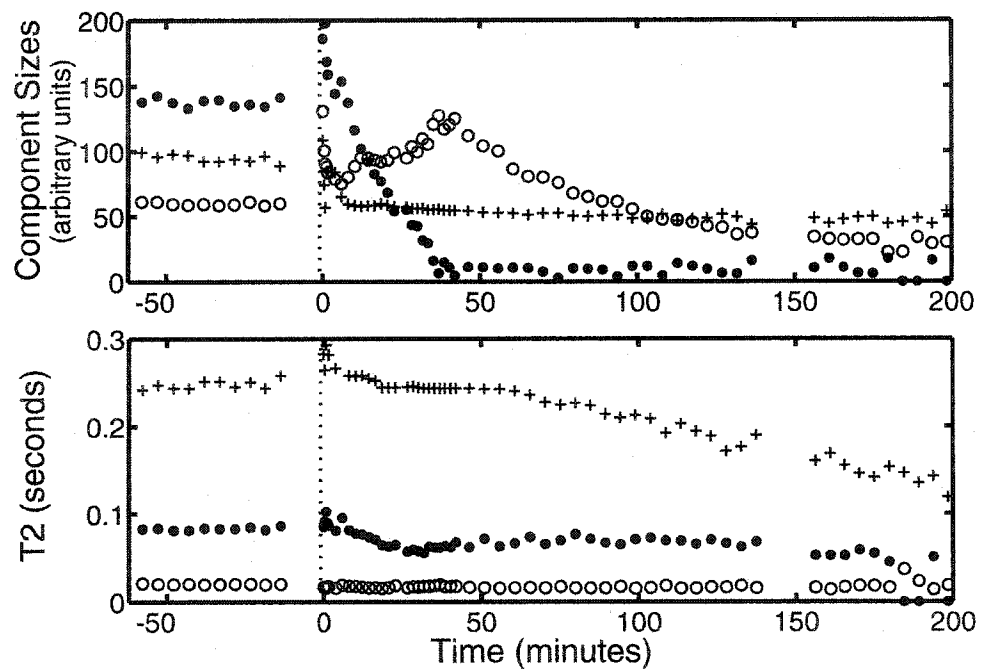


Figure 4-2. A plot of the T_2 component sizes (top) and their corresponding T_2 times (bottom) obtained from a sheathed nerve sample before and after switching the perfusate at time = 0 from a normal solution to one containing 10-mM Mn^{2+} .

Figure 4-3 shows a plot of the same type of experiment as described above, but with the epineurium removed. The same basic trends in component sizes and relaxation times can again be seen, with the main differences being the rapidity of change and the total depletion of the intermediate-lived component. Experiments using Gd-DTPA with and without the epineurium removed revealed similar trends as for Mn^{2+} , with the primary

difference being an increase of approximately 50% in the depletion time of the intermediate-lived component (results not shown).

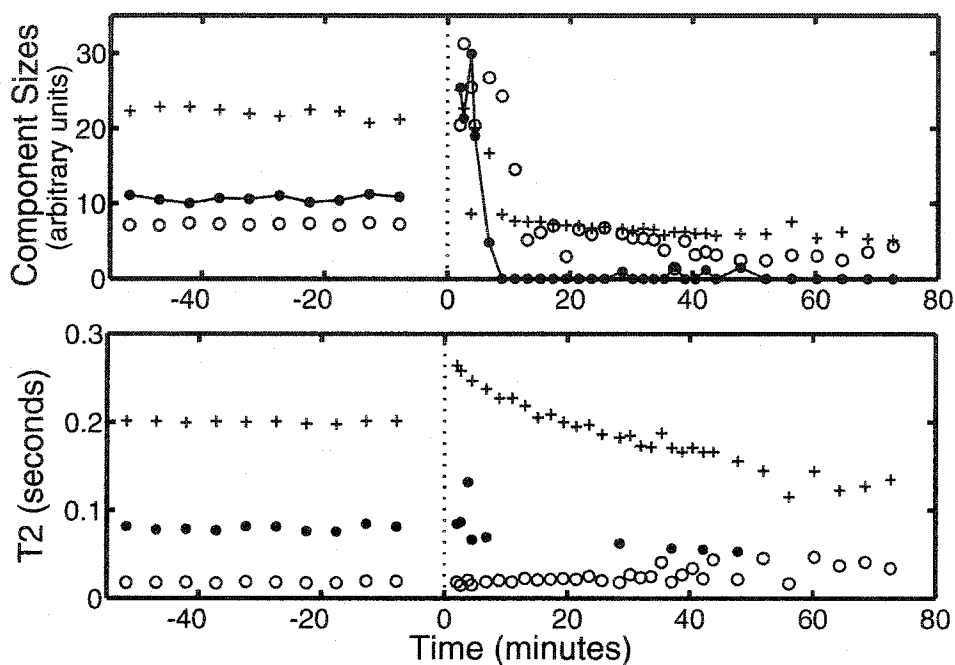


Figure 4-3. A plot of the T_2 component sizes (top) and their corresponding T_2 times (bottom) obtained from a desheathed nerve sample before and after switching the perfusate at time = 0 from a normal solution to one containing 10-mM Mn^{2+} .

4.4 Discussion

Experiments with paramagnetic agents consistently showed the intermediate-lived T_2 component being affected prior to either of the other components. A gradual reduction in the relaxation time of the longest-lived component was observed, but on a time scale much longer than that of loss of signal from the intermediate-lived T_2 component (Figures 4-2 and 4-3). The primary finding of this study is thus that the intermediate-lived component of the proton T_2 spectrum of amphibian peripheral nerve originates from the endoneurium water of the nerve and the longest-lived from the axonal water. This conclusion follows when one considers that the axonal and myelin compartments have access to the outside environment (perfusate) only through the

endoneurium, due to the physical structure of nerve tissue. Thus, if one of the T_2 components is being preferentially affected before the others, it is most likely to represent the endoneurium tissue compartment. The slower, more gradual reduction in relaxation time of the longest-lived component would then result from movement of the paramagnetic agent from the endoneurium into the axonal space, either through the myelin or the nodes of Ranvier. It is interesting to note that the intermediate-lived component is affected roughly five times faster by the paramagnetic agent in the desheathed (epineurium removed) preparation than in whole nerve. This finding would lend further support to the assignment of the intermediate-lived component to the endoneurium, as one would expect the paramagnetic agents to enter that compartment more rapidly without the epineurium acting as a diffusion barrier. Granted, the long-lived component was affected faster in the desheathed sample as well, but at a proportionally longer timescale than the intermediate-lived. That the proton T_2 spectrum originates primarily from the water proton follows from > 98% of the spectrum being found to result from exchangeable H_2O (Figure 4-1b).

Let us assume, for the sake of discussion, that the assignment is opposite to what was stated above. In this case, the axonal water would be receiving the faster influx of paramagnetic agent, being (as the assumption goes) the intermediate-lived component. Now, if this were the case, the agents cannot be diffusing through the endoneurium, as this would have a rapid effect on the long-lived component, which was not seen. The only other point of entry to the axons, without passing through the endoneurium, is through the open ends. Taking this as the point of entry for the paramagnetic agents, one could, presumably, see the same results as were displayed in Figure 4-2, with the assignment reversed. However, this assumption will fail when one views the results for the desheathed preparation (Figure 4-3), as the removal of the epineurium would have no impact on the diffusion rate of the agents through the axoplasm, and therefore one would not expect to see a change in the rapidity of response for the intermediate-lived component.

In contrast to the decline and extinction of the intermediate-lived T_2 component, the size of the shortest-lived, but not the longest-lived component, was observed to increase markedly and then decrease following introduction of a paramagnetic agent into the perfusate (Figures 4-2 and 4-3). It is possible that the transient change in the shortest-lived component resulted from an effect of the paramagnetic agent on a proton population other than that of the endoneurium water. For example, the agent may have affected the myelin in such a manner as to allow water from the endoneurium or axonal compartments to accumulate in the myelin compartment in a transient manner. However, the change in the shortest-lived component may also represent an artifact of the NNLS analysis of the T_2 decay curves. That is, as the endoneurium concentration of the paramagnetic agent increased following its introduction into the perfusate, the T_2 relaxation time of the endoneurium water declined. During the period of time when the relaxation time of the endoneurium water was similar to that of the shortest-lived component, the NNLS analysis would attribute the endoneurium water signal to that of the shortest-lived component, resulting in an increase in the size of the shortest-lived component. As the relaxation time of the endoneurium water continued to decline, the size of the shortest-lived component would return to its pre-agent value, and that of the paramagnetic-agent containing endoneurium water fall below the level of detection (~ 3 ms).

In an attempt to test the above hypothesis, a computer simulation was performed in which T_2 spectra were calculated following introduction of a paramagnetic-agent containing perfusate. The resulting spectral parameters were then compared to those obtained experimentally. The model was based upon the solution of Fick's second law of diffusion (diffusion equation). As changes in the spectral parameters of the longest-lived component were observed to occur at a slower rate than those of either the shortest- or intermediate-lived T_2 components, and since following extinction of the intermediate-lived component the shortest-lived component was still present (Figures 4-2 and 4-3), the paramagnetic agent was assumed to have access to only the endoneurium. Further,

paramagnetic agent present in the endoneurium was assumed to have no effect upon the relaxation times of either the myelin water or axonal water protons. In order to simplify the computation, the nerve was viewed as a homogeneous cylinder of radius a and endoneurium diffusion coefficient D_1 . This structure was presumed to contain the endoneurium water and was surrounded by a layer of epineurium and perineurium that had an outer radius b and a diffusion coefficient D_2 (Figure 4-4). At time $t = 0$, this modeled tissue was placed in a well-stirred bathing solution having a constant paramagnetic agent concentration of C_0 . Initially, the concentration of paramagnetic agent in the tissue was zero ($C(r,0) = 0 \quad | 0 \leq r < b$).

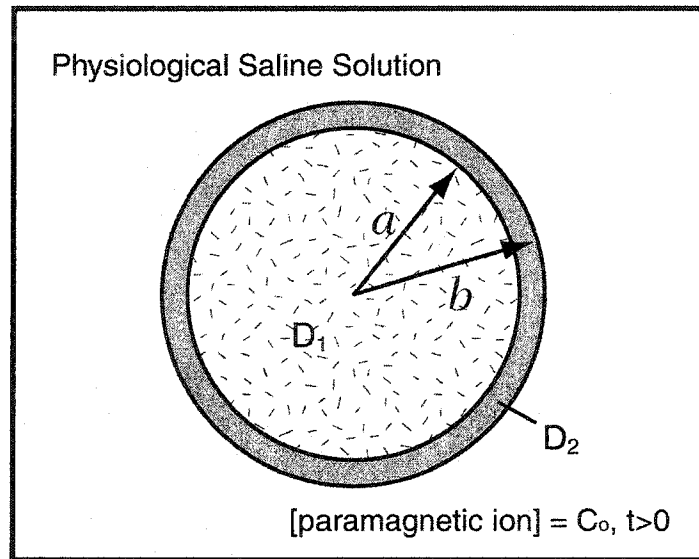


Figure 4-4. Geometric construction of a sheathed cylinder for the purposes of simulation. D_1 and D_2 refer to the diffusion coefficients assigned to the inner section and the outer sheath, respectively.

The diffusion equation

$$\frac{\partial C}{\partial t} = D \nabla^2 C \quad [4.1]$$

can be solved in cylindrical coordinates to provide the equations [22]:

$$C(r,t) = C_0 + \pi D_2^2 C_0 \sum_{s=1}^{\infty} e^{-D_1 \alpha_s^2 t} J_0(r \alpha_s) J_0(a \alpha_s) X(\tilde{D} a \alpha_s, \tilde{D} b \alpha_s) F_1(\alpha_s) \quad | 0 \leq r < a, \quad [4.2]$$

$$C(r,t) = C_0 + \pi D_2^2 C_0 \sum_{s=1}^{\infty} e^{-D_1 \alpha_s^2 t} J_0^2(a \alpha_s) X(\tilde{D} r \alpha_s, \tilde{D} b \alpha_s) F_1(\alpha_s) \quad | a < r < b \quad [4.3]$$

where $C(r,t)$ is the concentration of the paramagnetic agent at radius r and time t within the nerve or sheath, $X(x,y) = J_0(x)Y_0(y) - Y_0(x)J_0(y)$, where J_0 and Y_0 are zeroth-order Bessel functions of the first and second kind, respectively, and $\pm \alpha_s, s=1, 2, \dots$, are roots of

$$D_1 J_0'(a \alpha) X(\tilde{D} a \alpha, \tilde{D} b \alpha) - \tilde{D} D_2 J_0(a \alpha) X_1(\tilde{D} a \alpha, \tilde{D} b \alpha) = 0 \quad [4.4]$$

where $\tilde{D} = \sqrt{D_1/D_2}$, $X_1(x,y) = \frac{\partial}{\partial x} X(x,y)$, $J_0'(r)$ is the first derivative of $J_0(r)$, and

$$\frac{1}{F_1(\alpha_s)} = \left[\frac{1}{4} \pi^2 a^2 \alpha_s^2 D_1 (D_1 - D_2) J_0'^2(a \alpha_s) X^2(\tilde{D} a \alpha_s, \tilde{D} b \alpha_s) \right] - D_2^2 J_0^2(a \alpha_s). \quad [4.5]$$

Once solutions for the concentration functions were found, they were translated into a time-dependent, radial T_2 distribution, $T_2(r,t)$, using the relation:

$$\frac{1}{T_2(r,t)} = \frac{1}{T_2(0)} + R_T C(r,t) \quad [4.6]$$

where $T_2(0)$ was the assumed transverse-relaxation time of the endoneurium in the absence of a paramagnetic agent and R_T was the transverse relaxivity constant. The values used in the simulation for a and b were 0.735 mm and 0.750 mm, respectively [23]. Transverse-relaxation decay curves for this endoneurium region were then generated as a function of time following exposure of the nerve to a paramagnetic agent. This was accomplished by segmenting the cylindrical nerve into N concentric shells, each with average radius r_k , with $k=1$ to N . The T_2 behavior of each shell was

determined by the expression for $T_2(r,t)$ in equation [6], and the resulting signal of each was summed together as in the following expression:

$$\text{Signal}_{\text{Inter-axonal}}(n\text{TE}) \approx \sum_{k=1}^N V_k \cdot \exp(-n\text{TE}/T_2(r_k, t)) \quad [4.7]$$

where V_k is the fractional volume of the k^{th} shell, TE is the inter-echo time, and t is the time following the introduction of the paramagnetic agent. N was set to 100 for these simulations. To best mimic our experimental results, four thousand echoes were used with an inter-echo time of 1.6 ms. Signal from the other T_2 components were then added with typical experimental parameters (both in proportion and T_2), as monoexponential decays. Finally, random noise sets at typical experimental levels were added to these simulated decay curves, and the resulting data were analysed by our NNLS routine. Spectral parameters from these simulations were determined from the NNLS best fits, just as with experimental data, and plotted out as a function of time (Figures 4-5 and 4-6).

Spectra were generated for both sheathed and desheathed nerve using various diffusion coefficients, assuming that either the intermediate-lived or the longest-lived component corresponds to the endoneurium. Comparison to experimental Mn^{2+} and Gd-DTPA spectra revealed that only the assumption of the intermediate-lived component corresponding to the endoneurium resulted in qualitative agreement between the computer generated (Figures 4-5 and 4-6) and experimental (Figure 4-2) spectra. For the case of Mn^{2+} , the diffusion coefficients D_1 and D_2 that resulted in agreement were approximately $3 \times 10^{-7} \text{ cm}^2/\text{s}$ and $5 \times 10^{-9} \text{ cm}^2/\text{s}$, respectively, while for Gd-DTPA the coefficients were somewhat smaller. The assumption of the intermediate-lived component corresponding to the endoneurium yielded theoretical spectra that contained the basic features of the experimental, in particular, the extinction of the intermediate-lived component, a concomitant rise and fall in the size of the shortest-lived component, and a relative constant size of the longest-lived component during the extinction of the intermediate-lived component. In contrast, assignment of the longest-lived component to the endoneurium resulted in theoretical spectra in which the longest-lived component

underwent extinction, and both the shortest- and intermediate-lived components exhibited a rise and fall in size during the extinction of the longest-lived component (Figure 4-6). Thus, assignment of the intermediate-lived, but not the longest-lived component, to the endoneurium compartment resulted in theoretical spectra in agreement with experimental spectra and provided an explanation for the rise and fall of the shortest-lived component consistent with the paramagnetic agent having access to only the endoneurium.

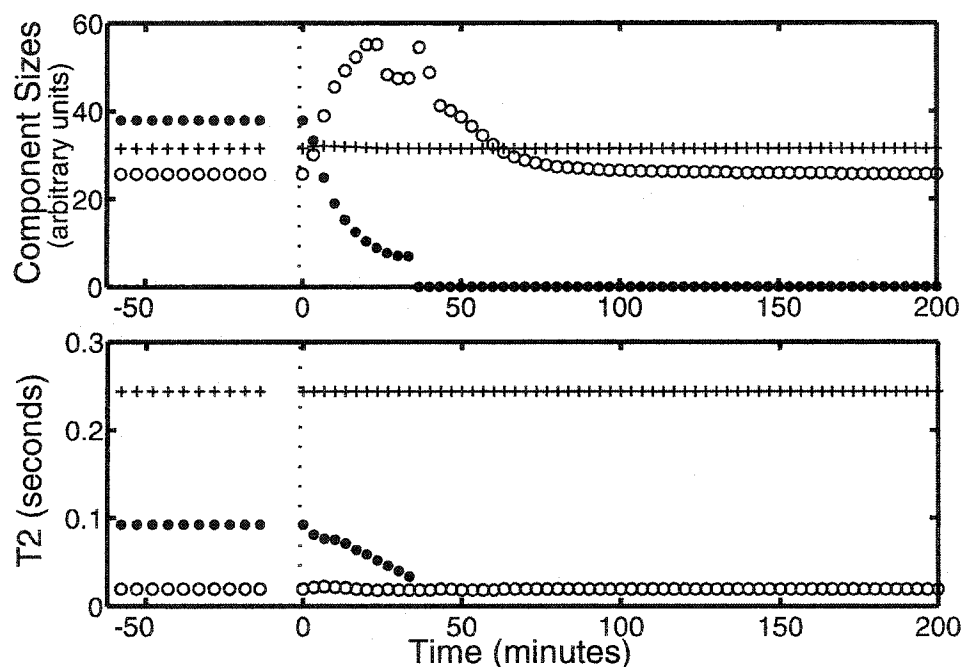


Figure 4-5. A computer simulation of the T_2 component sizes (top) and corresponding T_2 times (bottom) from a nerve with the sheath intact in which 10-mM Mn^{2+} is introduced to the surrounding bathing solution at time = 0. In this simulation, the radius of the nerve was taken to be 0.735 mm, and surrounding this was a 15- μ m thick sheath. The diffusion coefficients of the nerve tissue and sheath were taken to be 3×10^{-7} cm²/s and 5×10^{-9} cm²/s, respectively. Here, it was assumed that the intermediate-lived component corresponded to the endoneurium.

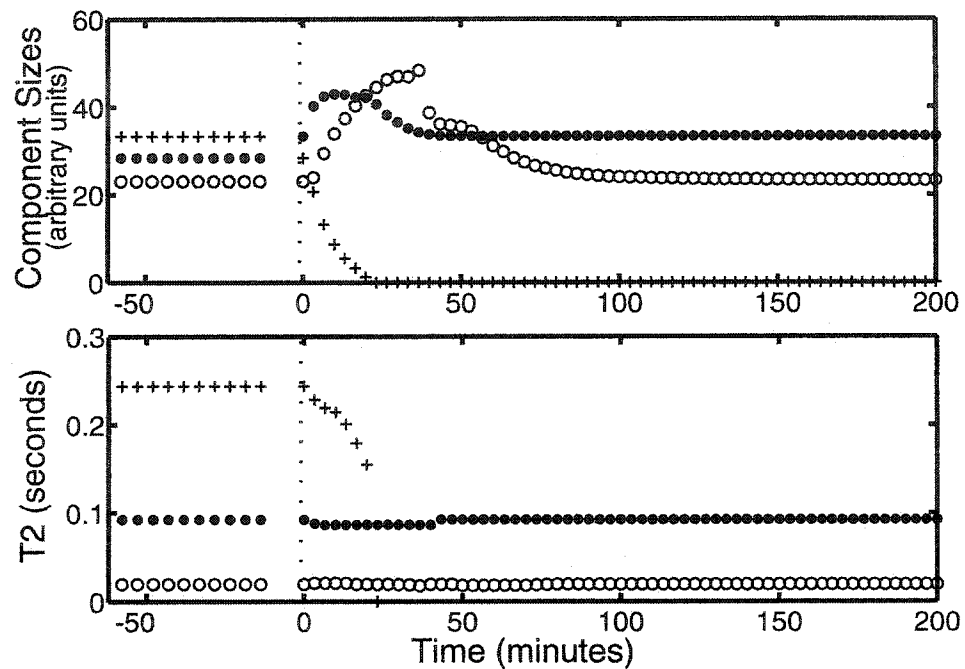


Figure 4-6. A computer simulation of the T_2 component sizes (top) and corresponding T_2 times (bottom) from a nerve with the sheath intact in which 10-mM Mn^{2+} is introduced to the surrounding bathing solution at time = 0. All dimensions and coefficients were kept the same as those for the simulation shown in Figure 4-5, the only difference being that in this simulation it was assumed that the longest-lived component corresponded to the endoneurium.

Although we are not aware of diffusion-coefficient studies of Mn^{2+} or Gd-DPTA in the endoneurium or epineurium of nerve, diffusion coefficients have been reported of $(4.2 - 8.9) \times 10^{-7} \text{ cm}^2/\text{s}$ for Mn^{2+} in brine-cured pork [24] and $1.4 \times 10^{-6} \text{ cm}^2/\text{s}$ for Gd-DPTA in cartilage [25]. Although 2-6 times larger than our estimated values, there is reasonable agreement given the differences in tissues and paramagnetic agents concentrations involved, and the simplification of our model. Our estimated diffusion coefficients for the sheath (D_2) which are two orders of magnitude smaller than those for the endoneurium most likely reflects the fact that the multilayered sheath serves as a diffusion barrier to a number of substances [26]. Wadhvani et al. [26] report values of $(1.3 - 14.0) \times 10^{-5} \text{ ml} \cdot \text{s}^{-1} \cdot \text{g}^{-1}$ for the permeability-surface area of Mn^{2+} through rat

perineurial sheath. With the approximation that the diffusion coefficient within the sheath equals the permeability multiplied by the thickness of the sheath, for a nerve 1 mm in diameter and having a sheath of thickness 15 μm [22], their reported values correspond to diffusion coefficients in the sheath of $(1 - 10) \times 10^{-9} \text{cm}^2/\text{s}$, our estimated value falling within this range. From this we conclude that our estimated values for diffusion coefficients are in reasonable agreement with related values available in the literature.

Unlike the use of the NMR tube where the saline solution is stationary and situated within a relatively uniform region of the B_1 field of the RF coil, flowing solution is present in the perfusion chamber inflow and outflow tubes which extends beyond the coil into a non-uniform region of the field. When nerve was not present in the chamber, the resulting spectra exhibited predominantly one T_2 peak at approximately 1500 ms, similar to that observed when only normal solution is present in a NMR tube. However, a small amount of signal (<5%) was typically scattered throughout the lower T_2 regions. While this signal did not affect the number of components associated with the nerve, it may have slightly altered the spectral values associated with the peaks. However, because of the dramatic relative changes seen upon the introduction of paramagnetic agents, the possibility of some spectral distortion due to flow effects is insufficient to affect the conclusion that the intermediate-lived, and not the longest-lived component, disappeared as a result of Mn^{2+} or Gd-DTPA being introduced.

There is a sudden change in the size of the long-lived component after the introduction of a paramagnetic agent (Figures 4-2 and 4-3). While it is possible that this is a flow distortion, experiments presented in the next chapter would indicate that this drop is due instead to an interaction of the buffer with the nerve surface: an interaction removed by the knockout of the buffer component by paramagnetic agents.

This study has the advantage of not requiring quantitative results to make an component-compartment assignment, as compared to studies which compare estimated

compartment water populations to those of the measured spectral parameters [10,27]. As was mentioned in Chapter 1, solution algorithms for interpreting multi-exponential data cannot always be relied upon to produce quantitatively accurate results for all spectral components. Additionally, the slow exchange model must be fully assumed for the quantitative results to hold, and the situation may be more complex than that. The findings in this study are in agreement with those of Peled et al. [11], although the methods performed here are possibly more convincing, in part because this study relies on a direct experimental result, and as well, more than one nerve preparation was involved.

4.5 Conclusions

The primary finding of this study is that the intermediate-lived component of the proton T₂ spectrum of amphibian nerve originates from the endoneurium water of the nerve and the longest-lived from the axonal water. It was found that greater than 98% of the proton spectrum on which the above conclusion is based originates from freely exchangeable water. A transient change observed in the shortest-lived component of the spectra during the wash-in period of a paramagnetic agent into the endoneurium may be understood as an artifact resulting from the NNLS fitting of the T₂ decay curves. Following extinction of the intermediate-lived component of the spectra, and over a time period of hours, evidence exists for the entrance of the paramagnetic agents employed into the axonal space of the nerve, resulting in a gradual reduction in T₂ time of the longest-lived component.

4.6 References

- [1] English AE, Joy RM, Henkelman RM. Pulsed NMR relaxometry of striated muscle fibres. *Magn Reson Med* 1991;21:264-281.
- [2] François A, Van Gerven L, Atassi G, Eisendrath H, Gielen M, Willem R. Analysis by the Carr-Purcell-Meiboom-Gill sequence of the influence of P388 Leukemia and of *cis*-diamminedichloroplatinum(II) in kidneys and spleens of mice. *Magn Reson Med* 1988;7:449-462.
- [3] Henkelman RM, Stanisz GJ, Kim JK, Bronskill MJ. Anisotropy of NMR properties of tissues. *Magn Reson Med* 1994;32:592-601.
- [4] Poon CS, Henkelman, RM. Practical T_2 quantitation for clinical applications. *J Magn Reson Imaging* 1992;2:541-553.
- [5] Saab G, Thompson RT, Marsh GD. Multicomponent T_2 relaxation of in vivo skeletal muscle. *Magn Reson Med* 1999;42:150-157.
- [6] Shioya S, Haida M, Fukuzaki M, Kurita D, Tsuji C, Ohta Y, Yamabayashi H. Nuclear magnetic resonance study of lung water compartments in the rat. *Am J Physiol* 1997;272:L772-L778.
- [7] MacKay AL, Whittall KP, Adler J, Li DKP, Paty DW, Graeb DA. In-vivo visualization of myelin water in brain by magnetic resonance. *Magn Reson Med* 1994;31:673-677.
- [8] Stanisz GJ, Henkelman RM. Diffusional anisotropy of T_2 components in bovine optic nerve. *Magn Reson Med* 1998;40:405-410.
- [9] Beaulieu C, Fenrich FR, Allen PS. Multicomponent water proton transverse relaxation and T_2 -discriminated water diffusion in myelinated and nonmyelinated nerve. *Magn Reson Imag* 1998;16:1201-1210.

- [10] Vasilescu V, Katona E, Simplaceanu V, Demco D. Water compartments in the myelinated nerve, III: pulsed NMR results. *Experientia*. 1978; 34: 1443-1444.
- [11] Peled, S, Cory DG, Raymond SA, Kirschner DA, Jolesz FA. Water diffusion, T_2 , and compartmentalization in frog sciatic nerve. *Magn Reson Med* 1999; 42: 911-918.
- [12] Does M, Snyder RE. T_2 relaxation of peripheral nerve measured in vivo. *Magn Reson Imag* 1995;13:575-580.
- [13] Stewart WA, MacKay AL, Whittall KP, Moore GRW, Paty WD. Spin-spin relaxation in experimental allergic encephalomyelitis. Analysis of CPMG data using a non-linear least squares method and linear inverse theory. *Magn Reson Med* 1993;29:767-775.
- [14] Does M, Snyder RE. Multiexponential T_2 relaxation in degenerating peripheral nerve. *Magn Reson Med* 1996;35:207-213.
- [15] Jolesz FA, Polak JF, Adams DF, Ruenzel PW. Myelinated and nonmyelinated nerves: comparison of proton MR properties. *Radiology* 1987;164:89-91.
- [16] Whittall KP, MacKay AL, Graeb DA, Nugent RA, Li DKP, Paty DW. In-vivo measurement of T_2 distributions and water contents in normal human brain. *Magn Reson Med* 1997;37:34-43.
- [17] Menon RS, Rusinko MS, Allen PS. Proton relaxation studies of water compartmentalization in a model neurological system. *Magn Reson Med* 1992;28:264-274.

- [18] Vasilescu V, Margineanu DG, Katona E. Heavy water intake in tissues. II. H₂O-D₂O exchange in the myelinated nerve of the frog. *Experientia* 1977;33:192-194.
- [19] Wachowicz K, Snyder RE. A perfusion chamber suitable for the measurement of transverse relaxation spectra of tissue maintained in vitro. In: Proceedings of the 8th Annual Meeting of ISMRM, Denver, USA, 2000. p 1987.
- [20] Whittall, KP and MacKay, AL. Quantitative interpretation of NMR relaxation data. *J Magn Reson* 1989; 84:134-152.
- [21] Seo Y, Morita Y, Kusaka Y, Steward MC, Murakami M. Diffusion of water in rat sciatic nerve measured by ¹H pulsed field gradient NMR: compartmentalization and anisotropy. *Jpn J Physiol* 1996;46:163-169.
- [22] Jaeger JC. Heat Conduction in Composite Circular Cylinders. *Phil Mag and J Sci* 1941;32:324-335.
- [23] Snyder RE, Smith RS. Application of position-sensitive radioactivity detectors to the study of the axonal transport of β -emitting isotopes. In: Weiss DG editor. *Axoplasmic transport*. New York: Springer-Verlag: 1982. P442-453.
- [24] Guiheneuf T, Gibbs S, Fischer A, Hall L. Measurement of the diffusion coefficient of manganese ions in cured pork by one-dimensional ¹H magnetic resonance imaging. *Intern J Food and Technol* 1996;31:195-203.
- [25] Foy BD, Blake J. Diffusion of paramagnetically labelled proteins in cartilage: enhancement of the 1-d NMR imaging technique. *J Magn Reson* 2001;148:126-134.

- [26] Wadhvani KC, Murphy VA, Smith QR, Rapoport SI. Saturable transport of manganese (II) across blood-brain barrier of rat peripheral nerve. *Am J Physiol* 1992;262:R284-R288.
- [27] Fenrich FR. MSc thesis: A simulation and experimental study of water proton relaxation in white matter model. University of Alberta; 1992.

CHAPTER 5

AN EXAMINATION OF MAMMALIAN NERVE T_2 SPECTRAL CHARACTERISTICS

5.1 Introduction

T_2 spectral examinations of rat sciatic nerve have been performed in a number of previous studies [1-3]. In these, a three-component spectrum was consistently determined. The shortest-lived component has consistently been reported to arise from myelin water from experiments performed on a wide range of species [4-9]. The origin of the other two remaining components in the rat nerve T_2 spectrum is more uncertain, however. For peripheral nerve in general, the notion that axonal membranes and, in particular, myelin provide a barrier to rapid diffusion, provide a belief that the endoneurium and axoplasm thus separated give rise to the intermediate and long-lived spectral components [10,11]. Differing views have been reported in the past as to the order in which they correspond [4,12-15].

The use of manganese ions to assign the T_2 components of frog sciatic nerve to their appropriate tissue microstructures yielded a convincing argument that the intermediate and long-lived components correspond to the endoneurium and axonal space, respectively [14]. On the path towards a better understanding of the MR behaviour of human nerve tissues, a sound knowledge of spectral nerve characteristics in a mammalian subject is the next important step. Although one might think it likely that the T_2 spectral relationships would be the same in mammalian nerve as in their amphibian counterparts, the exact protein and collagen makeup of the respective nerve structures (being among the primary promoters of relaxation in tissue) is not necessarily the same, requiring that this idea be challenged. Following is an investigation into the T_2 spectral characteristics of rat sciatic nerve, with emphasis on determining the assignment of the microstructural origins of the intermediate- and long-lived components. Also examined was the effect of

the epineurium, the connective tissue which surrounds the nerve and separates the individual fascicles, on the spectra. Tissue interactions with water-based buffer solutions, and their impact on the resulting T_2 spectra were also investigated.

5.2 Method

All nerve samples studied were taken from adult Sprague Dawley rats. Three to four cm nerve segments were dissected out within one hour of euthanasia in CO_2 . The nerves were cleaned of any extraneous tissue and immediately placed in a physiologically appropriate buffer solution (130-mM NaCl, 3-mM KCl, 2-mM MgSO_4 , 2-mM CaCl_2 , 10-mM Dextrose, and 10-mM HEPES, buffered to a pH of 7.4). The epineurium was removed from seven of the nerves, which were then studied as single fascicle preparations. In total, 27 nerves were utilised in this study. All preparations were studied at room temperature (~ 20 degrees C).

NMR Tube Experiments

Nineteen nerve samples were examined in a 5-mm NMR tube. Ten of these were intact preparations and nine were single fascicles. Approximately half of these samples were bathed in a physiologically appropriate water-based buffer solution (as listed above). Five each of the single fascicle and intact preparations were bathed in FluorinertTM FC-77 (3MTM, London, ON), which is transparent to proton NMR techniques and is a barrier to the diffusion of water and ions. Whenever Fluorinert was used, the nerve sample was quickly but thoroughly blotted dry before immediately transferring it to the Fluorinert bath. In four of these occasions, two intact nerves and two single fascicles were briefly rinsed in a low concentration Mn^{2+} solution before being blotted dry and placed in the NMR tube.

To acquire T_2 decay curves, the NMR tubes were placed within the centre of a 4-loop solenoid coil measuring approximately 7 mm in diameter. Coil and tube were then positioned in the isocentre of a 3-Tesla whole body scanner, controlled by a S.M.I.S.

console. Phase-cycled CPMG experiments with 8 averages, an echotime of 1.6 ms, 2000 echoes, and a TR of 14 s were performed. Fifteen to twenty decay curves were acquired in this manner for each sample over a time period spanning 34 to 45 minutes.

Polyethylene Flow Chamber

Eight nerves samples were studied in a polyethylene flow chamber [16]. In these experiments, which usually lasted for more than 3 hours, the buffer solution was changed on-the-fly from the normal one described above to one containing 10-mM MnCl_2 . In order to maintain a constant osmotic pressure when the Mn^{2+} solution was introduced, the concentration of NaCl in that solution was reduced from 130 mM to 115 mM. The chamber, with an inner diameter of 4.5 mm and a inner height of about 4 mm, was placed inside an actively decoupled two-coil system designed to compensate for distortions caused by the flow [17]. This coil system consisted of a small solenoid receive-only coil (same dimensions as above), and a 7-cm inner diameter birdcage transmit coil. Phase-cycled CPMG experiments were performed with the same parameters as above.

Analysis

A non-negative least squares approach (NNLS) was utilised to decompose the raw decay curves into a decay spectrum [18]. 140 data points were quasi-logarithmically sampled and fitted to 105 decaying exponential functions, with decay times logarithmically ranging from between 0.5 ms to 4 seconds. This was repeated 10 times for each experimental decay curve, following which the ten resulting spectra were averaged.

At times, when the number of components in the T_2 spectrum was constant throughout an entire experiment (as determined by the NNLS algorithm), another analysis routine was implemented. In this routine, each of the components was modeled by a Gaussian line in logarithmic decay space. Three parameters defined the position and shape of each spectral line: width at half maximum, magnitude, and spectral location [1].

The routine begins by taking seed values for all these parameters (supplied by the NNLS results) and then optimizing them to minimize the χ^2 parameter of the fit. For some data sets from the NMR tube experiments this routine was found to improve the precision of fitted spectral components.

Histology

A number of the samples were fixed in gluteraldehyde for light microscopy. The sections were stained with Bacsich's Myelin stain.

5.3 Results and Discussion

5.3.1 The effect of water and removal of the epineurium on rat nerve tissue

To assess any effect a water-based buffer might have on T_2 spectral characteristics, rat nerve spectra, both with epineurium intact and with epineurium removed, were studied in either a water-based buffer or fluorinert. The average spectra obtained from each of these four conditions are displayed in Figure 5-1, normalized such that the short-lived component has a constant amplitude. This normalization criterion was chosen on the assumption that the tissue's myelin content (which is generally associated with the short-lived component) will be a constant throughout the four different experimental conditions. The mean and standard deviations for the spectral characteristics are detailed in Table 5-1.

The intact nerves (epineurium remaining) in both **a** and **c** have very similar spectra except for one significant discrepancy – the spectra taken from samples in water-based buffers have a long-lived component that is 2.4 times larger (on average) than that from nerve in fluorinert. The obvious difference between the two cases is the presence or lack of surface water in contact with the tissue. It is likely that this water in association with the surface of the nerve tissue has a T_2 coincident with that of the long-lived component derived from the nerve tissue itself. This explanation is corroborated by the fact that whenever a water-based buffer is switched from normal to one containing paramagnetic

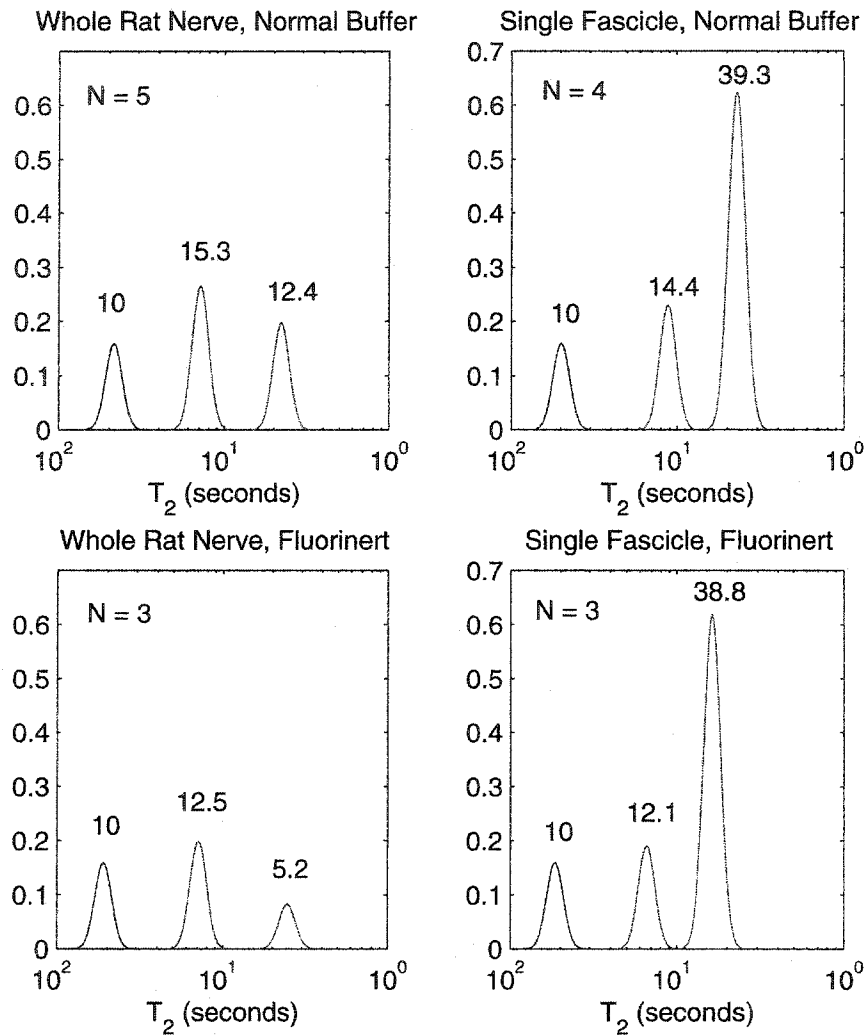


Figure 5-1. Spectra from rat sciatic nerve in four different circumstances. Spectra were reconstructed from average parameters in each case, using Gaussian peaks of equal width for easy visual comparison from one to another. Normalization of the spectra was achieved by setting the short-lived component to a constant magnitude of 10.

agents, the long-lived component of whole nerve will immediately drop in size by about 50 percent. This has implications for studies which seek to obtain quantitative T_2 spectral parameters from tissue bathed in buffer solution. One must take steps to account for any effect the water in the bathing solution may have on results. This is not to say that this

effect is always present with tissue in a water-based buffer solution. For example, there is no appreciable difference observed between the spectra in Figures 5-1b and 5-1d from single fascicles. A possible explanation for this has to do with surface area. Micrographs of epineurium reveal many folds of tissue that would supply a large surface for water to associate with. With the epineurium absent, however, this surface area is greatly reduced, making the presence of water irrelevant to the appearance of the spectra.

Tissue & Condition	T2 (ms)	SD (ms)	Size (%)	SD (%)	Size	SD
					Normalised to Short-Lived	
Whole Rat Nerve Normal Buffer (N=5)	19.7	0.3	26.5%	3.0%	10.0	1.1
	64.7	1.3	40.7%	6.3%	15.3	2.3
	231.4	8.7	32.8%	5.9%	12.4	2.2
Whole Rat Nerve Fluorinert (N=4)	18.9	0.9	36.1%	3.4%	10.0	0.9
	68.3	1.5	45.0%	1.4%	12.5	0.4
	244.8	1.7	18.8%	2.0%	5.2	0.5
Single Fascicle Normal Buffer (N=3)	20.5	0.7	15.7%	2.0%	10.0	1.3
	95.4	5.2	22.6%	7.2%	14.4	4.6
	240.7	24.0	61.7%	9.1%	39.3	5.8
Single Fascicle Fluorinert (N=3)	18.6	1.1	16.4%	0.9%	10.0	0.5
	65.8	5.3	19.8%	2.3%	12.1	1.4
	162.7	9.0	63.7%	1.4%	38.8	0.9

Table 5-1. Average T₂ spectral parameters from rat sciatic nerve in four different circumstances.

Another obvious difference present in Figure 5-1, and in all other experiments that utilise single fascicles is the abnormally large long-lived component. Unlike the increase in the long-lived component size due to surface water as described above, this feature is present in both water-buffer and fluorinert baths. Therefore, it has to represent a change in the nerve tissue itself, and not just a surface-water interaction. In order to evaluate any physical changes occurring in the nerve tissue that might account for this 7-fold increase in long-lived signal (based on Figures 5-1c and 5-1d), micrographs from both whole rat sciatic nerves and single fascicles were taken. Two such micrographs are displayed with equal magnification in Figure 5-2 a and b, respectively. Measurements from these

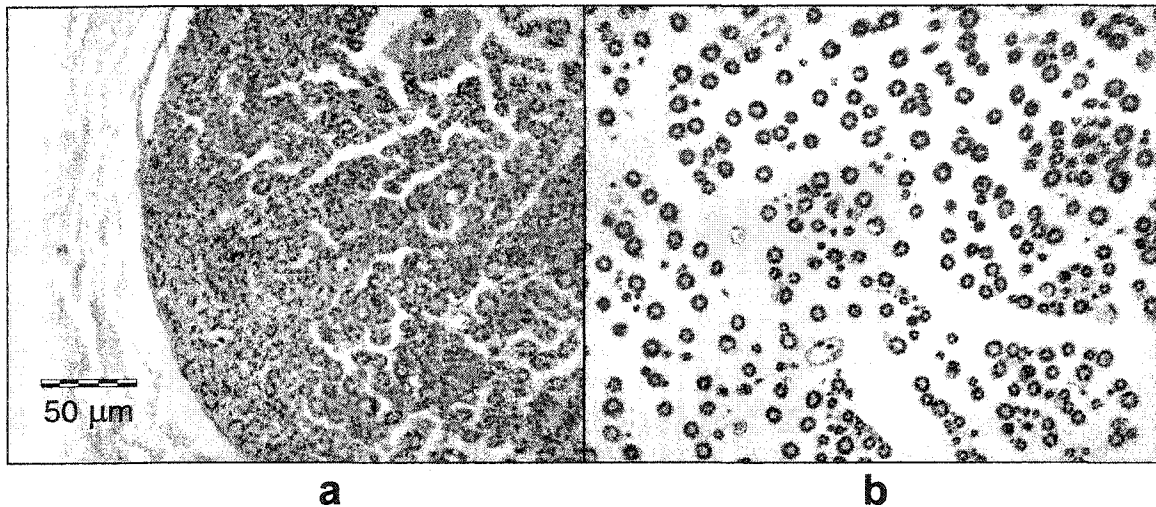


Figure 5-2. a. Rat nerve with epineurium intact. b. Rat nerve with epineurium removed (single fascicle). Note the increased spacing between axons.

pictographs reveal an approximate 6-fold increase in inter-axonal space when the epineurium is removed.

Because of the concurrent changes in microscopic structure and spectral characteristics, it was hoped that by properly associating these changes, one could establish a clear and definitive assignment of microstructures to the T_2 spectral components. As was stated earlier, the short-lived component has been generally associated with the water in myelin wrappings. The other two components have been more difficult to interpret. The results above would at first inspection be seen to support an assignment of the long-lived component to the endoneurium, seeing that both the size of this spectral component and the inter-axonal space increased simultaneously, and by similarly dramatic amounts. However, a dilution of the inter-axonal space would not only have a dramatic increase on its size, but it would have an equally dramatic effect on the resultant T_2 . For instance, using the equation $\frac{1}{T_2} = \frac{1}{T_{20}} + \alpha C$, where T_{20} is taken to be 1.54 seconds and the term αC is proportional to the concentration of transverse-

relaxation causing material, the dilution of the inter-axonal space by a factor of six would cause the long-lived component to rise from ~ 250 ms to ~ 830 ms. As little, if any, change occurs in the T_2 of the long-lived component, it would be incorrect to assign it to the endoneurium on the basis of these results.

On the other hand, if one were to assume the opposite assignment, where the intermediate component corresponds to the endoneurium, its T_2 would expectedly rise from ~ 70 ms to ~ 340 . This value is a little higher than the experimental position of the extra signal, but it is possible that it could correspond to it within the limitations of the above relaxation enhancement equation. Even so, one must note that the intermediate spectral component is still present in its expected position (Figures 5-1b and 5-1d), defying the notion that it has been driven up in T_2 by an influx of water into the endoneurium.

Thus it appears that these results do not directly support either assignment. It is possible that the endoneurium is not being diluted by an influx of buffer solution when the epineurium is removed, but rather microscopic water pockets are being formed within this space, having a relaxation rate roughly coincident with that of the long-lived component. If one were to accept this explanation, then the idea that the endoneurium corresponds to the intermediate-lived component would make more sense than the alternative, simply because one would not expect the microscopic pockets of water to take on the exact T_2 of that in which they reside, but a T_2 somewhere between this and that of bulk water.

5.3.2 The use of Mn^{2+} to assign components to physical compartments

In other studies, manganese ions have been used to assign the T_2 spectral components of frog nerve to tissue microstructures. The premise of these studies was that the endoneurium, being the most readily accessible microstructure to ions diffusing into the tissue, would be affected by the paramagnetic ions prior to other nerve structures.

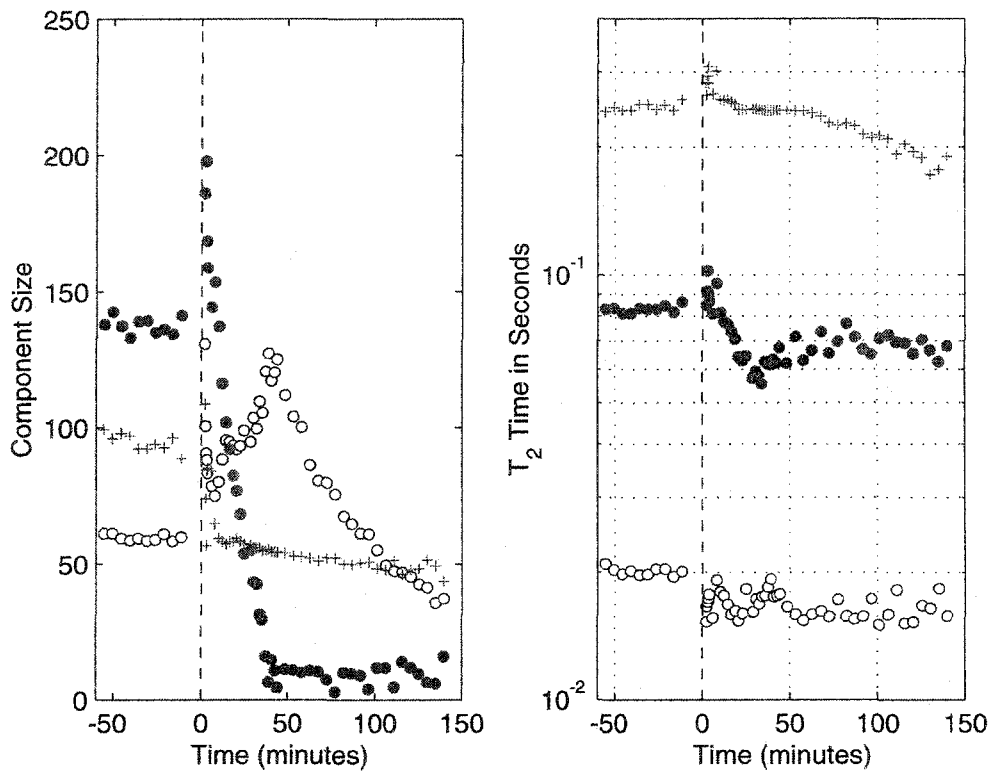


Figure 5-3. Frog nerve with 10-mM Mn^{2+} ions infused at time zero.

An observation of the concurrent changes in T_2 spectral components would then be able to reveal which component corresponds to the epineurium. Figure 5-3 shows the results of such an experiment on frog sciatic nerve. The bathing solution was switched from normal to one containing 10-mM Mn^{2+} at time zero. Note how the long-lived signal remains very stable in size (ignoring the sudden drop in size after the introduction of manganese, which is explained in the previous section), and drops less than 20% of a decade in T_2 over a period of two and a half hours. In contrast, the intermediate-lived component is strongly affected, and after a period of 40 minutes is virtually decimated – forced to merge with the short-lived component. After about 100 minutes, this signal has disappeared from the nerve spectra altogether (having stopped influencing the magnitude of the short), serving to assign the intermediate-lived component to the endoneurium.

The same type of experiment was performed on rat sciatic nerve tissue, with the hope that a component/compartiment assignment could be established in a similar manner. However, in rat nerve, the long-lived component no longer remained stable after the introduction of manganese. Thus it was no longer obvious which component was being flushed out first by the paramagnetic ions. Additionally, the decline in T_2 of the long-lived component created difficulties for the analysis and interpretation of the data. For example, when a longer-lived component is declining in T_2 , and falls through or close to the spectral position of another, an analysis algorithm will be unable to resolve the two components completely, and some of the magnitude of the longer will be merged with that of the shorter. (Note the temporary increase in the size of the short-lived component in Figure 5-3 as the intermediate-lived is being affected by Mn^{2+} ions.) If only one of the T_2 spectral components is changing, as in Figure 5-3, it is easy to account for this merging behaviour. When two components are changing simultaneously, however, as seems to be the case for rat sciatic nerve, the interpretation of the resultant spectral parameters is much more complex. Conclusions on the basis of these results are accordingly, less reliable. Figure 5-4 shows a typical set of results from the six experiments of the above type performed on rat sciatic nerve.

The many trends and changes observed in Figure 5-4 make interpretation difficult. One of the few assertions that can be made from such data is that both the intermediate and long-lived components are undergoing substantial changes in response to the 10-mM Mn^{2+} solution. One might conclude that the long-lived component is disappearing first, as it can no longer be followed after ~70 minutes. However, this is unlikely given the rise in magnitude and T_2 of the intermediate-lived component, coincident with the disappearance of the long. These rises indicate a merging of the two components. The degree to which the intermediate-lived component had itself fallen at the time of the merger and thereafter is uncertain.

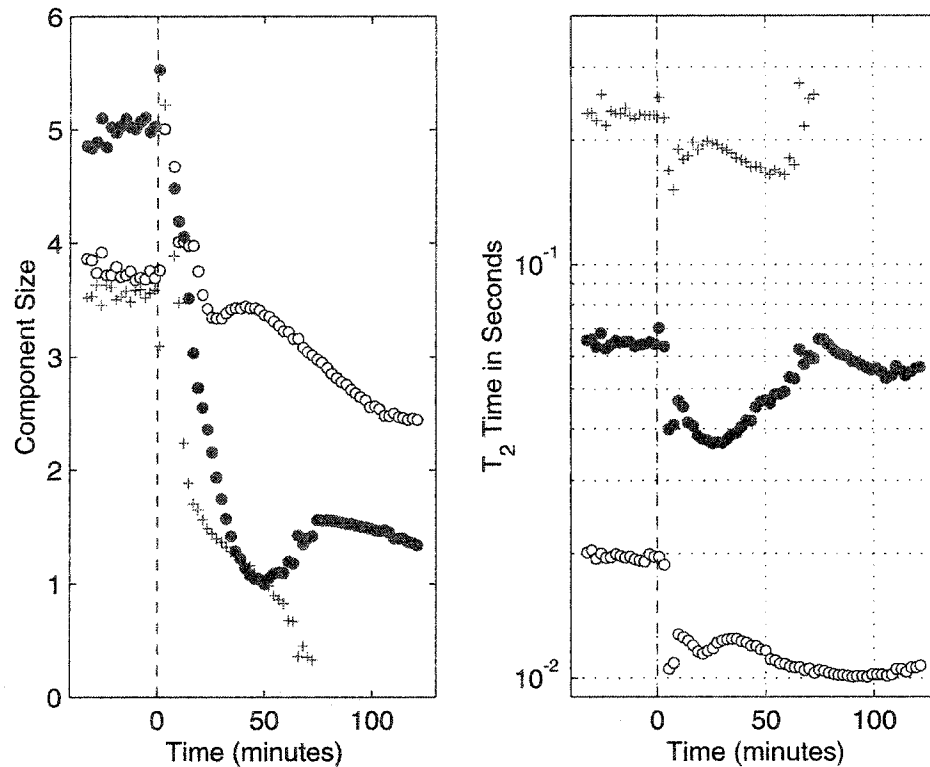


Figure 5-4. Solved spectral parameters for rat sciatic nerve. 10-mM Mn^{2+} ions were infused at time zero (dashed line).

In order to shed some light on the changes occurring in the long-lived component, a technique was employed that would force the short- and intermediate-lived components to merge. This was accomplished by raising the lower bound of the NNLS solution space from 0.5 ms to 5 ms. Although this is still well below the T_2 of the short-lived nerve component, the presence of 10-mM Mn^{2+} in the buffer will move its T_2 down from a typical value of 1.6 seconds to approximately 2 ms. With the lower bound in the solution space raised to 5 ms and the smoothing constraints in the algorithm present, the effect of this component reaches in to the lower part of the spectrum and has the effect of blurring the short- and the intermediate-lived components together. This merger leaves the long-lived component more distant in T_2 from other components, allowing its parameters to be

followed without risk of their mingling with another's. Figure 5-5 shows one of the rat nerve data sets analysed in this manner.

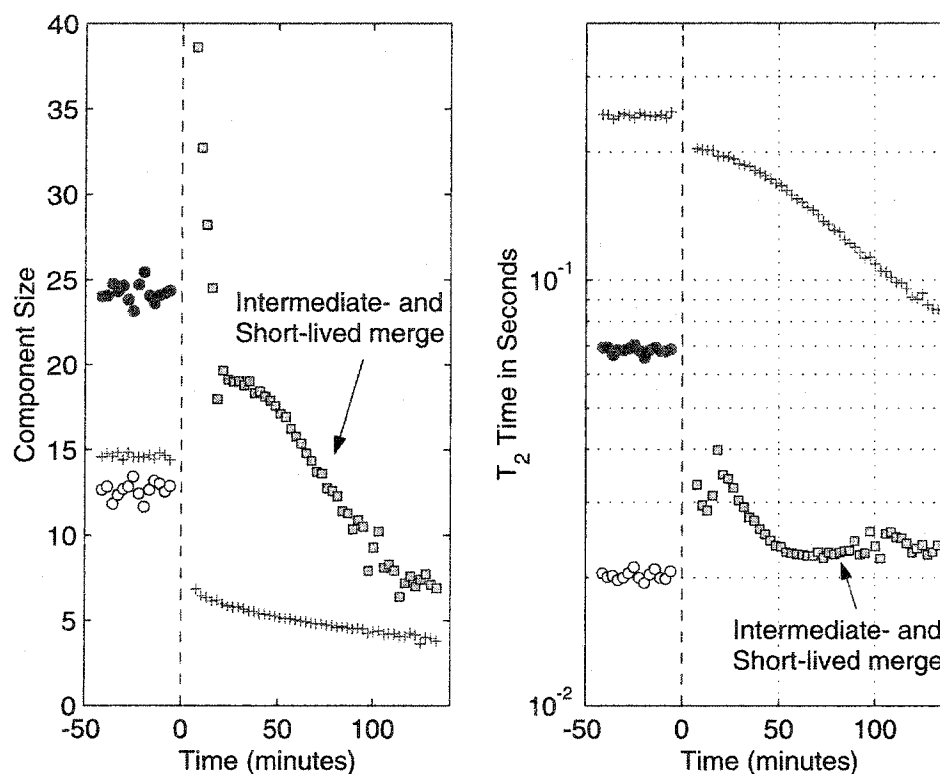


Figure 5-5. Experiment on rat sciatic nerve, with 10-mM Mn^{2+} ions infused at time zero. The short-lived and intermediate-lived components cannot be resolved after the introduction of manganese. The resultant merged component is represented with filled squares.

These data confirm that the long-lived component, although feeling the effects of the influx of Mn^{2+} ions as evidenced by its steady decline in T_2 , is not being saturated within a short time. Despite this confirmation, the behaviour of the intermediate-lived component is still unknown, and without this knowledge the component/compartiment assignment obviously cannot be made. Note: The sudden drop in its size after the buffer is switched is not due to a rapid integration of paramagnetic ions into the tissue, but rather to the removal of a surface water artefact as was discussed earlier.

Other experiments were explored in order to elucidate the response of the different components to Mn^{2+} ions. In one such experiment, a single fascicle was removed from the epineurium of the rat sciatic nerve, and underwent the same experimental procedure as above. The hope was that the removal of the epineurium would allow the paramagnetic ions faster access to the nerve tissue, and these would be able to completely saturate the endoneurium before being able to enter the axonal space. The spectral parameters from this experiment are displayed in Figure 5-6. Here, it is evident that the Mn^{2+} ions entered the tissue faster with the epineurium absent, due to the rapidity of the trends in the components compared to Figure 5-4. Unfortunately, this increased influx rate did not simplify the trends; it only accelerated them.

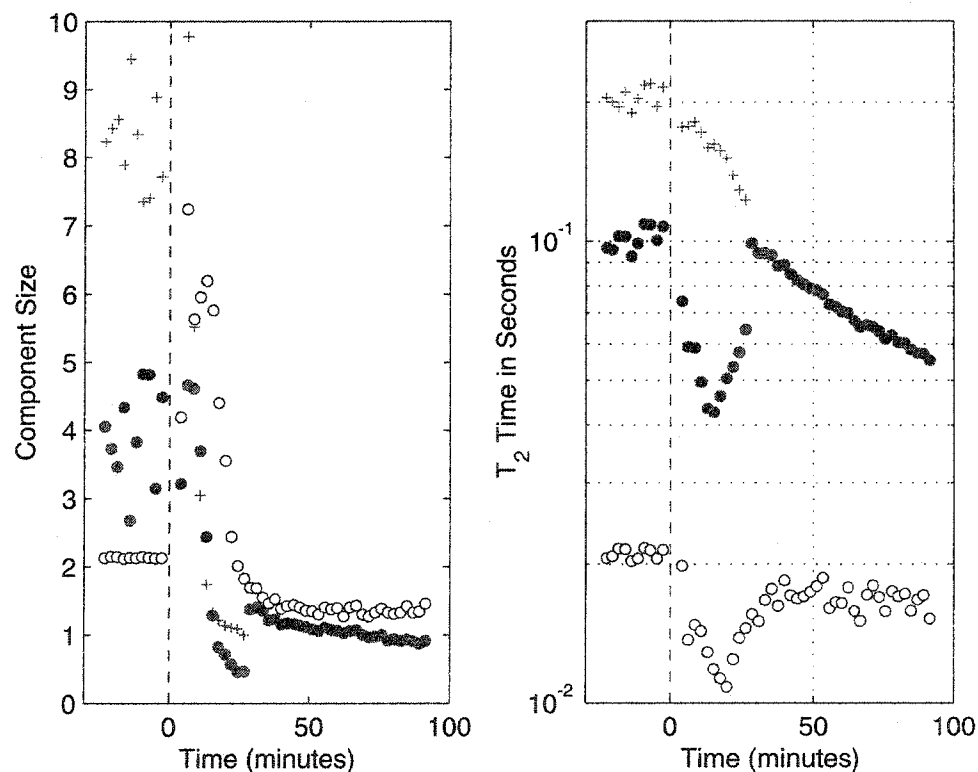


Figure 5-6. Repeat of experiment displayed in Figure 4, but using a single fascicle taken from rat sciatic nerve, instead of the entire nerve. Infusion of 10 mM Mn^{2+} begins at time zero (dashed line).

Another experiment explored the effects of low concentration of Mn^{2+} on nerve tissue, based on the concept that only subtle changes in spectral parameters would result: changes that would be less likely to cause interaction with other components. In this experiment, an intact rat sciatic nerve was laid on filter paper, and excess buffer solution was blotted off. Three to four drops of buffer containing 10-mM Mn^{2+} were then placed on the outer surface of the nerve. The nerve was immediately turned over, and the process repeated. The nerve was then blotted dry once more and placed in an NMR tube containing fluorinert, which, being immiscible to water and ions, including manganese, forced all the residual manganese adhering to the surface of the nerve to diffuse into the tissue. The solved spectral parameters from this experiment are shown in Figure 5-7.

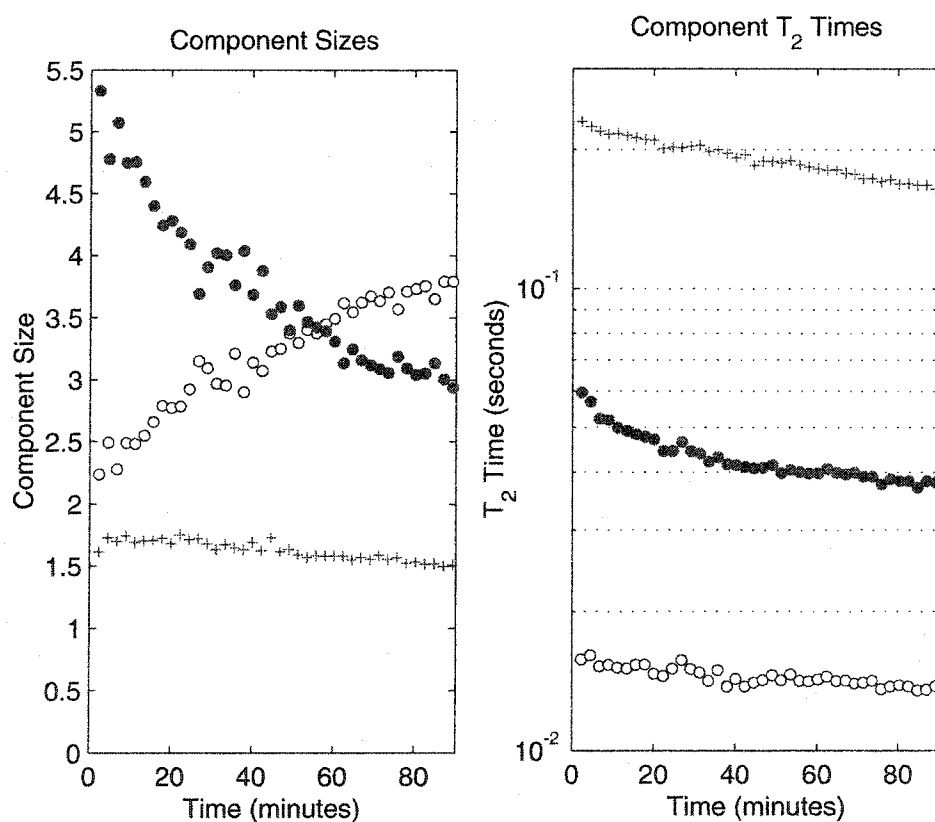


Figure 5-7. Spectral parameters of a rat sciatic nerve briefly exposed to Mn^{2+} , and then bathed in fluorinert.

It seems that the spectral changes were not subtle enough to avoid merging of components: one can see the size of the short-lived component increase as that of the intermediate-lived falls. Further, this extra short-lived signal cannot be coming from the long-lived component, since that remains quite stable here. Using this reasoning, one can build a more realistic picture of how the individual components behave. One simply assumes that all the gains in the short-lived component come from the original intermediate-lived component. The intermediate component can then be modeled as a weighted average of two spectral factors in $\log(T_2)$ space, where one factor is taken to be the gain in short-lived signal at a T_2 equal to that of the short-lived component. The second is the intermediate-lived component as solved above. Using this method, the plots **a** and **b** in Figure 5-8 were generated, showing how the spectral parameters would most-likely look if they remained independent. Figure 5-8c is an estimate of the Mn^{2+} concentration in the intermediate and long-lived components, based on the T_2 values in

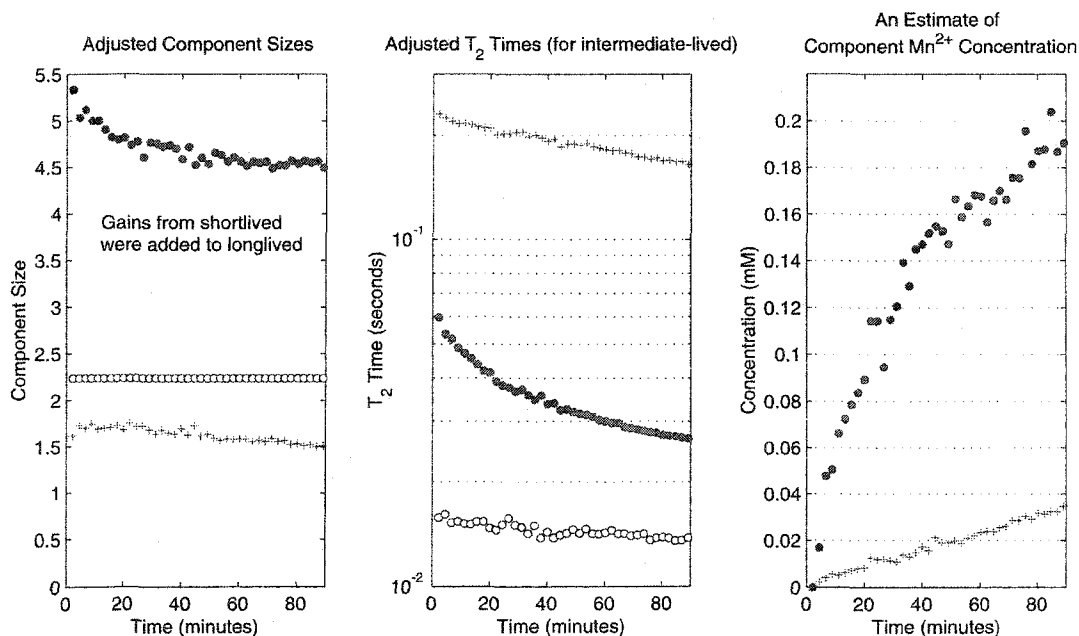


Figure 5-8. **a** and **b**: Modified spectral parameters of the data set shown in Figure 7. **c**: An estimate of the paramagnetic ion concentration based on the values in **b**.

Figure 5-8b, the assumption that the concentration was 0 at the time of the first spectrum, and the following equation:

$$C(t) = \frac{1/T_2(t) - 1/T_{20}}{\alpha_2}, \text{ where } \alpha_2 \text{ is the transverse relaxivity constant (}=50 \text{ mM}^{-1}\text{s}^{-1} \text{ for manganese ions).}$$

Looking at Figure 5-8b, it is evident that the relaxation rate of the intermediate component is falling faster and farther than that of the long-lived component. Nevertheless, seeing that they are both declining, this alone would be tenuous grounds for making conclusions about the compartment/component assignment. However, looking to the estimates of the Mn^{2+} concentration displayed in Figure 5-8c, the concentration in the intermediate-lived component is dramatically greater than that of the long-lived, ranging from between 10 times greater at the beginning to 6 times at 90 minutes. This is much more convincing evidence that the intermediate component is the more accessible one to ions diffusing into the nerve, namely the endoneurium. Why the axonal space would be more permeable to Mn^{2+} ions in rat nerve than in frog nerve is uncertain. A plausible explanation, however, may have to do with axonal diameter. Figure 5-9 shows a comparison between histological samples of rat sciatic and frog sciatic nerve photographed under identical magnification. These samples would indicate a significant difference between fibre sizes in the two species. Rough measurements from these photographs indicate a difference in axonal diameter to be on the order of 2. These estimates are supported in the literature, where rat sciatic nerve was measured to have a mean axonal diameter of 8.3 μm [19], as opposed to frog nerve, which according to a plot presented in Peled et al. [15] has a rough mean diameter of 14 μm . This doubling of diameter will bring about an associated quadrupling of axonal volume per fibre. As a result, assuming the rate of paramagnetic agent influx is the same in both cases, the effect on T_2 will be much more pronounced in the rat nerve.

Let us consider the Mn^{2+} concentration in the long-lived components in Figures 5-3 and 5-5. The frog nerve undergoes a drop in T_2 from about 250 ms to 180 ms in ~150 minutes, which using the equation given above, corresponds to about 0.03 mM. The T_2 drop in the long-lived component for rat nerve went from around 200 ms to 85 in the same amount of time. The corresponding concentration here is ~0.14 mM, about four to five times higher than that of the frog nerve. Therefore, it is possible that the different response to paramagnetic agents seen between the spectra of rat and frog are not due to fundamental differences in nerve physiology, but simply a difference in axon diameter.

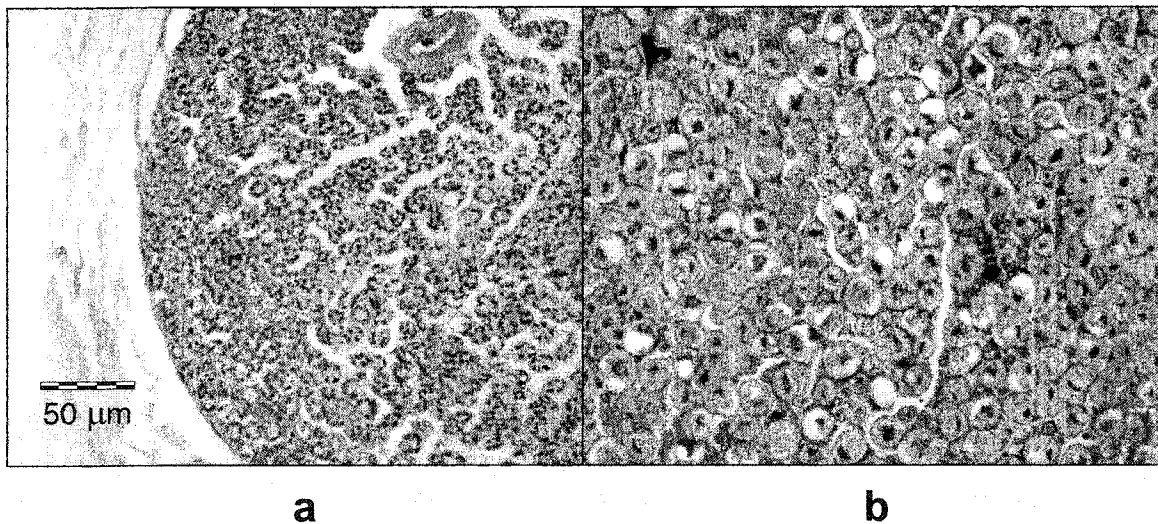


Figure 5-9. a. Rat sciatic nerve. b. Frog sciatic nerve. Both these micrographs were acquired with the same magnification.

But despite differences in how the two types of nerves respond, the component/compartments assignment appears to be the same. This is further verified by an experiment performed on a single fascicle. In this instance the tissue was rinsed for six seconds in 3-mM Mn^{2+} buffer, blotted dry and immediately placed in fluorinert. As can be seen in Figure 5-10, the manganese integrated very quickly into the intermediate component. The intermediate-lived component moves quickly from its usual decay time of ~70 ms to ~35 ms. The long-lived component begins at a typical value of ~200 ms, and falls only slightly to ~160 ms over the 20 minute experiment.

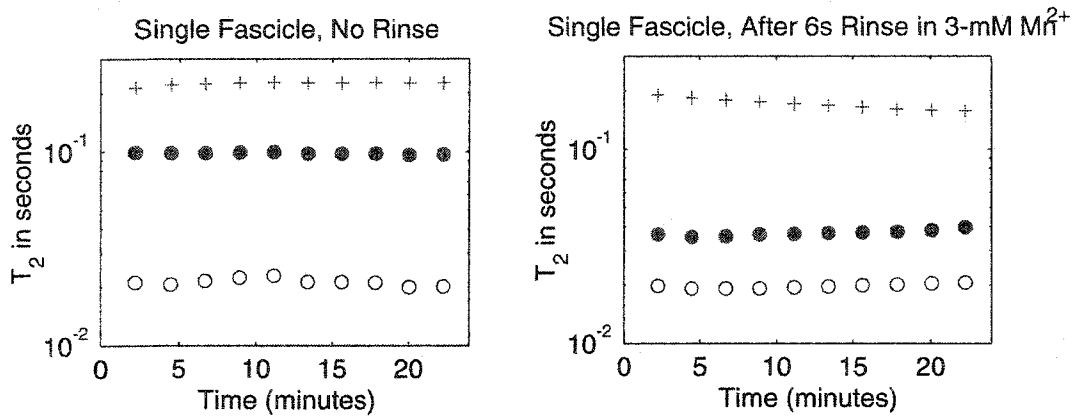


Figure 5-10. Comparison between normal spectral parameters of a single fascicle and one which was first rinsed in 3-mM Mn^{2+} for 6 seconds.

5.4 Conclusions

Although the results are more complex than that seen in frog nerve, experimental evidence indicates that the relationship of T_2 spectral components to microstructural compartments of rat sciatic nerve is the same, with the myelin water, endoneurium, and axoplasm corresponding to the short, intermediate, and long-lived components, respectively. Results also indicate a need for caution when using water-based buffer solutions, as in some circumstances the buffer can interact with the tissue and distort the appearance of the resulting spectrum.

5.5 References

- [1] Stanisz GJ, Midha R, Munro CA, Henkelman RM. MR properties of rat sciatic nerve following trauma. *Magn Reson Med.* 2001; 45: 415-20.
- [2] Wachowicz K, Snyder RE. Temperature dependence of the T_2 spectrum of peripheral nerve. In: *Proceedings of the 9th Annual Meeting of ISMRM, Glasgow, 2001*; p 1368.
- [3] Webb S, Munro CA, Midha R, Stanisz GJ. Is multicomponent T_2 a good measure of myelin content in peripheral nerve? 2003; 49: 638-645.
- [4] Beaulieu C, Fenrich FR, Allen PS. Multicomponent water proton transverse relaxation and T_2 -discriminated water diffusion in myelinated and nonmyelinated nerve. *Magn Reson Imag.* 1998; 16: 1201-1210.
- [5] Menon RS, Rusinko MS, Allen PS. Proton relaxation studies of water compartmentalization in a model neurological system. *Magn Reson Med.* 1992; 28: 264-274.
- [6] Stewart WA, MacKay AL, Whittall KP, Moore GR, Paty DW. Spin-spin relaxation in experimental allergic encephalomyelitis. Analysis of CPMG data using a non-linear least squares method and linear inverse theory. *Magn Reson Med.* 1993; 29: 767-775.
- [7] Menon, RS, Rusinko, MS, Allen, PS. Multiexponential proton relaxation in model cellular systems. *Magn Reson Med.* 1991; 20:196-213.
- [8] Fischer HW, Rinck PA, Van Haverbeke Y, Muller RN. Nuclear relaxation of human brain gray and white matter: analysis of field dependence and implications for MRI. *Magn Reson Med.* 1990;16: 317-334.

- [9] Does MD, Snyder RE. Multi-exponential T_2 relaxation in degenerating peripheral nerve. *Magn Reson Med.* 1996; 35: 207-213.
- [10] Jolesz FA, Polak JF, Ruenzel PW, Adams DF. Wallerian degeneration demonstrated by magnetic resonance: spectroscopic measurements on peripheral nerve. *Radiology.* 1984; 152: 85-87.
- [11] Does MD, Snyder RE. Multi-exponential T_2 relaxation in degenerating peripheral nerve. *Magn Reson Med.* 1996; 35: 207-213.
- [12] Vasilescu V, Katona E, Simplaceanu V, Demco D. Water compartments in the myelinated nerve, III: pulsed NMR results. *Experientia.* 1978; 34: 1443-1444.
- [13] Vasilescu V, Margineanu DG, Katona E. Heavy water intake in tissues, II: H_2O - D_2O exchange in the myelinated nerve of the frog. *Experientia.* 1977; 33: 192-194.
- [14] Wachowicz K, Snyder RE. Assignment of the T_2 components of amphibian peripheral nerve to their microanatomical compartments. *Magn Reson Med.* 2002; 47: 239-245.
- [15] Peled S, Cory DG, Raymond SA, Kirschner DA, Jolesz FA. Water diffusion, T_2 , and compartmentation in frog sciatic nerve. *Magn Reson Med.* 1999; 42: 911-918.
- [16] Wachowicz K, Snyder RE. A perfusion chamber suitable for the measurement of transverse relaxation spectra of tissue maintained in vitro. In: *Proceedings of the 8th Annual Meeting of ISMRM, Denver, 2000*; p 1987.
- [17] Wachowicz K, Bonilla I, Snyder RE. The use of a decoupled coil system and relaxation agents to improve perfusion chamber data. In: *Proceedings of the 11th Annual Meeting of ISMRM, Toronto, 2003*; p 2427.

- [18] Whittall KP, MacKay AL. Quantitative interpretation of NMR relaxation data. *J Magn Reson* 1989; 84: 134-152.

- [19] Canpolat L, Kukner A, Canpolat I, Ozan E. Ultrastructural and morphometric analysis of peripheral nerve regeneration within silicone tubes. *Tr. J. of Medical Sciences*. 1999; 29: 203-209.

CHAPTER 6

T₂ SPECTRAL CHARACTERISTICS OF HUMAN PERIPHERAL NERVE *IN VITRO*

6.1 Introduction

The transverse relaxation spectra of *in-vitro* peripheral nerve in frog, rat, and other species have been well characterized [1-6]. To this author's best knowledge, no study has been undertaken to investigate human nerve in this manner. Peripheral nerve has been successfully imaged, showing bright contrast compared to skeletal muscle in heavily T₂ weighted sequences [7-9]. This allows for the possibility that peripheral nerve may have a longer-lived signal component similar to that in frog or rat (>200 ms). (*In-vivo* C-P-M-G studies of skeletal muscle have reported ~90% of its signal relaxing with a T₂ time less than 50 ms, but also that a T₂ component exists up at around 110 ms [10].) Doubt as to the existence of this signal in human nerve comes from the fact that white matter has normally been characterized by a two-component spectrum consisting of short- and intermediate-lived signal. Since Chapters 4 and 5 have attributed the long-lived signal in frog and rat peripheral nerve to axoplasm (which one would assume to be of a similar nature in the CNS and PNS), the fact that human CNS is seen to lack this long-lived signal would raise questions about whether it is present in human peripheral nerves. It is possible that the spectrum and assignment of rat sciatic nerve cannot be used as a general mammalian peripheral nerve model. Thus, in the following work, the T₂ spectrum of normal human nerve samples was characterized, with special attention to the presence a long-lived component.

6.2 Method

6.2.1 Experimental Procedure

Twelve human peripheral nerve segments were obtained from the University of Alberta Comprehensive Tissue Centre. All proper ethics approval was obtained. After

the tissues were retrieved, they were placed in RPMI-1640 tissue medium (with sodium bicarbonate, and without L-glutamine and phenol red) and made available within one to eight hours. From the time they were obtained, one to two further hours were needed to prepare the nerves for relaxation experiments. The nerve samples were primarily saphenous retrieved from the ankle region, and ranging in diameter from ~0.8 mm to 3 mm.

The nerve samples were placed either in a perfusion system for MR experimentation, or in an NMR tube. In either case the tissue was continuously bathed in the RPMI medium, and in the case of the perfusion chamber, fresh bathing solution was constantly introduced into the chamber at a rate of 6.5 mL/hr. In one case, the nerve was carefully blotted dry before bathing it in a FluorinertTM FC-77 (3MTM, London, ON) solution. Fluorinert, being non-detectable to proton NMR, allows the nerve tissue to be studied with little to no interaction with surrounding bathing solution water. All experiments were performed at room temperature (~20 degrees C). Four different samples were subjected to paramagnetic agents in experiments. Either iron dextran, Mn^{2+} , or Gd-DTPA was used. The object of this technique was to investigate how the nerve decay signal was affected by the presence of a paramagnetic agent, and in what order the different spectral components were permeated with the agents. The iron dextran solution and Mn^{2+} solutions were administered via the perfusion chamber, after 10 to 20 baseline transverse decay curves had been acquired. In the case of Gd-DTPA, the nerve was dipped in a 500-mM solution for 10 seconds before being blotted dry and bathed in a Fluorinert bath.

In preparation for the MR experiments, the tissue in either the perfusion chamber or the NMR tube was centred in a 4-loop solenoid RF coil, and positioned in the isocentre of a 3 Tesla whole-body Magnex scanner controlled by an S.M.I.S. console. The small solenoid coil had a diameter of approximately 7 mm, and was used in pursuit of a high signal-to-noise ratio. Transverse-relaxation decay curves were acquired with a 2000

echo, 1.6 ms echo-time C-P-M-G sequence. Eight phase-cycled averages were performed for each acquired decay curve.

6.2.2 Analysis

To transform the 2000-echo decay curves into transverse relaxation spectra, the non-negative least squares algorithm (NNLS) was utilised [11]. One hundred and forty data points were randomly sampled in a quasi-logarithmic pattern, and fit to 105 mono-exponential functions, with decay times ranging logarithmically from 0.5 ms to 3 s. A minimum energy smoothing constraint was added to generate continuous spectral solutions. To utilise more of the data points, this procedure was repeated 20 times, with the average results being taken as the estimate of the T_2 decay spectrum. The data was sampled logarithmically rather than simply using all acquired data points in order to generate a closer-to-uniform sampling of every spectral component. This seemed to create a more uniform response to added smoothing constraints.

6.3 Results

The characteristic appearance of human peripheral nerve T_2 spectra revealed a three-component spectrum, similar to that found in frog and rat nerve (Figure 6-1). The component parameters from seven transverse relaxation spectra acquired from human peripheral nerve are displayed below in Table 6-1. All these data were obtained from nerve samples bathed in water-based tissue medium.

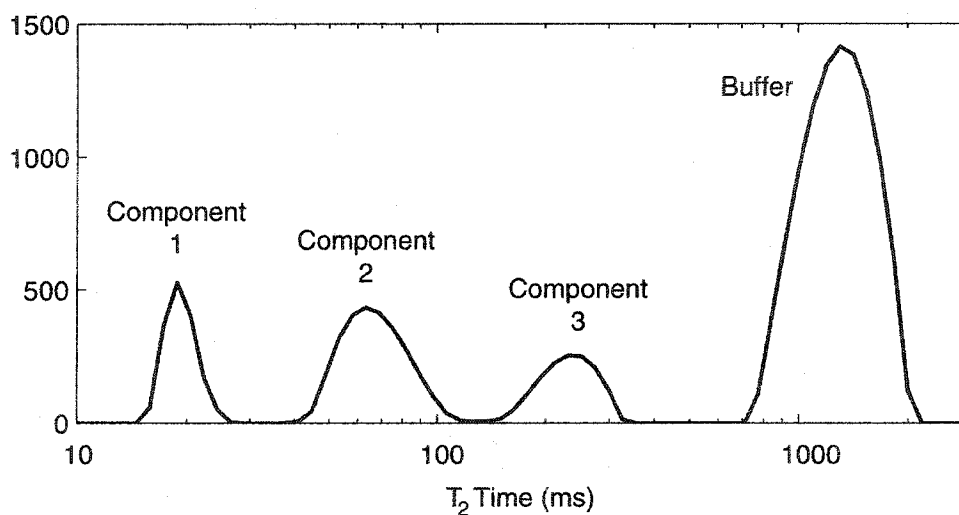


Figure 6-1. A typical T_2 spectrum of human peripheral nerve (saphenous) bathed in a water-based medium (RPMI).

Component 1				Component 2				Component 3			
Size (%)	S.D.	T_2 (ms)	S.D.	Size (%)	S.D.	T_2 (ms)	S.D.	Size (%)	S.D.	T_2 (ms)	S.D.
40.5	4.3	29.1	2.4	33.2	4.8	68.7	5.9	26.3	0.8	287.5	5.0
22.1	2.4	32.3	2.8	47.7	1.6	92.0	6.7	30.1	1.8	287.4	31.2
16.8	1.5	33.9	1.3	52.6	2.2	97.6	2.9	30.7	3.5	282.0	38.1
21.8	2.4	29.5	2.6	55.8	2.3	75.3	2.1	22.5	0.7	266.4	4.3
27.2	1.1	19.3	0.7	48.0	0.8	66.9	1.5	24.7	0.5	229.1	3.8
31.5	4.6	17.8	3.0	37.6	4.6	58.8	9.1	30.9	6.1	235.2	81.6
27.3	2.4	27.4	2.7	40.5	1.0	84.7	6.0	32.3	1.8	241.7	10.8
Component 1 Average				Component 2 Average				Component 3 Average			
27%	8%	27 ms	6 ms	45%	8%	78 ms	14 ms	28%	4%	261 ms	26 ms

Table 6-1. Spectral parameters for human peripheral nerves acquired in vitro while bathed in a water based tissue medium.

The relatively large variance in the component parameters (particularly with regards to time) is most likely due to the inconsistency of the exact section of nerve being retrieved. This data strongly indicates the presence of a long-lived component. It is interesting to note that the human nerve bathed in RPMI has T_2 spectral characteristics

very similar to those of rat nerve (Table 5-1), in fact they agree within error. A comparison of these results between human nerve and rat sciatic nerve is displayed below in Figure 6-2.

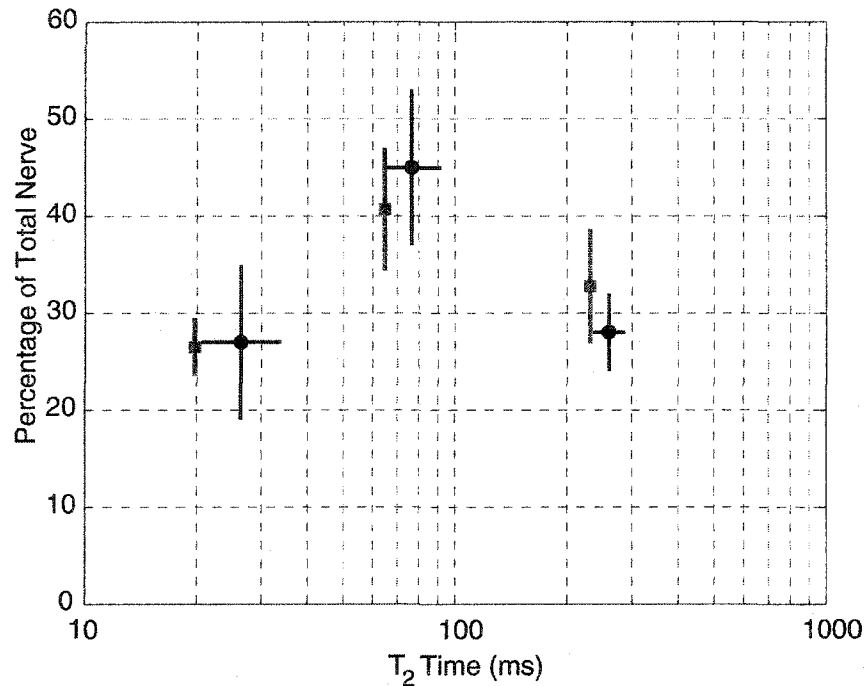


Figure 6-2. Plot of average component parameters for human nerve (circles), compared to the average parameter values for rat sciatic nerve in the similar experimental conditions (squares). The error bars represent the standard deviations of these parameters for T_2 time and spectral size. The error bars for the T_2 times are derived from the standard deviation in logarithmic space.

However, in studies with rat nerve, it was found that the long-lived component could be magnified by the presence of a water-based buffer. To test for this, one of the samples was bathed in Fluorinert rather than RPMI medium during data acquisition. The results are displayed in the spectrum in Figure 6-3 below. The long-lived component is a great deal smaller here than in the above RPMI results, but its presence remains clear.

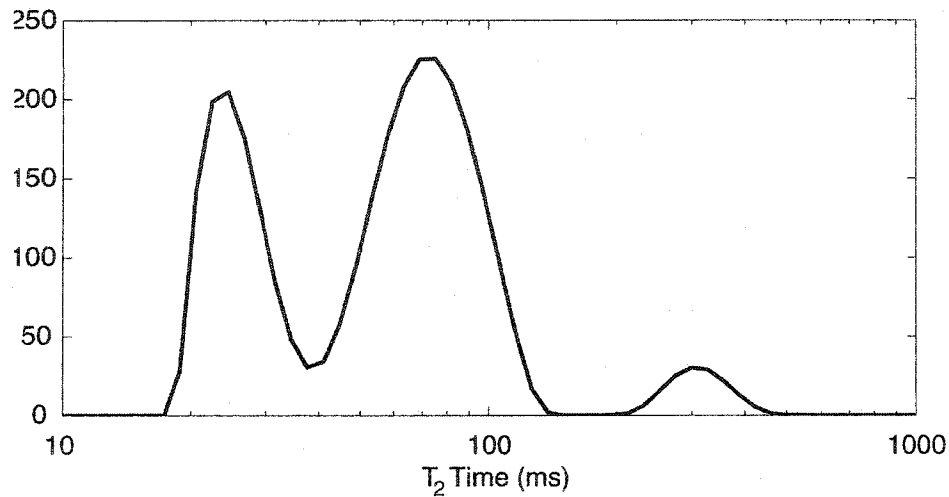


Figure 6-3. Human peripheral nerve sample (saphenous) in Fluorinert FC-77. The long-lived component is present, albeit small.

Experiments with paramagnetic ions had more ambiguous results. It was hoped that either the long-lived or intermediate-lived component would be affected more rapidly by the paramagnetic agent diffusing in, thus revealing information about the spectral relationship to microanatomy (similar to experiments described for frog sciatic nerve in Chapter 4). However, in this set of human nerve samples it was difficult to discern that one component was being affected before the other. This was primarily due to the fact that the intermediate-lived and the long-lived components were consistently seen to merge soon after the nerve was subjected to the agent (Figure 6-4). The reason for this merging is unclear. It is possible that the inherent shortcomings in multi-exponential analysis make it difficult to separate these components in this particular circumstance. (Perhaps the dramatic jump in signal size and later increase in T_2 of the short-lived component, presumably due to the reduction in T_2 of a portion of the merged component, causes the routine to lose some degree of specificity in the reduced amplitude longer-lived portion of the spectrum. This could especially be the case if, as is likely, the affected component is not reduced in T_2 as a whole, but increases its spectral width

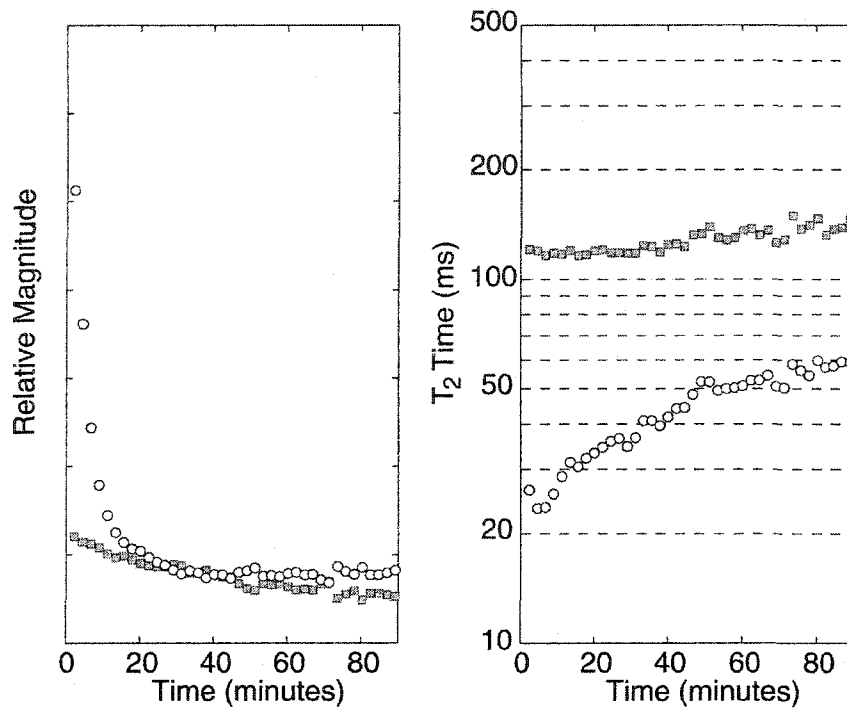


Figure 6-4. The relative magnitude and T_2 time of nerve components calculated from the data set involving Gd-DTPA. The nerve was dipped for 10 seconds in 500-mM Gd-DTPA 2 minutes before time 0.

during the transient period as Gd-DTPA diffuses in.) Whatever the case, one can clearly see the influence of longer-lived signal throughout the data set. In Figure 6-4 for example, the merged component (represented by squares), is positioned well above the expected T_2 of the intermediate-lived component displayed in Figure 6-2. The T_2 of the merged component is, at its lowest, 120 ms, which is a value one might expect to see in a weighted average of the intermediate- and long-lived components in logarithmic space. Furthermore, as time progresses, the T_2 of this merged component increases, indicating that the signal that is being lost (as seen in the magnitude plot) is that of a shorter-lived nature. One can only speculate as to the causes of the behaviour seen in the short-lived component, where the T_2 rises from its typical value of ~ 25 ms to ~ 60 ms. As was suggested earlier, perhaps a portion of the merged component is being increasingly

influenced by the Gd-DTPA, falling in T_2 , and being lumped together with the short-lived component.

6.4 Conclusions

Human peripheral nerve has been established as a multi-component T_2 spectrum, with strong evidence for three-components. The T_2 spectral characteristics of human nerve when bathed in a water-based buffer are quite similar to those of rat sciatic nerve, agreeing within error. This would suggest that rat nerve can be taken as a reasonable model for human nerve, at least from the perspective of transverse relaxation. The size of this long-lived component was seen to be reduced by the use of a Fluorinert bathing solution, which removes the effect of buffer-surface interactions. This reduction in magnitude was consistent with that seen in rat sciatic nerve in Chapter 5. The magnitude of the signal drop-off, however, as seen by a comparison of Figure 6-3 and Figure 6-1, was much greater than that of rat sciatic nerve. This could represent a difference between rat and human nerve characteristics. However, seeing that only one nerve sample above was analysed with the Fluorinert buffer, it is possible that the long-lived signal in Figure 6-3 is just uncharacteristically low. This is possible considering these nerves had sometimes been excised for up to nine hours before experiments could be performed, and the individual may have been deceased for hours before this. Thus, the condition of the nerve samples was not ideal, as compared to the rat nerve studies discussed in Chapter 5 where the nerve experiments began within one to two hours after the animal was euthanised. Considering how closely the human and rat nerve spectral characteristics compare, it would be surprising if they appeared radically different in a Fluorinert solution. More studies would be needed to establish typical T_2 spectral characteristics of human nerve in the absence of buffer water.

The studies using paramagnetic agents were unfortunately unclear as to which compartment was most accessible. A merging of the two longer-lived components prevented a clear analysis of the order in which the compartments were being affected.

As above, this could be a result of the poor state of the tissue samples. However, a slight rise in the merged component over time is suggestive of intermediate-lived signal dropping out of the component, while long-lived signal remains.

6.5 References

- [1] Vasilescu V, Katona E, Simplaceanu V, Demco D. Water compartments in the myelinated nerve, III: pulsed NMR results. *Experientia*. 1978; 34: 1443-1444.
- [2] Does MD, Snyder RE. T_2 relaxation of peripheral nerve measured in vivo. *Magn Reson Imag*. 1995; 13: 575-580.
- [3] Peled S, Cory DG, Raymond SA, Kirschner DA, Jolesz FA. Water diffusion, T_2 , and compartmentation in frog sciatic nerve. *Magn Reson Med*. 1999; 42: 911-918.
- [4] Stanisiz GJ, Midha R, Munro CA, Henkelman RM. MR properties of rat sciatic nerve following trauma. *Magn Reson Med*. 2001; 45: 415-20.
- [5] Wachowicz K, Snyder RE. Temperature dependence of the T_2 spectrum of peripheral nerve. In: *Proceedings of the 9th Annual Meeting of ISMRM, Glasgow, 2001*; p 1368.
- [6] Beaulieu C, Fenrich FR, Allen PS. Multicomponent water proton transverse relaxation and T_2 -discriminated water diffusion in myelinated and nonmyelinated nerve. *Magn Reson Imag*. 1998; 16: 1201-1210.
- [7] Dailey AT, Tsuruda JS, Filler AG, Maravilla KR, Goodkin R, Kliot M. Magnetic resonance neurography of peripheral nerve degeneration and regeneration. *Lancet*. 1997; 350: 1221-2.
- [8] Filler AG, Howe FA, Hayes CE, Kliot M, Winn HR, Bell BA, Griffiths JR, Tsuruda JS. Magnetic resonance neurography. *Lancet*. 1993; 341: 659-61.
- [9] Maravilla KR, Bowen BC. Imaging of the peripheral nervous system: evaluation of peripheral neuropathy and plexopathy. *Amer J Neurorad*. 1998; 19: 1011-1023.
- [10] Saab G, Thompson RT, Marsh GD. Multicomponent T_2 relaxation of in vivo skeletal muscle. *Magn Reson in Med*. 1999; 42:150-157.

- [11] Whittall KP, MacKay AL. Quantitative interpretation of NMR relaxation data. *J Magn Reson.* 1989; 84: 134-152.

CHAPTER 7

CONCLUSIONS

7.1 Component to Compartment Assignment of Frog and Rat Nerve

In the case of both frog and rat sciatic nerve, a three-component transverse relaxation spectrum was verified to those reported in the literature. Experiments performed on frog nerve utilising manganese ions revealed that the intermediate-lived spectral component was the one most easily accessed by the ions. Following from the notion that there are three main water pools in nerve tissue with limited exchange between them (water in axoplasm, endoneurium water, and myelin water), the manganese results were taken to reveal that the intermediate-lived component corresponds to the endoneurium water. This conclusion was reached on the basis that the endoneurium is the compartment most easily accessible via diffusion. (In order for the axoplasm to be invaded by the Mn^{2+} ions, it must first pass through the endoneurium.) Given that there has already been much evidence that myelin water corresponds to the short-lived spectral component, the component to compartment assignment on the basis of these results is: 1) short-lived component – myelin water, 2) intermediate-lived component – endoneurium, and 3) long-lived component – axoplasm.

Results using this technique with rat sciatic nerve were less straight-forward. Rather than the intermediate-lived component being affected while the long-lived remained stable, both these components would experience changes in spectral parameters, and would often merge, making interpretations difficult. The merging that was seen was not necessarily an indication that the T_2 time of the intermediate-lived and the long-lived had become the same, but that the two spectral peaks had shifted together past the resolving power of the analysis routine (the resolving condition being that the two peaks be approximately greater than a factor of two apart.). A later experiment in which a rapid but limited influx of Mn^{2+} was administered to a nerve sample through a

blotting technique allowed the long-lived component to remain more independent, and allowed some insight into the concentration levels of Mn^{2+} affecting the different components. It was shown that although the long-lived component was being affected by manganese ions to a considerably greater extent than that seen in frog nerve, the concentration of Mn^{2+} affecting the intermediate-lived component rose at a much greater rate than it did for the long-lived. Based on these findings, it was concluded that the same component to compartment assignment used for frog nerve was appropriate for rat. It was postulated that the differences seen between frog and rat nerve could be due to a larger frog axon diameter.

It was also discovered during this study that the presence of a water-based bathing solution can have significant contribution on the measured T_2 spectra of nerve tissue, specifically in the long-lived component. Evidence derived from the use of FluorinertTM (3MTM, London ON) as a bathing solution suggested this to be the result of a tissue surface / water interaction. The degree of spectral distortion from this interaction seemed to depend on the smoothness of the tissue surface.

7.2 Human Peripheral Nerve Studies

A pioneering *in-vitro* T_2 relaxation study on human peripheral nerve was performed. Human peripheral nerve (primarily saphenous) was found to have a three-component transverse-relaxation spectrum. Experiments utilizing paramagnetic agents as performed on frog and rat were inconclusive due to the merging behaviour of the intermediate- and long-lived components, like that seen in rat nerve, but to a greater extent. This may be due to inherent properties of the human peripheral nerve, or perhaps due to the agedness of the nerve (up to 9 hours post-excision) at the time of experiment. This work provides a foundation for future study.

7.3 NMR In-Vitro Perfusion System

A device was developed that was capable of continually providing fresh buffer to a tissue sample while simultaneously acquiring data. The rationale behind this project was to be able to maintain oxygen requirements to tissue over long studies, and secondly, for the ability to switch buffer solution content on the fly. The use of this system to switch solutions instead of the traditional approach (removing the tissue from the NMR tube and replacing it into a new solution) increased the precision of the measured spectral precision by an approximate factor of 5.

An early version of this system involved the use of a single coil for both transmission and reception. Some problems were found with this design, however, that related to the flow of buffer solution during data acquisition. Thus, a second system was designed that involved a decoupled two-coil setup, with a larger volume coil for transmission, and a smaller coil for reception. This two-coil system was found to remove most of the data distortions that were due to the presence of flow.

7.4 Future Directions

7.4.1 Human Nerve

Further experiments directed towards investigating the assignment of the T_2 spectral components of human peripheral nerve to microanatomy need to be performed. Given the difficulty experienced when using paramagnetic agents with human nerve in the previous chapter, a different approach will likely need to be taken, perhaps along the lines of the experiments on rat nerve discussed in Section 5.3.2 where the amount of agent accessible to the nerve was curtailed. As well, although the long-lived component was unarguably present in the spectra obtained with the tissue bathed in RPMI, a water-based buffer solution, the single experiment that revealed the magnitude of this component to drop drastically when in a Fluorinert buffer indicates that repetitions of this latter experiment would allow one to establish human nerve as a three-component spectrum with greater certainty.

Finally, the ultimate goal would be to obtain human peripheral nerve T_2 spectra *in vivo*. Lower SNR and larger echo spacings would pose difficulties not seen in the *in vitro* work presented in the previous chapters. However, if one were to be able to overcome these difficulties, the technique would offer potential for diagnostic capabilities.

7.4.2 Analysis Technique

The three-component spectrum consistently measured and reported for frog and rat nerve may be an overly simplistic picture of the true transverse-relaxation spectrum. Subtle spectral characteristics caused by such things as the presence of the epineurium, for example, may go unnoticed due to the lack of spectral resolution as seen through the analysis routine. As demonstrated by the merging of components seen in Chapters 5 and 6 when manganese ions were introduced, the ability to resolve components more accurately would be a significant step forward for this type of study. Of course, that the exponential function is extremely non-orthogonal implies some significant inherent resolution limitations to any method of translating relaxation data to the spectral domain. However, there may well be methods, or combinations of methods that allow one to glean more information out of one's data. With this in mind, a modification to the standard method of applying the NNLS routine to the multi-exponential problem is outlined in Appendix 1.

APPENDIX 1

ALTERNATIVE ANALYSIS TECHNIQUE

A1.1 Introduction

Multi-exponential analysis has a wide range of applications in many scientific disciplines. Relaxometry in NMR has the potential to reveal a great deal of information, yet it has never been used to its full potential because of the spectral distortion and poor resolution offered by available analysis techniques. It would behoove the NMR community, as well as other scientific disciplines, to explore different approaches to multi-exponential analysis so that information that is presently hidden in experimental data might be unlocked. The following is a novel approach to this problem that offers some modest advantages over present techniques, and holds promise for future development.

A1.2 Theory

The difficulty in performing multi-exponential analysis is owing largely to the non-orthogonality of the decaying exponential function. An example of this is illustrated in Figure A1-1 a. Here, a plot of a mono-exponential decay curve (solid) is compared to the average (dashed) of two different decay curves, with decay constants increased and decreased by the same factor from the original. Note the relatively small difference function plotted in Figure A1-1b. This difference function has a very consistent form and can be described as follows:

$$D(t, f) = \exp(-t/\tau) - \left[\frac{1}{2} \exp\left(-f \times \frac{t}{\tau}\right) + \frac{1}{2} \exp\left(-\frac{1}{f} \times \frac{t}{\tau}\right) \right], \quad [\text{A1.1}]$$

where t is time, τ is the decay constant of the original decay curve, and f is a stretch/shrink factor.

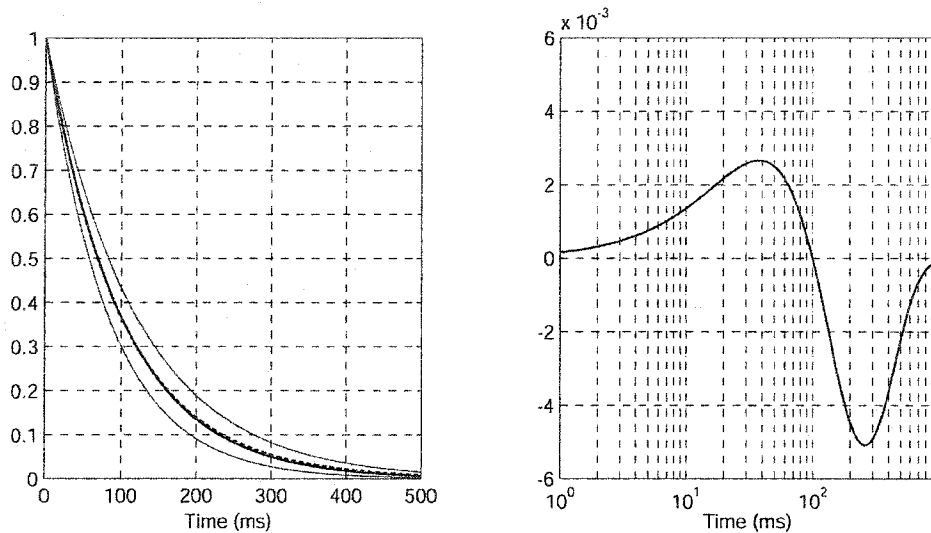


Figure A1-1. a) A plot of a monoexponential decay curve (solid) with a decay constant of 100 ms against a plot of the average (dashed) of two different curves, with decay constants increased and decreased by a factor of 1.2 from 100 ms. b) The difference function (single decay minus average of the two lines described in a).

Now if one sets $t = e^x$, a linear sampling of x will generate a logarithmic sampling of time. One can also set $\tau = e^T$, where T will be a logarithmic sampling of the decay constant, which is appropriate considering most decay spectra are described in logarithmic space. Using these substitutions, Equation A1-1 becomes:

$$D(x, f) = \exp(-e^{(x-T)}) - \left[\frac{1}{2} \exp(-f \times e^{(x-T)}) + \frac{1}{2} \exp\left(-\frac{e^{(x-T)}}{f}\right) \right]. \quad [A1.2]$$

Thus, the difference function takes on a form which is dependent solely on the factor f , and completely independent of the decay time t . The variable $T = \ln(\tau)$ only has the effect of translating the function horizontally. Figure A1-2 demonstrates the response of the difference function to changes in the factor f .

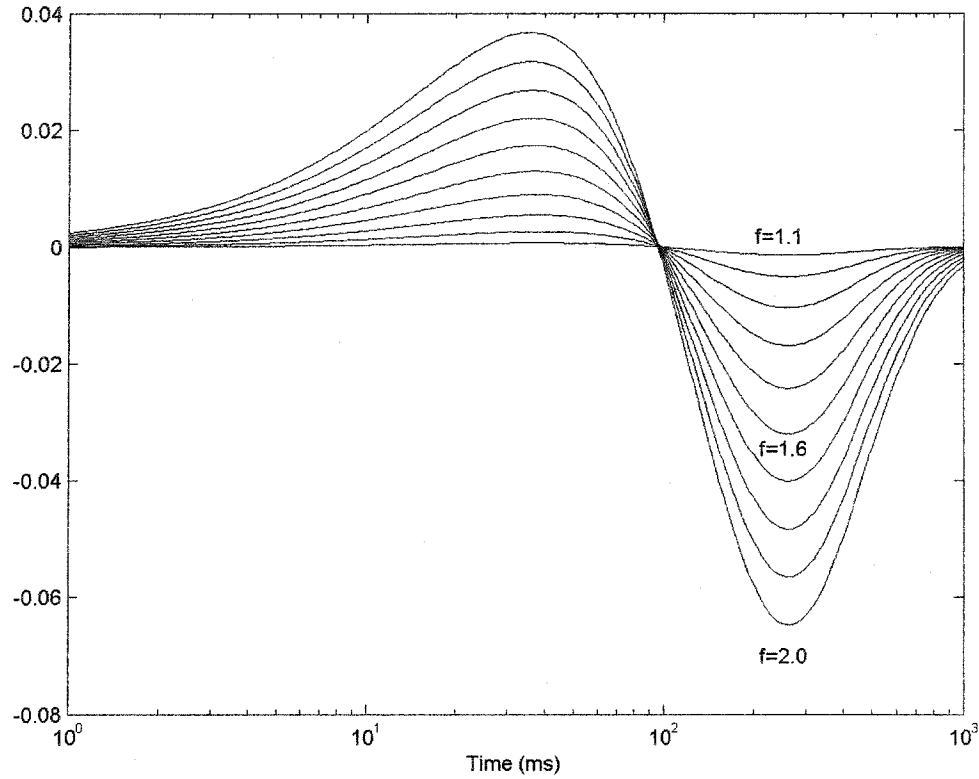


Figure A1-2. The difference function as it varies over a range of factor values (f). An increasing f value has the primary effect of vertically magnifying the difference function.

Now consider an arbitrary decay spectrum $S(T)$. The time domain signal produced by this spectrum would be:

$$Y(x, f) = \int S(T) \exp(-e^{(x-T)}) dT. \quad [\text{A1-3}]$$

If one could manipulate the time variable t such that $t^- = f \times t$, then

$$Y^-(x, f) = \int S(T) \exp(-f \times e^{(x-T)}) dT, \text{ and if } t^+ = f \div t, \text{ then} \quad [\text{A1-4}]$$

$$Y^+(x, f) = \int S(T) \exp\left(-\frac{e^{(x-T)}}{f}\right) dT. \quad [A1-5]$$

Therefore, obtaining the difference data from these time signals would yield:

$$\begin{aligned} D_s(x, f) &= Y(x) - \left(\frac{1}{2}Y^-(x) + \frac{1}{2}Y^+(x)\right) \\ &= \int S(T) \left\{ \exp(-e^{(x-T)}) - \left[\frac{1}{2} \exp(-f \times e^{(x-T)}) + \frac{1}{2} \exp\left(-\frac{e^{(x-T)}}{f}\right) \right] \right\} dT \\ &= \int S(T) \cdot D(x+T, f) dT \\ &= S(T) \otimes D(x, f), \end{aligned} \quad [A1.6]$$

which finally reveals that the difference data $D_s(x, f)$ is equivalent to the convolution of its ideal decay spectrum by the difference function $D(x, f)$.

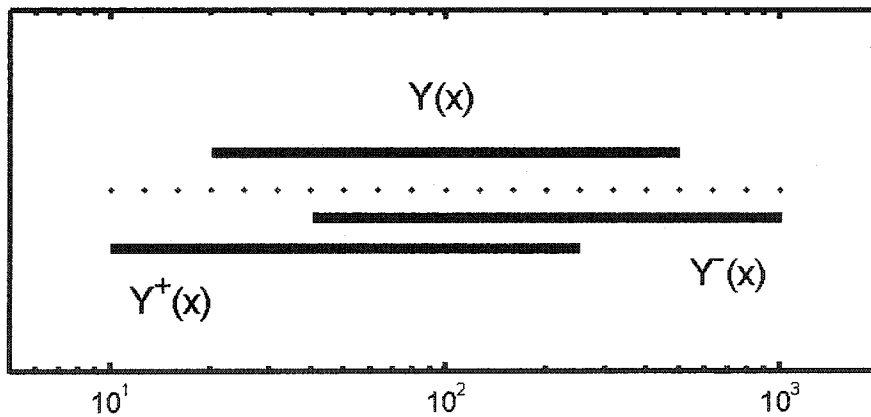


Figure A1-3. A schematic of how one might obtain compressed and magnified data sets $Y^-(x)$ and $Y^+(x)$ if data were sampled logarithmically.

Obtaining the time compressed and magnified data sets Y^- and Y^+ experimentally would be very straightforward in cases where logarithmic time sampling is possible. One would simply obtain those sets by utilizing three groups of consecutive data points, each shifted by the same number of points apart (Figure A1-3). Clearly, however, this logarithmic sampling is not always feasible, as is the case with transverse relaxation. In this case, where data points are sampled linearly in time, there are two options for obtaining the above data sets. Firstly, one could acquire three experimental decay curves, each with a different TE. This option has some obvious disadvantages. For one, the use of different echo times may result in differing rates of relaxation between acquisitions, complicating the technique. Also, this method would obviously increase scan time by a factor of three. A simpler alternative would be to assign the factor f to be a whole number, say 2 or 3. In this case, different sets of echo multiples can be compared to determine the difference data (i.e. 1, 2, 3, 4; 2, 4, 6, 8; and 4, 8, 12, 16). This latter method would not suffer any signal to noise loss compared to the first, as the noise should be uncorrelated in time.

Now that the difference data can be calculated, the source decay spectrum can be calculated by deconvolving the difference function from the data (Equation A1-6). It is unfortunate that the deconvolving function $D(x,f)$ is so broadened in time, as this makes the use of frequency domain methods unworkable. As a result, least-squares fitting seems the most appropriate method to achieve deconvolution. The non-negative least squares routine can be set up as follows:

$$\begin{bmatrix} D(x_1 + T_1) & D(x_1 + T_2) & \cdots & D(x_1 + T_N) \\ D(x_2 + T_1) & D(x_2 + T_2) & \cdots & D(x_2 + T_N) \\ \vdots & \vdots & \ddots & \vdots \\ D(x_M + T_1) & D(x_M + T_2) & \cdots & D(x_M + T_N) \end{bmatrix} * \begin{bmatrix} S_1 \\ S_2 \\ \vdots \\ S_N \end{bmatrix} = \begin{bmatrix} D_s(1) \\ D_s(2) \\ \vdots \\ D_s(M) \end{bmatrix} \quad [\text{A1.7}]$$

A1.3 Method

To test how this technique would respond in practice, computer simulated decay curves were generated with 4000 echoes, and a TE of 1 ms. Three component Gaussian and delta function decay spectra were used to simulate the data. Noise was added to these decay curves to yield a signal to noise ratio ranging from 100 up to 6000. Both delta function fits and constrained solutions were generated using an f factor of 2. In the case of delta function fits the routine would be left to run over 1000 times, after which a limiting distribution of the resulting spectra could be estimated. Spectra obtained using this difference method were compared to results from the traditional fitting technique using the same data sets.

A1.4 Results and Discussion

It is evident from looking at the size of the convolving function (Figure A1-2) as compared to the raw decay data (normalised to 1) that this technique will suffer a significant drop in SNR as compared to the traditional technique which directly analyses the raw data. For example, using an f factor of 2, the maximum amplitude of the convolving function is 0.0647, yielding a drop in SNR of $\frac{1}{0.0647 \times \sqrt{3/2}} \approx 12.6$.

However, this loss in SNR does not prove to be as negative to the capabilities of the technique as the above number would indicate. Figure A1-4 to A1-7 show a comparison of results between the traditional and the new technique when analysing data of different kinds. The first is a delta function data set (Figure A1-4). In this example, both methods are seen to perform comparably well, with perhaps a little more spectral resolution using the traditional technique. The next example, however, (Figure A1-5) reveals the new technique producing a spectrum that is better biased towards the centre of the source peaks than that of the traditional technique. The traditional technique, while generating spectral peaks with weighted averages well matched to the proper location, produce peripheral bias points, as seen around the 60 ms spectral line. This is seen even more dramatically when the SNR is increased to 6000 in Figure A1-6. However, when the

SNR is dropped to low values, the new technique begins to perform more poorly than the traditional, as is seen in Figure A1-7, where an SNR of 100 was used.

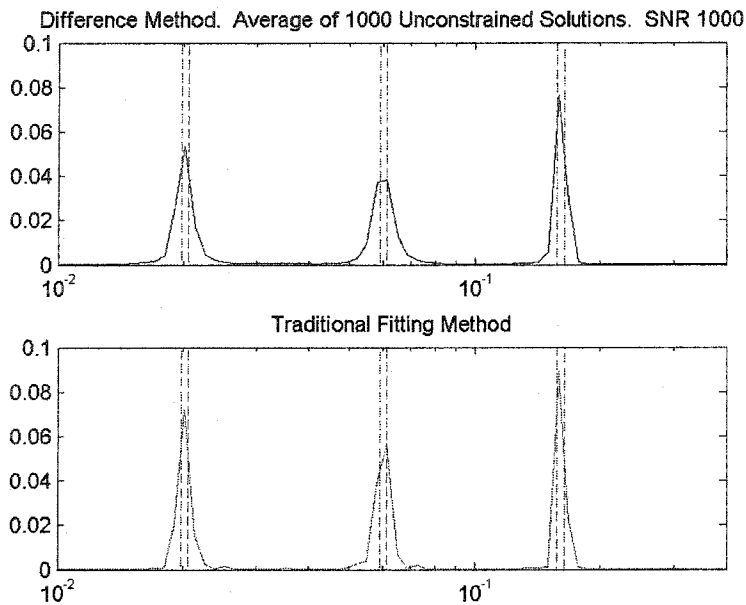


Figure A1-4. A comparison of the techniques when applied to a data set with a delta function source spectrum (dashed).

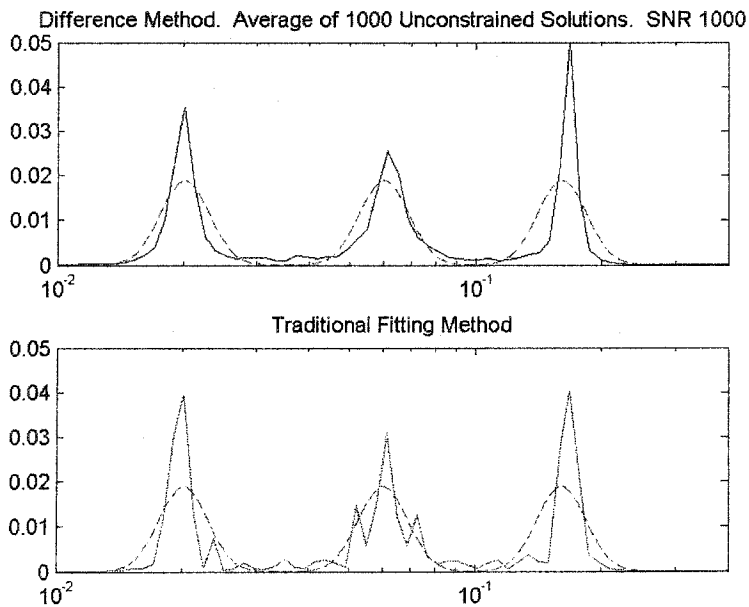


Figure A1-5. A comparison of the techniques when applied to a data set with a continuous Gaussian line source spectrum (dashed), SNR=1000.

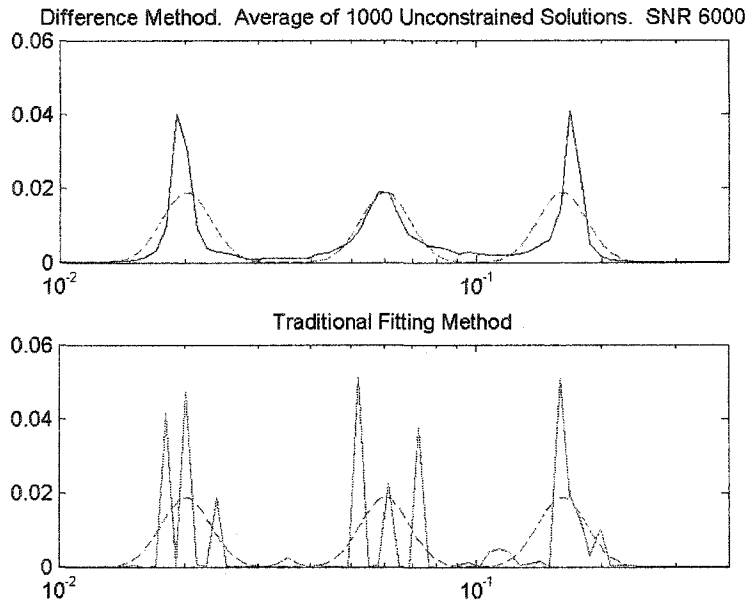


Figure A1-6. A comparison of the techniques when applied to a data set with a continuous Gaussian line source spectrum (dashed), SNR=6000.

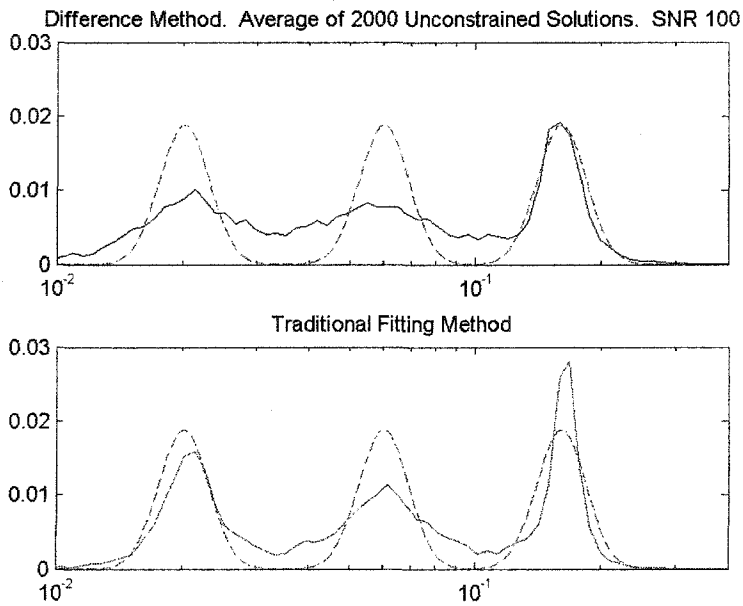


Figure A1-7. A comparison of the techniques when applied to a data set with a continuous Gaussian line source spectrum (dashed), SNR=100.

Despite the aforementioned problem with SNR, there are reasons why one might expect advantages to come from using this method. Firstly, as this technique involves taking differences between selected data in the same set, it will be completely immune to problems with DC offsets in experimental data. In order to accommodate this DC problem, the traditional technique must employ an extra variable to the solution vector, adding uncertainty to an already uncertain solution. Additionally, the difference technique will be more resistant to distortions caused by the presence of Rician noise in the raw data curves (Figure A1-8). (This will only be an issue when magnitude data are used, which is sometimes unavoidable.) This resistance is derived from the fact that distortions due to Rician noise will only be significant when the SNR becomes low, as in the tail end of the relaxation curve. Since this technique involves the averaging of a short section the decay curve with a long one, up to half of this distortion can be eliminated. Note in Figure A1-8 how the solution for the 60 ms peak is deviated from center using the traditional fitting method, whereas the difference method locates the correct spectral location. This illustrates the robustness of the new technique to data sets with Rician noise.

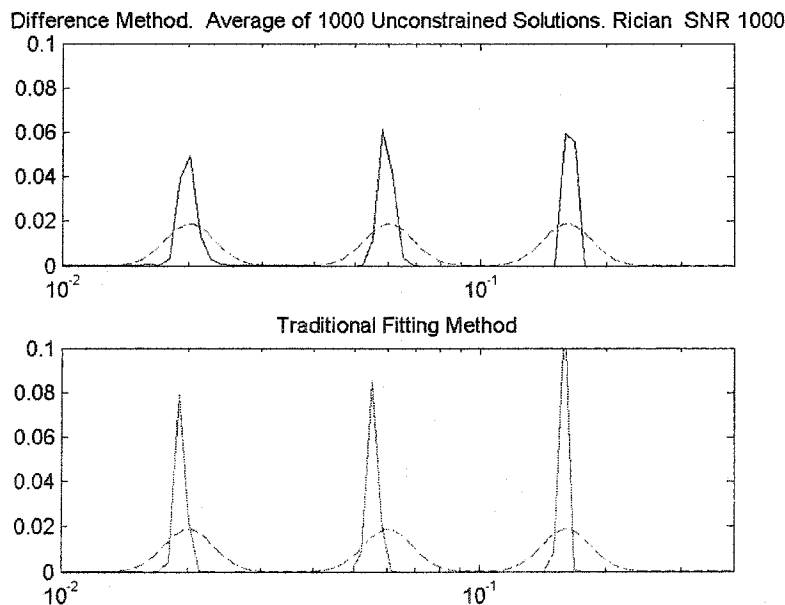


Figure A1-8. A comparison of the techniques when applied to a data set with Rician noise. The dashed line represents the ideal source spectrum.

A1.5 Conclusions

Except for problems encountered with low SNR, the new technique performed quite well compared to the traditional NNLS approach. Spectra were seen to exhibit less bias around the central part of a spectral line than that of the traditional NNLS, and will *a priori* be immune to problems with DC offset. The technique was demonstrated to be resistant to problems associated with Rician noise, which may be encountered when analysing magnitude data.